The Computational Modelling of Heavy Atom Chemistry

UNIVERSITY OF CAMBRIDGE

A thesis

by ***Chris-Kriton Skylaris***

submitted for the degree

of Doctor of Philosophy

Hughes Hall

Cambridge

July 1999

Στους Γονείς μου

Acknowledgements

I am grateful to my supervisor Professor Nicholas C. Handy F.R.S. and Dr Andrew Willetts for their enthusiastic support and wise advice throughout my research in Cambridge. They have been a constant source of inspiration and motivation for learning. The interaction with Dr Laura Gagliardi, Dr Andrew G. Ioannou, Dr Adrian M. Simper and Dr Steven Spencer has been a valuable and rewarding experience. I would like to thank Dr Roger D. Amos for his constructive suggestions. The friendly and scientifically fruitful atmosphere created by all the other members of the Theoretical Sector of the University's Chemistry Department is a memory I will treasure. Last but not least, I would like to thank BNFL and EPSRC for their deep interest in my research and for providing the funding.

Declaration of originality

This thesis describes research carried out in the Department of Chemistry at the University of Cambridge between April 1996 and July 1999. The contents are my original work except where otherwise indicated. This thesis is the result of my own work and includes nothing which is the outcome of work done in collaboration. I further state that this thesis is not substantially the same as any that I have submitted for a degree or diploma or other qualification at any other University nor is any part of it being concurrently submitted for any such degree, diploma or other qualification.

Abstract

The Kohn-Sham formalism for Density Functional Theory (DFT) is a remarkable tool which in principle can solve exactly Schrödinger's equation at the computational cost of the independent particle model. The recognition of this great potential led to the development of MAGIC, a modern, extensible computer program intended for calculations on industrially relevant heavy atom molecules. This thesis describes the author's contribution to MAGIC. The implementation of the overlap, kinetic and nuclear attraction integrals is presented. Also, a new method for the calculation of Effective Core Potential integrals, conceptually simpler than previous methods, is described. A broad range of test results demonstrate the efficiency and verify the correctness of the implementation. The auxiliary basis fitted density Coulomb energy approximation is a key feature of MAGIC that reduces computation time by an order of magnitude compared to conventional methods. Extensive tests of current auxiliary basis sets are performed and criteria are developed for controlling the resulting error. The evaluation of the two-electron integrals is performed with the reduced multiplication scheme of the Rys quadrature. Two-electron integrals account for the bulk of the computational effort of a direct SCF calculation and therefore the careful optimisation of the relevant computer code is of paramount importance. Efficiency is enhanced considerably by estimating the magnitude of two-electron integrals and rejecting them when they are negligible. Convergence of DFT calculations is assisted with various techniques. Emphasis is placed on Density Matrix Search (DMS) methods as a means of improving the initial approximation to the density and a novel DMS method based on more rigorous theoretical background is developed. Geometry optimisations, achieved by an analytic gradient and

the BFGS algorithm, are checked by tests. Finally applications to large inorganic systems with the current version of MAGIC, allow for an interpretation of chemistry from a different point of view to experiment and show the strengths, weaknesses and potential of this theoretical approach.

Contents

Chapter 1

Introduction

1.1 Chemistry from a theoretical point of view

Chemistry has a long history and is usually thought to be both an art and a science. This is due to the great difficulties encountered in describing the nature of matter whose behaviour at the microscopic level is governed by laws not directly linked to our experience in the macroscopic world. Thus, chemical reactions and properties have been rationalised mainly from the empirical point of view. An enormous number of man-hours of research into observing reactions has led to the classification of molecules according to their composition, reactivity, size, etc. Rules and predictions have been derived from this classification. However, due to their empirical nature, they only apply broadly and the final test is always experiment. Although this flexibility represents some of the pleasure of being a chemist, there is nevertheless something undesirable in this empirical approach to chemistry compared to the precision of other sciences. For example, a chemist will usually try several different synthetic paths for the preparation of a molecule. On the other hand, much of physics is constructed on a firm mathematical basis. Physical laws are supposed to allow for the exact description of nature; where they fail, they have to be revised to do so. There are no clear borders between the sciences and some of the laws of physics have been introduced indirectly to the study of chemistry, in the form of spectroscopic techniques that have become an indispensable tool for

the characterisation of molecules. However the direct description of chemistry by mathematics and physical laws is not as straightforward. The quote by A. Compte (1838) : "Every attempt to employ mathematical methods in the study of chemical questions must be considered profoundly irrational. If mathematical analysis should ever hold a prominent place in chemistry - an aberration which is highly impossible - it would occasion a rapid and widespread degradation of that science" represents the view of a significant number of chemists even today.

We possess no direct insight into the constituents of matter and their behaviour. As a consequence, efforts to explain matter have progressed very slowly. The concept of the atom that the philosopher Demokritos suggested in the fourth century B.C. was only extensively re-examined and confirmed experimentally in the 19th century. Progress from this point onwards however accelerated and in 1925 the wave equation

$$\hat{H}\Psi = E\Psi \tag{1.1}$$

discovered by Erwin Schrödinger formed the basis for the mechanics of microscopic particles, or *Quantum Mechanics*. Quantum mechanics developed into a major branch of physics and in the late 1920's the theory had already matured to a significant extent. The mathematical equations with the potential to describe exactly essentially everything that can be known about the behaviour of atoms and molecules, as manifested in chemical reactions, existed. The often quoted comment "The underlying physical laws necessary for the mathematical theory of ... the whole of chemistry are thus completely known, and the difficulty is only that the exact application of these laws leads to equations much too complicated to be soluble" by Paul A. M. Dirac in 1929 provides a good summary of the situation. An alternative interpretation of this comment may be that our point of view of nature is not always the most convenient.

The apparently insurmountable difficulties in the application of quantum mechanics into the chemical properties of matter did not deter research but strengthened it. Since the theory was known, research was focused on developments of methodologies and approximations that would allow the extraction of useful information from the virtually insoluble equations of quantum mechanics. This research

produced many concepts that provided chemists for the first time with at least a qualitative picture of the nature of the chemical bond and reactivity. The molecular orbitals, the hybridization theory and the Hückel molecular orbital theory are amongst numerous concepts developed during this era that found appreciable application in chemistry. *Quantum chemistry*, or the application of quantum mechanics to solve chemical problems, was established. A major breakthrough occured in the 1970's as computers became widely available. The power to perform an enormous number of arithmetic operations in a very short period of time opened new horizons. The approximations became more rigorous and approached more closely to the solution of Schrödinger's equation, through breaking down the solution process into many small steps. The GAUSSIAN 70 program [1] of Pople was the first tool of computational chemistry to become available. It was a general, robust program able to perform calculations on molecules defined by the user.

Nowadays, quantum chemistry, or electronic structure theory has come a long way and has reached a state of maturity. A variety of methods exist, ranging from the Hartree-Fock (HF), or independent particle approximation to Full Configuration Interaction (CI) that is essentially the exact solution of Schrödinger's equation. Hartree-Fock theory is rather poor in terms of accuracy, but is computationally very cheap and can be applied to large molecules. Full CI on the other hand includes the whole of the correlation energy (everything that's missing from non-relativistic Hartree-Fock) but is extremely expensive and can be applied to molecules of 10 electrons or less. Intermediate situations to these two extremes exist. Some of them, in increasing level of sophistication, are: Møller-Plesset perturbation theory (MP), CI, Multi-Configuration Self Consistent Field (MCSCF), Multi-Reference CI (MRCI), Complete Active Space second order Perturbation Theory (CASPT2) and Coupled Cluster (CC) [2, 3, 4].

Maybe the ultimate goal of computational chemistry is to be able to predict the properties of any molecule and furthermore to furnish the optimum synthetic route for it. This objective is still far from current capabilities and it is likely that it will continue to be so in the future. However, it is believed that computational chemistry can provide significant assistance to improving the efficiency of applied

chemistry.

1.2 The MAGIC project

Heavy atom chemistry is a challenging topic, often of interest to the nuclear industry, and computational chemistry may have a lot to offer. Here the motivation and general planning behind such a use of computational chemistry are presented.

1.2.1 The nuclear fuel cycle

The use of nuclear fission for the generation of energy presently accounts for 25-30% of the World's energy supply[5]. This creates a problem however in what to do with the spent nuclear fuel. One solution is simply to dispose of it. A more elegant and environmentally aware solution however is to reprocess it to extract materials of use. This will clearly involve recovery of any uranium-235, which forms the basis of the fission process itself. It will also include extraction of plutonium, which is formed in the reactor from uranium-238.

There are a number of advantages to recycling in this way. As the uranium-235 content of naturally occurring uranium ore is very low, the fuel is enriched before being used. This keeps the size of reactors down and means that the fuel has to be changed less often. However, such enrichment, typically by diffusion or centrifuge, is expensive. In the spent fuel the uranium-235 content is typically higher than in nature and so less enrichment is necessary. Hence the cost of producing fresh fuel is reduced. Another advantage is in the conservation of resources, a topic of ever growing importance. This may also be extended to the use of ex-military material, where the alternative is simply a difficult disposal procedure. Finally, one easy way of restricting access to plutonium is to store it in a mixed fuel; it is a straightforward procedure to generate such a mixed fuel within the reprocessing cycle.

Spent nuclear fuel consists of actinide elements and their fission products. The first step in reprocessing is therefore to separate uranium and plutonium from the fission products. This involves a liquid separation between aqueous and organic phases. The spent nuclear fuel is first dissolved in nitric acid. Any insoluble ma-

terial can be filtered at this stage. The rest is passed through a mixture of an organic solvent, typically tri-n-butylphosphate in odourless kerosene (TBP/OK), and water. The important uranyl and plutonyl nitrates are coordinated by TBP and are extracted in the organic phase. Most of the other nitrates simply dissolve in the water and are extracted in the aqueous phase. In this way the uranium and plutonium may be separated, together with some contaminants. The next stage is to separate the uranium from the plutonium. This may be achieved by changing the oxidation state of the plutonium. For example, U(IV) in hydrazine reduces the extractable Pu(IV) complex to the practically inextractable Pu(III) complex.

Once the uranyl nitrate has been separated, it is heated to produce uranium trioxide, which may be subsequently reduced to give uranium dioxide. It is this which provides the basic fuel for the reactor. Before use however it needs to be enriched. For this reason it is converted to uranium hexafluoride; this is a convenient choice because it is gaseous under the conditions of the diffusion experiment and fluorine has only one isotope. It is subsequently converted to uranium metal or back to uranium dioxide for use in the reactor. The plutonyl nitrate may also be heated to produce plutonium dioxide but because of the presence of impurities conversion to plutonium oxalate and heating to give the dioxide is more typical.

The metal nitrates, which were extracted in the aqueous phase, must now be disposed of. These are classified as high-level waste. They are denitrated and vitrified ready for long term storage. Material from the recycling process, for example cladding materials from the fuel rods, is classified as intermediate-level waste and is encapsulated in cement. Other low-level waste is simply buried in vaults.

It is clear that a good understanding of the chemistry of these systems can be used in a number of areas. For example, in the area of liquid separation a number of criteria need to be satisfied for a good extractant. These include: a high distribution ratio for uranyl and plutonyl nitrates, which is sensitive to the acidity; a different affinity for different actinide elements, in particular uranium and plutonium; negligible affinity for the fission products; stability towards chemical and radiolytic breakdown; low toxicity, with harmless degradation products which are simple to dispose of.

It would be interesting to explore if quantum chemistry can be used to model some of the molecules; in particular the change in their energetic properties in different environments can now be studied. In combination with experiment, such understanding may lead to the use of improved extraction methods. The potential saving involved, due to the need for less experimental work, is considerable. Hence it may be possible to extract uranium and plutonium more efficiently or, for example, to extract other actinide elements effectively. A further example might be to look for an extractant for the heat-releasing elements (Cs and Sr) which cause problems later in waste storage, or for technetium which affects the efficiency of the uranium/plutonium separation.

A second area in which theoretical chemistry could be used is in describing the final waste storage procedure. It is important to engineer properties of the glasses in which the high-level waste is vitrified. For example, they must incorporate the maximum amount of waste material. They should be sufficiently reactive, so that they incorporate the waste, but also durable so that they do not need to be maintained over long periods of time. With a good theoretical model, such properties may be predicted, as well as the likely effects of waste incorporation on the glass structure. Similarly, in the case of intermediate-level waste, the cement properties such as chemical stability and leach behaviour may be predicted. Quantum chemistry may provide parameters for a more reasonable model of the system, or in some cases it may even provide the model.

1.2.2 MAGIC: the software

So far our discussion established an outline of the types of applications to be studied. The next logical step is to decide how to perform these calculations. Many quantum chemistry programs are currently available that in principle could perform calculations on such molecular systems. They were meant however for very accurate calculations on small molecules and in any case they contain a plethora of methods that simply cannot by applied due to the size of the systems of study. Another drawback is that most available programs have been developing constantly over the last 20 years and now they contain an enormous amount of code that is dif-

ficult to understand or amend. For the same reason the programming conventions used in many existing programs do not take into account recent computer science developments that increase flexibility and functionality.

Therefore the development from the beginning of a program specifically for calculations on large molecules containing heavy atoms is necessary. Such a choice also allows one to address effectively the problems of the robustness of the program. This refers not only to how the program executes but also, for example, in the ease with which it may be moved between different computer platforms. The program developed for this purpose is called *MAGIC*.

The choice of the scientific model was based on consideration of both the complex molecular systems to be examined and the properties that can be predicted reasonably well. It is clear that this should be a relativistic model. A full Dirac-Fock 4-component analysis is rejected due to the size and complexity of the systems. A 2-component analysis is therefore favoured, although it is not clear which of the Douglas-Kroll (DK) [6] or Chang-Pellissier-Durand (CPD) [7] treatments is more reliable. Both of these were therefore included in MAGIC. They will not be discussed however further in this thesis apart from mentioning that they are expensive compared to the use of relativistic effective core potentials, which form the basis of the model. The implementation of the DK and CPD methods was carried out by Dr Adrian M. Simper with contributions by Dr Laura Gagliardi.

As most of chemistry takes place in the liquid phase, solvent modelling is important. The simplest approach is to use a cavity model [8] where the liquid is represented by a bulk continuum with a fixed dielectric constant. A multipole expansion of the solute density is performed and it is through this that the effect of the interaction with the solvent is introduced to the model. The modelling of solvent effects will not be discussed further here except for mentioning that it is likely that the most severe approximation lies in not allowing specific interaction between the solvent molecules and the solute. One way to overcome this is to perform a calculation on a small collection of solute and solvent molecules using the quantum mechanical model. This soon becomes too expensive and one has to consider the use of mixed quantum mechanical/molecular mechanical [9] models. The

implementation of solvent effects was carried out by Dr Steven Spencer.

The choice of a quantum mechanical method is crucial to the predictive success of the entire model. The inclusion of electron correlation in the model is important. The high-level correlated techniques, such as CI [10] or CC [11], are however too expensive when applied to such large systems. Also, although they may be conceptually straightforward, their implementation is often much less so. Density functional theory (DFT), which is outlined in section 1.3, includes correlation at an affordable computational cost and is therefore the obvious choice.

Every effort has been made during the development of MAGIC to keep the structure of its code as simple and short as possible. Typically, most subroutines have a length of the order of 50 lines. Variable names are long and descriptive, according to conventions set by the developers, and comments are included in places where ambiguity might arise. Where possible, external mathematical library routines are used. A modular format ensures functionality and ease to develop and debug code. This means that every distinct part of a calculation is a different module. Modules are combined together in scripts in order to form the stages of various types of calculations. Data are passed between the modules with a special binary disk storage facility called *archive*. The archive is also used to store the results of a calculation, such as the density, orbitals, etc. for subsequent access and processing by tools, i.e. modules that process the results of a calculation. The archive as well as some other computer science related features are written in C while the subroutines for the scientific tasks are written in FORTRAN. It is important that MAGIC should be straightforward to run. This is addressed by the use of the Cerius^2 [12] visualisation software, to which MAGIC has been interfaced, even though it can be run without it. Overall it is intended that maximum development effort should be directed into improvement of the scientific model and minimum effort in trying to understand the existing computer science.

1.3 Density Functional Theory

1.3.1 Density as the basic variable

Quantum mechanics is built around the wavefunction Ψ (equation (1.1)) which is a complex function of many variables. It is an *ab initio* theory which means that no quantity is taken for granted apart from the fundamental physical constants. On the other hand the accurate description of the wavefunction is a tremendously difficult task. An alternative approach is based on the first-order diagonal one-electron *spinless density matrix* to which we will refer from now on as the "density"

$$\rho(\mathbf{r}) = [\rho_1(\mathbf{r}', \mathbf{r})]_{\mathbf{r}'=\mathbf{r}} \tag{1.2}$$

with

$$\rho_1(\mathbf{r}_1', \mathbf{r}_1) = N \int \cdots \int \Psi(\mathbf{r}_1' s_1, \mathbf{x}_2, \ldots, \mathbf{x}_N) \Psi^*(\mathbf{r}_1 s_1, \mathbf{x}_2, \ldots, \mathbf{x}_N) ds_1 d\mathbf{x}_2 \ldots d\mathbf{x}_N$$

where N is the number of particles, s_1 is a spin coordinate, $\mathbf{r}_1$ is a space coordinate and $\mathbf{x}_2$ is a space and spin coordinate. The rigorous justification for the transition from the wavefunction to the density was provided in 1964 by Hohenberg and Kohn[1] [14]. Their first theorem states that given a mathematical form for the Hamiltonian operator $\hat{H}$ of a system there is a one-to-one correspondence between the ground state density ρ_{GS} and the external potential $v(\mathbf{r})$ and the number of electrons N. Therefore the density ρ_{GS} provides $v(\mathbf{r})$ and N that determine the Hamiltonian, which in turn is able to provide all the information we can know about the system through the wavefunction. The proof of this fundamental statement which constitutes the first Hohenberg and Kohn theorem is based on the logic of *reductio ad absurdum* and is very simple.

Theorem 1.1 *Suppose that there are two external potentials v and v' differing in more than an additive constant, corresponding to two different systems. Further-*

[1]The Density functional formalism was originaly developed in the space of v-representable densities, i.e. those due to some external potential $v(\mathbf{r})$. One can work just as well in the space of N-representable densities which is the space of densities derived from an antisymmetric wavefunction Ψ for N fermions (electrons in our case) [13]. The space of N-representable densities is a superspace of the v-representable densities.

more suppose that each of the two potentials produces the same density ρ_{GS} for the ground state of its system, through their Hamiltonian operators $\hat{H}$ and $\hat{H}'$ respectively. If the ground state energies for the two external potentials are E_{GS} and E'_{GS} respectively, the variational principle leads to the following two relations

$$\begin{aligned} E_{GS} < \langle \Psi'_{GS}|\hat{H}|\Psi'_{GS}\rangle &= \langle \Psi'_{GS}|\hat{H}'|\Psi'_{GS}\rangle + \langle \Psi'_{GS}|\hat{H}-\hat{H}'|\Psi'_{GS}\rangle \\ &= E'_{GS} + \int \rho_{GS}(\mathbf{r})[v(\mathbf{r}) - v'(\mathbf{r})]d\mathbf{r} \qquad (1.3) \\ E'_{GS} < \langle \Psi_{GS}|\hat{H}'|\Psi_{GS}\rangle &= \langle \Psi_{GS}|\hat{H}|\Psi_{GS}\rangle + \langle \Psi_{GS}|\hat{H}'-\hat{H}|\Psi_{GS}\rangle \\ &= E_{GS} - \int \rho_{GS}(\mathbf{r})[v(\mathbf{r}) - v'(\mathbf{r})]d\mathbf{r} \qquad (1.4) \end{aligned}$$

and by adding them together we obtain

$$E_{GS} + E'_{GS} < E'_{GS} + E_{GS} \qquad (1.5)$$

which is clearly wrong and therefore the external potential defines uniquely the ground state density.

As a consequence, it must be possible to express the ground state energy as a functional of the ground state density.

$$E_{GS} = E_v[\rho_{GS}] = \int \rho_{GS}(\mathbf{r})v(\mathbf{r})d\mathbf{r} + F_{HK}[\rho_{GS}] \equiv \langle \Psi_{GS}|\hat{H}|\Psi_{GS}\rangle \qquad (1.6)$$

This statement leads naturally to a variational principle which is the second Hohenberg and Kohn theorem.

Theorem 1.2 *According to the first Hohenberg and Kohn theorem any trial density ρ_t defines an external potential $v_t(\mathbf{r})$ which in turn defines a Hamiltonian operator $\hat{H}_t$ with wavefunction Ψ_t. This sequence allows us to write down the variational principle for wavefunctions in terms of densities*

$$\langle \Psi_t|\hat{H}|\Psi_t\rangle = \int \rho_t(\mathbf{r})v(\mathbf{r})d\mathbf{r} + F_{HK}[\rho_t] = E_v[\rho_t] \geq E_v[\rho_{GS}] \qquad (1.7)$$

where $v(\mathbf{r})$ and $\hat{H}$ are the external potential and Hamiltonian of the system with ground state density ρ_{GS}. Therefore the ground state density ρ_{GS} minimises $E_v[\rho]$.

1.3.2 The Kohn-Sham equations

The Kohn-Sham (KS) formulation of Density Functional Theory (DFT) [15, 16] is a further development that casts DFT in the form of single particle equations. It is in principle an *exact* single-particle description of a many particle system. For this unique feature, and its accompanying simplicity, it is widely used.

In quantum mechanics the expectation value $\langle O \rangle$ of the observable O, represented by the operator $\hat{O}$, is given by the integral

$$\langle O \rangle = \langle \Psi \mid \hat{O} \mid \Psi \rangle \tag{1.8}$$

where the wavefunction Ψ is assumed to be normalized. Density functional theory, based on the first Hohenberg and Kohn theorem, replaces the operator $\hat{O}$ by a functional F_O which produces the expectation value $\langle O \rangle$ when the density ρ is its argument

$$\langle O \rangle = F_O[\rho] \tag{1.9}$$

The task of DFT formalisms then is to find accurate forms for the functionals which yield the observables and also ways of calculating the electronic density accurately.

The starting point is the ground state energy of a closed-shell system which is represented by the following functional form:

$$E_v[\rho_{GS}] = E_T[\rho_{GS}] + \int \rho_{GS}(\mathbf{r}) v(\mathbf{r}) d\mathbf{r} + E_J[\rho_{GS}] + E_{xc}[\rho_{GS}] + U_{NN} \tag{1.10}$$

where the energy has been written as a sum of terms which are familiar to us from wavefunction quantum mechanics. We recognise $E_T[\rho_{GS}]$ as the kinetic energy, and

$$E_J[\rho_{GS}] = \frac{1}{2} \int \int \frac{\rho_{GS}(\mathbf{r}) \rho_{GS}(\mathbf{r}')}{\mid \mathbf{r} - \mathbf{r}' \mid} dr dr' \tag{1.11}$$

$$E_{xc}[\rho_{GS}] = \int F(\rho_{GS}, \nabla \rho_{GS}, \ldots) dr \tag{1.12}$$

are the Coulomb energy (classically interpreted as charge distribution self-interaction energy) and the exchange and correlation energy respectively. The second term in equation (1.10) is the nuclear attraction energy and the fifth term is the internuclear repulsion energy (a constant under the Born-Oppenheimer approximation).

Kohn-Sham theory postulates the existence of a *noninteracting reference system* whose density is equal to that of the system under study. The purpose of the non-interacting reference system is to provide a unique (up to a unitary transformation) decomposition of the density ρ_{GS} in terms of orbitals.

$$\rho_{GS}(\mathbf{r}) = 2\sum_{i=1}^{N/2} \mid \psi_i(\mathbf{r}) \mid^2 \tag{1.13}$$

Here it is assumed that there is an even number of particles. The theory applies equally well if N is odd with only a trivial extension along the lines of unrestricted Hartree-Fock theory. The kinetic energy functional is redefined as

$$E_T[\rho_{GS}] = 2\sum_{i=1}^{N/2} \langle \psi_i \mid -\frac{1}{2}\nabla^2 \mid \psi_i \rangle \tag{1.14}$$

which is the *exact* kinetic energy of the noninteracting reference system (with ψ_i being the occupied orbitals of the reference system) but not of the real system.

Looking back to equation 1.10, and provided that the density ρ_{GS} is exact, we can observe that $E_J[\rho_{GS}]$ is exact for the real system (the reference system does not have Coulomb energy due to the lack of interelectronic interactions), $\int \rho_{GS}(\mathbf{r})v(\mathbf{r})dr$ is exact only for the real system and $E_T[\rho_{GS}]$ is exact only for the reference system.

$E_v[\rho_{GS}]$ is the total electronic and nuclear energy of the real system, and since we have changed the definition of its $E_T[\rho_{GS}]$ component, we must redefine $E_{xc}[\rho_{GS}]$ as a functional which yields the correction to the kinetic energy for the real system, the correction due to self-interaction in the Coulomb energy $E_J[\rho_{GS}]$ and the exchange and correlation energy for the real system. The difficulty now is that the explicit form of $E_{xc}[\rho_{GS}]$ is unknown and approximations, often semiempirical in nature, have to be used.

According to the second Hohenberg-Kohn theorem the correct ground state density ρ_{GS} for the system minimises the energy $E_v[\rho]$. Finding the density ρ_{GS} then involves the minimisation of the energy subject to the constraint that the number of electrons N remains constant. This leads to the folowing Euler equation with the Lagrange mutliplier μ

$$\mu = v_{eff}(\mathbf{r}) + \frac{\delta E_T[\rho]}{\delta\rho(\mathbf{r})} \tag{1.15}$$

where the effective KS potential $v_{eff}(\mathbf{r})$ is defined by

$$\begin{aligned} v_{eff}(\mathbf{r}) &= v(\mathbf{r}) + \frac{\delta E_J[\rho]}{\delta \rho(\mathbf{r})} + \frac{\delta E_{xc}[\rho]}{\delta \rho(\mathbf{r})} \\ &= v(\mathbf{r}) + \int \frac{\rho(\mathbf{r}')}{\mid \mathbf{r} - \mathbf{r}' \mid} d\mathbf{r}' + v_{xc}(\mathbf{r}) \end{aligned} \tag{1.16}$$

and $v_{xc}(\mathbf{r})$ is called the *exchange-correlation potential.*

We have assumed that the density of the real system can be expressed as the sum of squares of $N/2$ orbitals. The determination of these orbitals ψ_i requires the minimisation of the energy functional of equation (1.10) with respect to the orbitals, subject to orthonormality constraints. This leads to the following single-particle equations

$$\left[-\frac{1}{2}\nabla^2 + v_{eff}(\mathbf{r}) \right] \psi_i = \epsilon_i \psi_i \tag{1.17}$$

where $v_{eff}(\mathbf{r})$ plays the role of an external potential. Therefore the Hamiltonian of the non-interacting reference system is

$$\hat{H}_{eff} = \sum_{i=1}^{N} \left\{ -\frac{1}{2}\nabla_i^2 + v_{eff}(\mathbf{r}_i) \right\} \tag{1.18}$$

and its *exact wavefunction* is a Slater determinant of the orbitals ψ_i. These $N/2$ orbitals will afford the ground state density ρ_{GS} which minimises $E_v[\rho]$.

In practice the orbitals corresponding to the $N/2$ lowest eigenvalues ϵ_i of the noninteracting reference system are chosen. From equations (1.17) and (1.16) it can be seen that a set of complicated, non-linear equations needs to be solved to determine the orbitals. This is done by an iterative scheme that is designed to find a self-consistent solution.

Kohn-Sham DFT calculations on collections of molecules are feasible. An important extension by Car and Parrinello [17, 18] combines density functional theory with classical molecular dynamics and makes possible the calculation of molecular properties at finite temperatures.

1.4 Gaussian basis functions

In calculations on polyatomic molecules, the Kohn-Sham orbitals are expressed as linear combinations from a set of basis functions. Gaussian basis functions have

been used almost exclusively for this purpose since they were first introduced into quantum chemistry by S. F. Boys in 1950 [19] and MAGIC is no exception to this rule.

A primitive Cartesian Gaussian function centred at point $\mathbf{A}$, is represented by the following formula:

$$\begin{aligned} g_{A_i}(\mathbf{r};\alpha_i,a_x,a_y,a_z,\mathbf{A}) &= (x-A_x)^{a_x}(y-A_y)^{a_y}(z-A_z)^{a_z} \\ &\times \exp(-\alpha_i \mid \mathbf{r}-\mathbf{A} \mid^2) \end{aligned} \tag{1.19}$$

We define $\lambda = a_x + a_y + a_z$ and we call it the angular momentum number of the Gaussian function, in analogy with the nomenclature of the orbital functions of atoms. Gaussians belonging to the same angular momentum constitute a shell and, carrying the analogy with atomic functions further, we name the shells by the letters $s, p, d, \ldots$ when λ is equal to $0, 1, 2, \ldots$ respectively.

The normalisation constant for this function is

$$n_{A_i} = \sqrt{\frac{(8\alpha_i)^\lambda a_x! a_y! a_z!}{(2a_x)!(2a_y)!(2a_z)!}} \left(\frac{2\alpha_i}{\pi}\right)^{\frac{3}{4}} \tag{1.20}$$

A contracted Gaussian function with K_A being its *degree of contraction* is defined by

$$\begin{aligned} G_A(\mathbf{r};a_x,a_y,a_z,\mathbf{A}) &= \sum_{i=1}^{K_A} c_i\, n_{A_i}\, g_{A_i}(\mathbf{r};\alpha_i,a_x,a_y,a_z,\mathbf{A}) \\ &= (x-A_x)^{a_x}(y-A_y)^{a_y}(z-A_z)^{a_z} \\ &\times \sum_{i=1}^{K_A} c_i\, n_{A_i} \exp(-\alpha_i \mid \mathbf{r}-\mathbf{A} \mid^2) \end{aligned} \tag{1.21}$$

As can be seen from the above equation, the contracted Gaussian is a linear combination of normalised primitive Gaussians, centred at the same point and of the same angular momentum. The purpose of the contraction is to alter the radial part of the Gaussian functions in order to make it more suitable for our calculations. Usually the exponents and contraction coefficients are selected so as to make the contracted functions resemble atomic orbitals. Over the years a huge number of contracted Gaussian basis sets have been developed to cover the needs of different computational approaches [20]. It turns out that the normalisation constant for the

contracted Gaussian does not depend on the kind of angular momentum component of the contracted Gaussian. It is given by the following expression

$$N_A = \frac{1}{2^{\frac{\lambda}{2}+\frac{3}{4}}} \frac{1}{\left(\sum_{j,k=1}^{K_A} c_j c_k \frac{(\alpha_j \alpha_k)^{\frac{\lambda}{2}+\frac{3}{4}}}{(\alpha_j+\alpha_k)^{\lambda+\frac{3}{2}}} \right)^{\frac{1}{2}}} \tag{1.22}$$

The normalisation of each primitive cartesian Gaussian g_{A_i} participating in a contraction is the product of n_{Ai} and N_A of equations (1.20) and (1.22). For practical purposes that will become clearer later, we rearrange the terms between the two normalisation constants to create two new normalisations

$$n'_{A_i} = (8\alpha_i)^{\frac{\lambda}{2}} \left(\frac{2\alpha_i}{\pi} \right)^{\frac{3}{4}} \tag{1.23}$$

and

$$N'_A = N_A \left(\frac{a_x! a_y! a_z!}{(2a_x)!(2a_y)!(2a_z)!} \right)^{\frac{1}{2}} \tag{1.24}$$

The benefit of using this normalisation scheme is that we can use the same value of n'_{A_i} to normalise with it all components of a shell (it does not depend on a_x, a_y, a_z). Then contraction follows and a normalisation of contracted functions with N'_A, whose value differs for each component of G_A.

A further advantage of primitive Cartesian Gaussian functions is that their derivative with respect to the coordinates of their centre is simply a sum of two other primitive Cartesian Gaussian functions centred on the same centre. For example, the derivative of g_{A_i} from equation (1.19), with respect to A_x is

$$\frac{\partial g_{A_i}(\mathbf{r}; \alpha_i, a_x, a_y, a_z, \mathbf{A})}{\partial A_x} =$$
$$2\alpha_i g_{A_i}(\mathbf{r}; \alpha_i, a_x+1, a_y, a_z, \mathbf{A}) - a_x g_{A_i}(\mathbf{r}; \alpha_i, a_x-1, a_y, a_z, \mathbf{A}) \tag{1.25}$$

with analogous formulae for differentiation with respect to A_y and A_z.

1.5 Quadrature for exchange-correlation potential matrix elements

The solution of the Kohn-Sham equations requires the calculation of the Kohn-Sham matrix, which, in a fashion similar to the Fock matrix in Hartree-Fock theory, is

the sum of the matrix elements of operators. The matrix elements of the exchange-correlation potential are needed for this purpose.

$$\langle G_A | v_{xc} | G_B \rangle \tag{1.26}$$

The analytical computation of these elements is not feasible due to the complicated form of the functionals in use. Therefore, a lot of effort has been made by researchers in the construction of efficient quadrature schemes for numerical evaluation of these integrals. Here, the quadrature scheme used in MAGIC and the parameters it involves, are discussed briefly.

The integration grid is a combination of octahedrally symmetric distributions of points centred at the coordinates of every atom. Let us examine one of these octahedral, atomic grids of which the molecular quadrature grid is made. Concentric spheres of points are used around an atom.

1.5.1 Atomic quadrature grid

Radial quadrature

The Log3 quadrature scheme of Mura and Knowles [21] that is optimised for integration of Gaussian functions is used to generate the radial distribution of points and weights w_r. The Log3 scheme is described in some detail in subsection 2.8.3. Atoms are divided into six groups depending on their atomic number.

Group	Atomic number
1	1-2
2	3-10
3	11-18
4	19-36
5	37-54
6	55-104

The number of radial points for each atom is given by

$$n_r = 20 + 5(\text{Group} + \text{LOG3} - 2) \tag{1.27}$$

where the parameter LOG3 is defined by the user. The default value of LOG3 is 2.

Angular quadrature

The angular distribution of points on each sphere is provided by the octahedral symmetry angular quadrature grids of Lebedev [22, 23, 24, 25]. Lebedev has found that several groups of angular quadrature schemes with octahedral symmetry are possible. In practice, for the atomic quadrature grids only one group is necessary and a choice was made based on the theoretical efficiency of the grids that Lebedev reports. The chosen angular quadrature grids are able to integrate exactly spherical polynomials (spherical harmonics) up to degree L given by the following formula

$$L = 12 \times \text{LEBEDEV} + 5 \tag{1.28}$$

where the paramerer LEBEDEV is specified by the user. It can take the values 1, 2, 3 or 4 and its default value is 2. The number of points n_a of the angular grid is given by the formula.

$$n_a = \frac{1}{3}(L^2 + 2L + 7) \tag{1.29}$$

For LEBEDEV equal to 1,2,3 and 4 grids are generated with 110, 302, 590 and 974 points respectively. The Cartesian coordinates of the points on the surface of the unit sphere and the corresponding weights are generated by the implementation using the grid parameters provided by Lebedev.

1.5.2 Molecular quadrature grid

The atomic quadrature grids are combined together with an adaptation of the multi-centre numerical integration scheme of Becke [26]. A relative weight function $w_A(\mathbf{r})$ is assigned to each nucleus. The relative weight functions satisfy the requirement

$$\sum_{A=1}^{N_{AT}} w_A(\mathbf{r}) = 1 \tag{1.30}$$

where N_{AT} is the number of atoms. Now, if $F(\mathbf{r})$ is the integrand of the exchange-correlation matrix element, it can be partitioned into a sum of atom-localised integrands $F_A(\mathbf{r}) = w_A(\mathbf{r})F(\mathbf{r})$ since

$$F(\mathbf{r}) = \sum_{A=1}^{N_{AT}} F_A(\mathbf{r}) \tag{1.31}$$

and the molecular integral can be split accordingly into a sum of atomic integrations. The optimum weight function $w_A(\mathbf{r})$ should approach 1 close to the Ath atom and 0 away from it in order to use efficiently the atomic quadrature grids of subsection 1.5.1 to evaluate the integral. For this purpose, the confocal elliptic coordinate μ_{AB} is introduced for every distinct pair of atoms A and B

$$\mu_{AB} = \frac{r_A - r_B}{|\mathbf{A} - \mathbf{B}|} \tag{1.32}$$

where r_A and r_B is the distance of point $\mathbf{r}$ from A and B respectively. The elliptic coordinates will provide a natural way of partitioning the area surrounding each atom. A further adjustment is made in order to take into account the different sizes of the atoms by defining a new coordinate ν_{AB}

$$\nu_{AB} = \mu_{AB} + a_{AB}(1 - \mu_{AB}^2) \tag{1.33}$$

with

$$a_{AB} = \frac{\frac{\chi_{AB}-1}{\chi_{AB}+1}}{\left(\frac{\chi_{AB}-1}{\chi_{AB}+1}\right)^2 - 1} \quad \text{and} \quad \chi_{AB} = \frac{R_A}{R_B} \tag{1.34}$$

where R_A and R_B are defined as the radii of the atoms. In the implementation the radii are defined as half the distance of closest approach in the elemental structure [27]. With the coordinate ν_{AB} the boundary between atoms A and B no longer lies at the midpoint of the line joining them. A "cutoff profile" function $s(\nu_{AB})$ is now defined, according to the definition by Handy et. al. [28, 29]

$$\frac{ds}{d\nu_{AB}} = C(1 - \nu_{AB}^2)^{10} \tag{1.35}$$

This function satisfies the requirements $s(-1) = 1$, $s(1) = 0$ and a number of its first derivatives at $\nu_{AB} = -1$ and $\nu_{AB} = 1$ are zero. The cutoff profile is used to define "fuzzy Voronoi polyhedra" or cells for each atom through the following functions.

$$P_A(\mathbf{r}) = \prod_{B \neq A}^{N_{AT}} s(\nu_{AB}) \tag{1.36}$$

$P_A(\mathbf{r})$ has a value close to unity if $\mathbf{r}$ lies inside the cell of atom A and near zero outside the cell. Finally, the normalisation of the cell functions yields a formula for the weight functions.

$$w_A(\mathbf{r}) = \frac{P_A(\mathbf{r})}{\sum_{B=1}^{N_{AT}} P_B(\mathbf{r})} \tag{1.37}$$

In practice the points of the atomic quadrature grids are calculated in Cartesian coordinates and stored together in the archive. The corresponding weight of every point $\mathbf{r}_i$ is the product of its radial weight w_{ri}, its angular weight w_{ai} and its molecular weight w_{Ai} (if it comes from the atomic grid of atom A). The quadrature weights are also stored in the archive. In this form the molecular quadrature grid is accessed whenever a MAGIC module needs it.

Chapter 2

One electron Integrals

2.1 Interpolatory integration formula

We wish to evaluate exactly a definite integral of the function $f(t)\exp(-t^2)$ in the interval $(-\infty,\infty)$ by a sum of n terms [30]. The function $f(t)$ is a polynomial of degree $\leq n-1$. Each term in the sum will be a product of a coefficient (weight) A_k and the value of $f(t)$ evaluated at a point t_k

$$\int_{-\infty}^{\infty} f(t)\exp(-t^2)dt = \sum_{k=1}^{n} A_k f(t_k) \tag{2.1}$$

The points $\{t_k\}_{k=1}^{n}$ are chosen arbitrarily. The polynomial $f(t)$ can be expressed in terms of its values at those points according to [1]

$$f(t) = \sum_{k=1}^{n} \frac{\alpha(t)}{(t-t_k)\alpha'(t_k)} f(t_k) \tag{2.2}$$

where

$$\alpha(t) = \prod_{k=1}^{n}(t-t_k) \quad \text{and} \quad \alpha'(t_k) = \left.\frac{d\alpha(t)}{dt}\right|_{t=t_k} \tag{2.3}$$

The integral we wish to evaluate becomes

$$\int_{-\infty}^{\infty} f(t)\exp(-t^2)dt = \int_{-\infty}^{\infty} \sum_{k=1}^{n} f(t_k)\frac{\alpha(t)}{(t-t_k)\alpha'(t_k)}\exp(-t^2)dt$$

[1] The righthandside of eq 2.2 is an interpolating polynomial which takes the same values as $f(t)$ in the n points t_k. It is identical with $f(t)$ since both are of degree $n-1$ and take the same value at n points.

$$= \sum_{k=1}^{n} \left[\int_{-\infty}^{\infty} \frac{\alpha(t)}{(t-t_k)\alpha'(t_k)} \exp(-t^2) dt \right] f(t_k)$$

$$= \sum_{k=1}^{n} A_k \; f(t_k) \tag{2.4}$$

This proves that the integral of equation 2.1 can be evaluated *exactly* as a sum of n terms. Equation (2.4) serves also as a definition of a formula for the weights A_k. This result is called the *interpolatory integration formula* and it is characterised by the fact that any n distinct points $\{t_k\}_{k=1}^{n}$ can be used.

At this point it is useful to observe that if the interval of integration was not $(-\infty, +\infty)$ but $[a, b]$ where a, b are real numbers or infinity, the interpolatory integration formula would still be valid, even if some or all of the points t_k did not belong to $[a, b]$. Since we have total freedom to select the points t_k, it is worth investigating if there is some particular set of points which is preferable in the sense that it would allow for exact integration with $f(t)$ being a polynomial of degree higher than $n-1$.

2.2 Gaussian Quadrature

Let the points $\{t_k\}_{k=1}^{n}$ be the zeros of the nth degree Hermite polynomial $H_n(t)$. We will prove that for this choice of points, equation 2.1 is exact for $f(t)$ being a polynomial of degree $\leq 2n-1$.

Theorem 2.1 *Assume that equation 2.1 is exact for $f(t)$ being any polynomial of degree $\leq 2n-1$. Therefore it must be exact for $f(t) = \alpha(t)Q_1(t)$ where $\alpha(t)$ is defined in equation 2.3 and $Q_1(t)$ is any polynomial of degree $\leq n-1$. By substituting the expression for $f(t)$ into equation 2.1 we get*

$$\int_{-\infty}^{\infty} \alpha(t)Q_1(t) \exp(-t^2) dt = \sum_{k=1}^{n} A_k \alpha(t_k) Q_1(t_k) = 0 \quad \textit{because} \quad \alpha(t_k) = 0 \tag{2.5}$$

which shows that $\alpha(t)$ is orthogonal to all polynomials of degree $\leq n-1$.

The converse now, assume that $\alpha(t)$ is orthogonal to all polynomials of degree $\leq n-1$ (which means that it must be a multiple by a constant factor of the nth degree Hermite polynomial. This justifies our selection of the t_k's at the beginning

of this section). Let $f(t)$ be a polynomial of degree $\leq 2n-1$. Then $f(t)$ can be written as

$$f(t) = \alpha(t)Q_2(t) + \rho(t) \tag{2.6}$$

where $Q_2(t)$ and $\rho(t)$ are both polynomials of degree $\leq n-1$ and are the result and the remainder respectively of the division of $f(t)$ by $\alpha(t)$. Equation 2.1 becomes

$$\int_{-\infty}^{\infty} f(t)\exp(-t^2)dt = \int_{-\infty}^{\infty} \alpha(t)Q_2(t)\exp(-t^2)dt + \int_{-\infty}^{\infty} \rho(t)\exp(-t^2)dt \tag{2.7}$$

The first term on the right vanishes because of our postulated orthogonality. Then, because the degree of $\rho(t)$ is $\leq n-1$, the interpolatory formula of equation 2.1 is exact and using it yields

$$\int_{-\infty}^{\infty} f(t)\exp(-t^2)dt = \sum_{k=1}^{n} A_k\rho(t_k) \tag{2.8}$$

or, since $\alpha(t_k) = 0$, equation 2.6 gives $\rho(t_k) = f(t_k)$ which when substituted into equation 2.8 gives the final result

$$\int_{-\infty}^{\infty} f(t)\exp(-t^2)dt = \sum_{k=1}^{n} A_k f(t_k) \tag{2.9}$$

which is exact for $f(t)$ being any polynomial of degree $\leq 2n-1$.

2.3 Overlap integrals

The overlap integral plays the role of the metric in the matrix form of the SCF equations and appears in most expressions when a non-orthogonal basis set is used, as is the case with Gaussian basis sets. The calculation of these integrals is a very fast and simple process and many methods are available. We will derive the equations required to evaluate overlap integrals by Gaussian quadrature on which the current implementation is based. We want to evaluate the integral:

$$\langle g_A \mid g_B \rangle = \int g_A(\mathbf{r};\alpha,a_x,a_y,a_z,\mathbf{A})\, g_B(\mathbf{r};\beta,b_x,b_y,b_z,\mathbf{B})\, d\mathbf{r} \tag{2.10}$$

Now according to the product rule for Gaussian functions

$$\begin{aligned} & g_A(\mathbf{r};\alpha,a_x,a_y,a_z,\mathbf{A})\, g_B(\mathbf{r};\beta,b_x,b_y,b_z,\mathbf{B}) = \\ & k_{ab}(x-A_x)^{a_x}(x-B_x)^{b_x}(y-A_y)^{a_y}(y-B_y)^{b_y} \\ \times\ & (z-A_z)^{a_z}(z-B_z)^{b_z} g_L(\mathbf{r};\Lambda,0,0,0,\mathbf{L}) \end{aligned} \tag{2.11}$$

where $k_{ab} = k_{abx}k_{aby}k_{abz}$. The coordinate $\mathbf{L}$, the exponent Λ and the constant k_{abx} are defined by

$$L_x = \frac{\alpha A_x + \beta B_x}{\alpha + \beta}, \qquad \Lambda = \alpha + \beta \tag{2.12}$$

$$k_{abx} = \exp\left(-\frac{\alpha\beta}{\alpha+\beta}(A_x - B_x)^2\right) \tag{2.13}$$

with analogous expressions for the y and z coordinates. The overlap integral is therefore expanded as follows

$$\begin{aligned}
\langle g_A \mid g_B \rangle &= k_{ab} \int_{-\infty}^{\infty} (x - A_x)^{a_x} (x - B_x)^{b_x} \exp(-\Lambda(x - L_x)^2) dx \\
&\times \int_{-\infty}^{\infty} (y - A_y)^{a_y} (y - B_y)^{b_y} \exp(-\Lambda(y - L_y)^2) dy \\
&\times \int_{-\infty}^{\infty} (z - A_z)^{a_z} (z - B_z)^{b_z} \exp(-\Lambda(z - L_z)^2) dz \\
&= k_{ab} \langle a_x \overset{x}{\mid} b_x \rangle \langle a_y \overset{y}{\mid} b_y \rangle \langle a_z \overset{z}{\mid} b_z \rangle
\end{aligned} \tag{2.14}$$

The triple integral has been factorised now into a product of three equivalent integrals. We show how to evaluate $\langle a_x \overset{x}{\mid} b_x \rangle$. We use the change of variables $t = \sqrt{\Lambda}(x - L_x)$. Therefore

$$x = \frac{t}{\sqrt{\Lambda}} + L_x \quad \text{and} \quad dx = \frac{dt}{\sqrt{\Lambda}} \tag{2.15}$$

and the integral becomes

$$\langle a_x \overset{x}{\mid} b_x \rangle = \frac{1}{\sqrt{\Lambda}} \int_{-\infty}^{\infty} \left(\frac{t}{\sqrt{\Lambda}} + L_x - A_x\right)^{a_x} \left(\frac{t}{\sqrt{\Lambda}} + L_x - B_x\right)^{b_x} \exp(-t^2) dt \tag{2.16}$$

The integrand in the above integral now has the form "polynomial in t of degree $a_x + b_x$ times $\exp(-t^2)$ " and is evaluated by Gaussian quadrature as described in section 2.2.

The elements of the overlap matrix $\mathbf{S}$ are overlap integrals between normalised contracted Gaussian functions. Therefore overlap integrals over primitive Gaussian functions are accumulated to form the elements of the overlap matrix.

$$(\mathbf{S})_{AB} = N_A N_B \langle G_A | G_B \rangle = N_A N_B \sum_{i=1}^{K_A} \sum_{j=1}^{K_B} c_i c_j n_{A_i} n_{B_i} \langle g_{A_i} | g_{B_i} \rangle \tag{2.17}$$

2.4 Kinetic energy Integrals

The kinetic energy matrix elements between primitive Cartesian Gaussian functions are

$$-\frac{1}{2}\langle g_A|\nabla^2|g_B\rangle = -\frac{1}{2}\int g_A(\mathbf{r};\alpha,a_x,a_y,a_z,\mathbf{A})\,\nabla^2 g_B(\mathbf{r};\beta,b_x,b_y,b_z,\mathbf{B})\,d\mathbf{r} \qquad (2.18)$$

The derivative of a primitive Gaussian is equal to the sum of two primitive Gaussians with angular momentum higher and lower by one. By taking this into account we can expand (2.18) in terms of overlap integrals.

$$\begin{aligned}
- \quad & \frac{1}{2}\langle g_A|\nabla^2|g_B\rangle = \\
- \quad & \frac{1}{2}b_x(b_x-1)\langle g_A(\mathbf{r};\alpha,a_x,a_y,a_z,\mathbf{A})|g_B(\mathbf{r};\beta,b_x-2,b_y,b_z,\mathbf{B})\rangle \\
- \quad & \frac{1}{2}b_y(b_y-1)\langle g_A(\mathbf{r};\alpha,a_x,a_y,a_z,\mathbf{A})|g_B(\mathbf{r};\beta,b_x,b_y-2,b_z,\mathbf{B})\rangle \\
- \quad & \frac{1}{2}b_z(b_z-1)\langle g_A(\mathbf{r};\alpha,a_x,a_y,a_z,\mathbf{A})|g_B(\mathbf{r};\beta,b_x,b_y,b_z-2,\mathbf{B})\rangle \\
+ \quad & \beta[2(a_x+a_y+a_z)+3]\langle g_A(\mathbf{r};\alpha,a_x,a_y,a_z,\mathbf{A})|g_B(\mathbf{r};\beta,b_x,b_y,b_z,\mathbf{B})\rangle \\
- \quad & 2\beta^2\langle g_A(\mathbf{r};\alpha,a_x,a_y,a_z,\mathbf{A})|g_B(\mathbf{r};\beta,b_x+2,b_y,b_z,\mathbf{B})\rangle \\
- \quad & 2\beta^2\langle g_A(\mathbf{r};\alpha,a_x,a_y,a_z,\mathbf{A})|g_B(\mathbf{r};\beta,b_x,b_y+2,b_z,\mathbf{B})\rangle \\
- \quad & 2\beta^2\langle g_A(\mathbf{r};\alpha;a_x,a_y,a_z;\mathbf{A})|g_B(\mathbf{r};\beta,b_x,b_y,b_z+2,\mathbf{B})\rangle
\end{aligned} \qquad (2.19)$$

The next step is to expand each of the overlap (triple) integrals above into products of three one-dimensional integrals. Then, they can be regrouped as follows.

$$\begin{aligned}
- \quad & \frac{1}{2}\langle g_A|\nabla^2|g_B\rangle = \\
- \quad & k_{ab}\left\{\left[\frac{1}{2}b_x(b_x-1)\,\langle a_x \overset{x}{|} b_x-2\rangle + 2\beta^2\langle a_x \overset{x}{|} b_x+2\rangle\right]\langle a_y \overset{y}{|} b_y\rangle\langle a_z \overset{z}{|} b_z\rangle\right. \\
- \quad & \left[\frac{1}{2}b_y(b_y-1)\langle a_y \overset{y}{|} b_y-2\rangle + 2\beta^2\langle a_y \overset{y}{|} b_y+2\rangle\right]\langle a_x \overset{x}{|} b_x\rangle\langle a_z \overset{z}{|} b_z\rangle \\
- \quad & \left[\frac{1}{2}b_z(b_z-1)\langle a_z \overset{z}{|} b_z-2\rangle + 2\beta^2\langle a_z \overset{z}{|} b_z+2\rangle\right]\langle a_x \overset{x}{|} b_x\rangle\langle a_y \overset{y}{|} b_y\rangle \\
+ \quad & \left.\beta 2(b_x+b_y+b_z)+3\;\langle a_x \overset{x}{|} b_x\rangle\langle a_y \overset{y}{|} b_y\rangle\langle a_z \overset{z}{|} b_z\rangle\right\}
\end{aligned} \qquad (2.20)$$

Each of the one dimensional integrals in the above expression is calculated using the Gaussian quadrature subroutines that calculate the overlap integrlals. The elements of the kinetic energy matrix $\mathbf{T}$ are integrals between contracted Gaussian

functions and are calculated by accumulating the kinetic energy integrals over primitive Gaussian functions in a fashion similar to that of equation (2.17).

2.5 Rys Polynomials

2.5.1 Definition of Rys polynomials

The manifold of *Rys polynomials* [31] is defined by the polynomials $J_n(t,x)$ which are orthonormal on the interval $t \in [-1,1]$ or the $R_n(t,x)$ polynomials orthonormal on $t \in [0,1]$. This orthonormality is defined with respect to the weight function $w(t) = \exp(-xt^2)$:

$$\int_{-1}^{1} \exp(-xt^2) J_n(t,x) J_m(t,x) dt = \delta_{nm} \tag{2.21}$$

$$\int_{0}^{1} \exp(-xt^2) R_n(t,x) R_m(t,x) dt = \delta_{nm} \tag{2.22}$$

where t is the dummy variable of integration and x is a real parameter. The J_n are polynomials of degree n while the R_n are chosen to be even polynomials of degree $2n$. The R_n are proportional to the even members of J_n, according to the relation: $R_n(t,x) = \sqrt{2} J_{2n}(t,x)$. Since R_n is an even polynomial in t of degree $2n$, it can be written as:

$$R_n(t,x) = \sum_{k=0}^{n} C_{kn}(x) t^{2k} \tag{2.23}$$

Now let us suppose that the value of x is fixed. By definition, for up to a given n, the square $(n+1)\times(n+1)$ matrix $\mathbf{C}(x)$ is upper triangular. Furthemore, observe that R_n is orthogonal to all t^{2m} with $m < n$ because each t^{2m} can be written as a linear combination of R_i's, $i = 0, \ldots, m$ which are all orthogonal to R_n. Substitution of 2.23 into the orthogonality relation gives:

$$\begin{aligned} \delta_{mn} &= \int_0^1 R_m R_n \exp(-xt^2) dt = \sum_{k=0}^{m} C_{km} \int_0^1 t^{2k} R_n \exp(-xt^2) dt \\ &= \sum_{k=1}^{m} C_{mk}^{\dagger} \sum_{l=0}^{n} \left[\int_0^1 t^{2(k+l)} \exp(-xt^2) dt \right] C_{ln} = \sum_{k=0}^{m} \sum_{l=0}^{n} C_{mk}^{\dagger} F_{kl} C_{ln} \end{aligned}$$

or in matrix notation:

$$\mathbf{C}^{\dagger}\mathbf{F}\mathbf{C} = \mathbf{I} \tag{2.24}$$

As the elements of **C** below the diagonal are zero, this equation can be solved for the elements of **C**. It defines the Rys polynomials $R_0 \ldots R_n$ as a set of Schmidt orthogonalised functions, linear combinations of the original set of functions $\{t^{2i}\}_{i=0}^{n}$.

The product of R_i and R_j can be expressed as a linear combination of R_0 up to and including R_{i+j}.

$$R_i R_j = \sum_{k=0}^{i+j} b_{ijk} R_k, \quad b_{ijk} = \int_0^1 R_i R_j R_k \exp(-xt^2) dt \tag{2.25}$$

The above simple formula for b_{ijk} is a result of orthonormality. The coefficients b_{ijk} are nonzero only if the indices i, j and k satisfy the "triangle inequality" which states that no index should be greater than the sum of the other two.

2.5.2 Rys Quadrature

We can use the orthonormality properties of the Rys polynomials in the interval $[0, 1]$ with respect to the weight function $\exp(-xt^2)$ to construct a set of quadrature points and weights, in the same way as we did with the Hermite polynomials in section 2.2. If we use only the positive roots $\{t_\alpha(x) > 0\}_{\alpha=1}^{n}$ of $R_n(t, x)$, then the orthonormality integral between R_i and R_j can be written as [2]

$$\int_0^1 R_i(t,x) R_j(t,x) \exp(-xt^2) dt = \sum_{\alpha=1}^{n} R_i(t_\alpha, x) R_j(t_\alpha, x) W_\alpha(x) = \delta_{ij} \tag{2.26}$$

where the weights $W_\alpha(x)$ are calculated by a formula similar to the formula for the weights A_k of equation (2.4). The sum is the exact expression of the integral in terms of *Rys (polynomial) quadrature*. According to section 2.2, the quadrature is exact when $2i + 2j \leq [2(2n) - 1]$, or $i + j < 2n$ since we are dealing only with even polynomials. Now suppose $f(t)$ is an even polynomial of degree $2m$ with $2m < 4n$. It can be written in terms of Rys polynomials as follows

$$f_m(t) = \sum_{i=0}^{m} a_i(x) R_i(t, x) \tag{2.27}$$

[2] Normally we should use all roots of the Rys polynomials but we are working under the tacit assumption that we will be integrating only even polynomials. Therefore the positive roots are sufficient provided that the weights are the usual weights multiplied by 2.

All integrals of the type

$$I_m(x) = \int_0^1 f_m(t) \exp(-xt^2) dt \tag{2.28}$$

can be evaluated exactly by Rys quadrature

$$I_m(x) = \sum_{\alpha=1}^{n} f_m(t_\alpha) W_\alpha(x) \tag{2.29}$$

using the n positive roots t_α of $R_n(t, x)$ and the weights $W_\alpha(x)$.

2.5.3 Calculation of Rys roots and weights

Rys quadrature has proved to be a very effective tool for generating many of the integrals that appear in quantum chemistry calculations. To obtain the roots and weights we use the original subroutines of King and Dupuis [31]. These subroutines employ Chebychev polynomial approximations and other curve fitting techniques to produce efficiently the quadrature parameters for all values of x and for $n = 1, 2, \ldots, 9$. They return the weights $W_\alpha(x)$ and the points $\{v_\alpha^2\}_{\alpha=1}^n$ defined by

$$v_\alpha^2 = \frac{t_\alpha^2}{1 - t_\alpha^2} \tag{2.30}$$

The Rys quadrature is exact provided we know the roots and the weights exactly. These subroutines were designed and tested in order to produce numbers accurate to at least one part in 10^{13} when used in double precision arithmetic, which is standard in our code. Therefore, the resulting errors should be comparable to the roundoff error of the computer and we need not be concerned about the accuracy of integrals that we calculate with Rys quadrature.

2.6 Nuclear Attraction Integrals

Nuclear attraction integrals are necessary in order to form the matrix elements of the electrostatic attraction of the electrons from the charge of the nucleus. We are interested in evaluating the following type of integral

$$\begin{aligned} & \langle g_A | \frac{1}{|\mathbf{r} - \mathbf{C}|} | g_B \rangle \\ = & \int g_A(\mathbf{r}; \alpha, a_x, a_y, a_z, \mathbf{A}) \frac{1}{|\mathbf{r} - \mathbf{C}|} g_B(\mathbf{r}; \beta, b_x, b_y, b_z, \mathbf{B}) \, d\mathbf{r} \end{aligned} \tag{2.31}$$

The procedure we have developed and implemented for this purpose is an adaptation of the Rys quadrature method for two electron integrals [31, 32]. It is a very efficient way of calculating these integrals which demonstrates yet another use of Rys quadrature. The formulas we develop in this section will serve as an introduction to the more complicated formulas used in the evaluation of two electron integrals, in section 3.9.

The first step is to express the nuclear attraction operator as a Gaussian transform (derived by a modification of a Laplace transform) [33]

$$\frac{1}{|\mathbf{r}-\mathbf{C}|} = \frac{1}{\sqrt{\pi}} \int_0^\infty s^{-\frac{1}{2}} \exp(-s|\mathbf{r}-\mathbf{C}|^2) ds \tag{2.32}$$

and apply the change of variables

$$s = u^2 \quad \epsilon\ [0,+\infty), \quad u = \sqrt{s}\ \epsilon\ [0,+\infty) \quad \text{and} \quad ds = 2udu \tag{2.33}$$

to get

$$\frac{1}{|\mathbf{r}-\mathbf{C}|} = \frac{2}{\sqrt{\pi}} \int_0^\infty \exp(-u^2|\mathbf{r}-\mathbf{C}|^2)\, du \tag{2.34}$$

Substitution of the above expression for the transformed nuclear attraction operator into equation 2.31 yields

$$\begin{aligned} \langle g_A|\frac{1}{|\mathbf{r}-\mathbf{C}|}|g_B\rangle &= \langle g_A|\frac{2}{\sqrt{\pi}}\int_0^\infty \exp(-u^2|\mathbf{r}-\mathbf{R_C}|^2)\, du|g_B\rangle \\ &= \frac{2}{\sqrt{\pi}}\int_0^\infty \langle g_A|\exp(-u^2|\mathbf{r}-\mathbf{C}|^2)|g_B\rangle\, du \\ &= \frac{2}{\sqrt{\pi}}\int_0^\infty M'_x(u)M'_y(u)M'_z(u)\, du \end{aligned} \tag{2.35}$$

where the integrand has split into a product of three one-dimensional integrals $M'_x(u), M'_y(u)$ and $M'_z(u)$. We can therefore manipulate each one of them separately. For $M'_x(u)$ we have

$$\begin{aligned} M'_x(u) &= k_{abx} \\ \times &\int_{-\infty}^{\infty} (x-A_x)^{a_x}(x-B_x)^{b_x}\exp(-\Lambda(x-L_x)^2)\exp(-(u^2(x-C_x)^2)dx \\ = &\ k_{abx}k_{lux}\int_{-\infty}^{\infty}(x-A_x)^{a_x}(x-B_x)^{b_x}\exp(-\zeta(x-Z_x)^2)dx \end{aligned} \tag{2.36}$$

where the definitions of $\mathbf{L}$, Λ and k_{abx} are given in equations (2.12) and (2.13). Also

$$\zeta = \alpha+\beta+u^2 \quad Z_x = \frac{\alpha A_x + \beta B_x + u^2 C_x}{\alpha+\beta+u^2} \tag{2.37}$$

and

$$p = \alpha + \beta \quad k_{lux} = \exp\left[\frac{-pu^2}{p+u^2}(L_x - C_x)^2\right] \tag{2.38}$$

It is easy to see now that for any value of u, the integral $M'_x(u)$ is one of the three components of an overlap integral and can be evaluated by Gaussian quadrature. For this purpose, a change of variables is carried out, as in equation (2.15) and the resulting integral is similar to that of equation (2.16)

$$\begin{aligned} M'_x(u) &= k_{abx} k_{lux} \frac{1}{\sqrt{\zeta}} \\ \times & \int_{-\infty}^{\infty} \left(\frac{x'}{\sqrt{\zeta}} + Z_x - A_x\right)^{a_x} \left(\frac{x'}{\sqrt{\zeta}} + Z_x - B_x\right)^{b_x} \exp(-x'^2) dx' \end{aligned} \tag{2.39}$$

To proceed further, one more change of variables is necessary, this time in the integral (2.35). This change, from u to t, is defined by

$$t^2 = \frac{u^2}{p+u^2}, \quad du = \frac{\sqrt{p}}{(1-t^2)^{\frac{3}{2}}} dt \tag{2.40}$$

in terms of which the quantities of equations (2.37) and (2.38) become

$$Z_x = L_x, \quad k_{lux} = \exp[-p(L_x - C_x)^2 t^2], \quad \text{and} \quad \zeta = \frac{p}{1-t^2} \tag{2.41}$$

$M_x(t)$ is now defined as a function of t. It will play a similar role to $M'_x(u)$

$$\begin{aligned} M_x(t) &= \frac{1}{\sqrt{1-t^2}} M'_x\left(\sqrt{p}\frac{t}{\sqrt{1-t^2}}\right) \exp[p(L_x - C_x)^2 t^2] \\ &= \frac{k_{abx}}{\sqrt{p}} \int_{-\infty}^{\infty} \left(x'\sqrt{\frac{1-t^2}{p}} + L_x - A_x\right)^{a_x} \\ &\times \left(x'\sqrt{\frac{1-t^2}{p}} + L_x - B_x\right)^{b_x} \exp(-x'^2)\, dx' \end{aligned} \tag{2.42}$$

$$\begin{aligned} &= \frac{k_{abx}}{\sqrt{p}} \sum_{i=1}^{[\frac{a_x+b_x}{2}]+1} \left(x'_i\sqrt{\frac{1-t^2}{p}} + L_x - A_x\right)^{a_x} \\ &\times \left(x'_i\sqrt{\frac{1-t^2}{p}} + L_x - B_x\right)^{b_x} w_i \end{aligned} \tag{2.43}$$

and $M_y(t)$ and $M_z(t)$ are defined in a similar manner. The sum (2.43) is the integral, expressed in terms of Gaussian quadrature, as we calculate it in practice. An observation is pertinent at this point: the expression of equation (2.43) is an

even polynomial in t of degree[3] $4[(a_x + b_x)/2]$. This is not immediately obvious because t appears in the form $\sqrt{1-t^2}$. However, if we were to carry out a binomial expansion on the terms in parentheses inside the integral of equation (2.42) we would split the integral in a sum of integrals containing powers of $x'\sqrt{1-t^2}$. All the integrals with odd powers of x' would vanish because of the odd parity of the integrand and symmetric interval of integration. Only terms with even powers of x' and consequently $\sqrt{1-t^2}$ would remain. The highest order term would be $(1-t^2)^{2[(a_x+b_x)/2]}$.

The nuclear attraction integral of equation (2.35) can now be written as

$$\langle g_A|\frac{1}{|\mathbf{r}-\mathbf{C}|}|g_B\rangle = \frac{2k_{ab}}{p\sqrt{\pi}}\int_0^1 M_x(t)M_y(t)M_z(t)\exp[-p(\mathbf{L}-\mathbf{C})^2t^2]dt \qquad (2.44)$$

where $k_{ab} = k_{abx}k_{aby}k_{abz}$ and $M_x(t)M_y(t)M_z(t)$ is an even polynomial in t of degree

$$n_{pol} = 4\left(\left[\frac{a_x+b_x}{2}\right] + \left[\frac{a_y+b_y}{2}\right] + \left[\frac{a_z+b_z}{2}\right]\right) \qquad (2.45)$$

At this stage we can finally evaluate the nuclear attraction integral using Rys quadrature with $N_{Rys} = [n_{pol}/4] + 1$ points. In practice, members of the same shell of primitive basis functions may require different number of points for the Rys quadrature. For example, the $g_A(\mathbf{r};\alpha,1,1,1,\mathbf{A})$, $g_B(\mathbf{r};\beta,0,0,0,\mathbf{B})$ pair of functions would require 1 quadrature point while the pair $g_A(\mathbf{r};\alpha,3,0,0,\mathbf{A})$, $g_B(\mathbf{r};\beta,0,0,0,\mathbf{B})$ requires 2 points. Hence, evaluation of the nuclear attraction integrals with the minimum number of quadrature points would require two calls to the subroutines that generate the Rys roots and weights for this combination of shells. With higher angular momentum the number of calls increases. We have found that for computational efficiency it is necessary to call the Rys subroutines as little as possible. Thus we call them only once per pair of shells and obtain the lowest number of points necessary to integrate *all* the integrals of a shell pair. So in practice we use

$$N_{Rys} = \left[\frac{\lambda_A+\lambda_B}{2}\right] + 1 \qquad (2.46)$$

As with the other one electron integrals we have seen so far, the nuclear attraction integrals over unnormalised primitive Gaussian functions are combined with con-

[3]Here the square brackets are used to denote the closest integer which is smaller than the real number inside the backets. For example, $[3.7] = 3$ and $[-3.7] = -4$.

traction coefficients and normalisation constants in order to form the matrix $\mathbf{V}^{nucl}$ of the nuclear attraction operator in the contracted Gaussian basis.

2.7 Effective Core Potentials

2.7.1 Introduction

The study of complexes of heavy elements by *ab initio* quantum chemical methods requires the incorporation of relativistic effects since it has been shown that they play a significant role in the properties of such compounds [34, 35]. To a great extent, the incorporation of such effects can be achieved through the use of *Effective Core Potentials* (ECP) (also called Pseudopotentials by some authors) or by some approximate method of solving the Dirac-Schrödinger equation adjusted to a many electron system [7, 6]. The design of ECPs is a compromise between two requirements: first they have to imitate the interactions of core electrons of a many electron atom with the valence electrons. Second, this imitation of core electrons has to be limited only to the valence region. This means that they have to produce valence orbitals that resemble the true valence orbitals in the valence region but have no features (nodes, etc.) in the core region. This requirement, which is not so trivial, is necessary to ensure that a smaller (i.e. valence only) basis set is needed for the atom in question. The ECPs are routinely used because in most cases they afford results of comparable accuracy to all-electron methods at reduced computational cost. Even in the cases of second, third and fourth row atoms, where relativistic effects are usually negligible, the use of ECPs is very common due to the computational savings that are achieved from the use of "valence only" basis sets.

The effective core potential operators of the functional form first proposed by Kahn et al. [36, 37] are widely used today. The only effort in using them in a molecular calculation rests in the evaluation of their one electron integrals which are their matrix elements with the Cartesian Gaussian functions of the basis set.

The matrix element of the ECP operator consists of two distinct types of integrals, one of which does not involve projection operators and one that does. A few methods and corresponding computer programs for evaluating these integrals are

known [37, 38, 39, 40]. The integral which involves the projection operators is by far the most difficult from a theoretical and practical point of view.

The purpose of this section is to introduce the reader to the theory behind the ECPs implemented in the code. As far as the implementation is concerned, a new method to calculate the second integral which is simple and fast will be described and compared to a much slower, benchmark original attempt. As with all of MAGIC, no limitations on the maximum angular momentum of basis functions and projection operators or the values of the parameters involved exist. Furthermore, the size of the molecular system to be studied is only restricted by the available computer resources.

2.7.2 The pseudopotential method of Weeks and Rice for a single valence electron

The method of Weeks and Rice [41] is very widely used because it avoids the complications of the frozen core orbital approximation and makes possible the neglect of the core orbitals. This results in computational savings both because it requires a smaller (valence only) basis set and also because it eliminates the need to calculate two-electron integrals between the valence and the core orbitals. In what follows we will give an outline of the formalism and the underlying physical principles. This information is essential for the understanding of the use of ECPs and their computational requirements which we will examine later. It is also quite interesting in itself as the theory involved is an elegant and successful approximation. ECPs are a way to express with mathematics the traditional notion of chemistry which attributes all chemical properties to the valence electrons.

We will consider an atom with a single valence electron (eg. Li, K, Ca^+, etc.) which we will treat explicitly. The rest of the electrons, N_{core} in total, which belong to complete groups we will distribute in a set of spin orbitals $\{\phi_i\}_{i=1}^{N_{core}}$. The eigenfunction and eigenvalue of the valence electron will be ϕ_v and ϵ_v respectively. We assume that the core and the valence orbitals are orthonormal, i.e.

$$\langle \phi_k | \phi_l \rangle = \delta_{kl} \qquad k, l = 1, ..., N_{core}, v \tag{2.47}$$

The eigenvalue equation for the valence orbital is

$$\hat{F}_v\phi_v = \epsilon_v\phi_v + \sum_{i=1}^{N_{core}} \lambda_{iv}\phi_i \tag{2.48}$$

where the λ_{iv} are Lagrange multipliers which impose orthogonality to the core orbitals. We do not know the form of the hermitian operator $\hat{F}_v$ at this stage, but we assume that it is not connected in any way to the core orbitals. The next step is the introduction of the following projection operators

$$\hat{\Omega} = \sum_{i=1}^{N_{core}} |\phi_i\rangle\langle\phi_i| \quad \text{and} \quad \hat{\Pi} = 1 - \hat{\Omega} \tag{2.49}$$

in terms of which we can rewrite equation (2.48) as

$$\hat{\Pi}\hat{F}_v\phi_v = \epsilon_v\phi_v \tag{2.50}$$

We can now define a valence pseudo-orbital ψ_v as an admixture of core orbitals to the valence orbital ϕ_v.

$$\psi_v = \phi_v + \sum_{i=1}^{N_{core}} \alpha_i\phi_i \quad \text{or} \quad \phi_v = \hat{\Pi}\psi_v \tag{2.51}$$

Substitution of the above expression for ϕ_v in (2.50) yields

$$\hat{\Pi}\hat{F}_v\hat{\Pi}\psi_v = \epsilon_v\hat{\Pi}\psi_v \tag{2.52}$$

We can rearrange (2.52) to obtain

$$(\hat{F}_v + \hat{V}_p)\psi_v = \epsilon_v\psi_v \tag{2.53}$$

where $\hat{V}_p$ is called the *generalised Phillips-Kleinman operator.*

$$\hat{V}_p = -\hat{\Omega}\hat{F}_v - \hat{F}_v\hat{\Omega} + \hat{\Omega}\hat{F}_v\hat{\Omega} + \epsilon_v\hat{\Omega} = -\hat{\Omega}(\hat{F}_v - \epsilon_v) - \hat{\Pi}\hat{F}_v\hat{\Omega} \tag{2.54}$$

It is easy to show that if we impose on $\hat{F}_v$ the condition that the the core orbitals ϕ_i are its eigenfunctions with eigenvalues ϵ_i (not generally true), $\hat{V}_p$ simplifies to

$$\hat{V}_{PK} = \sum_{i=1}^{N_{core}} (\epsilon_v - \epsilon_i)|\phi_i\rangle\langle\phi_i| \tag{2.55}$$

which is the Phillips-Kleinman [42] potential.

The formalism we have developed so far is exact and allows us to use the valence pseudo-orbital in place of the valence orbital. The pseudo-orbital is not restricted to be orthogonal to the core orbitals and furthermore we have the liberty to chose the coefficients α_i in any way we like. This non-uniqueness of the α_is is called "pseudopotential indeterminacy" and was reported by Cohen and Heine [43]. The importance and usefulness of this result lies in the fact that the valence pseudo-orbital ψ_v can be constructed in such a way as to resemble the true valence orbital ϕ_v in the valence region and have no features (nodes, etc.) in the core region. This leads to a smaller basis necessary to describe the valence space and it is the true computational saving we seek. Of course the construction of the valence pseudo-orbital subject to the requirement we just stated is not a trivial matter and many different procedures have been devised over the years for determining the coefficients α_i of equation (2.51). We will examine these in subsection 2.7.5, but for the moment we will assume the problem has been solved in a satisfactory way and we will proceed with the development of a local and more handy version for $\hat{F}_v + \hat{V}_p$.

In practice, an additional mathematical requirement (constraint) has to be imposed on the pseudo-orbital to lift the pseudopotential indeterminacy. It has been shown that this requirement can be incorporated into the pseudopotential Hamiltonian [44]. This is achieved by using a modified form for the effective potential

$$\hat{V}'_P = \sum_{i=1}^{N_{core}} |\phi_i\rangle\langle\chi_i| - \hat{\Pi}\hat{F}_v\hat{\Omega} \tag{2.56}$$

where the functions χ_i could in principle be arbitrary and will always produce a valence orbital $\phi_v = \hat{\Pi}\psi_v$ which satisfies equation (2.50) just as the generalised Phillips-Kleinman potential does. The generalised Phillips-Kleinman potential operator is obtained when

$$\chi_i = (\hat{F}_v - \epsilon_v)|\phi_i\rangle \tag{2.57}$$

The functional form of the χ_i determines now the shape of the pseudo-orbital. There are choices of χ_i possible that are not plagued by pseudopotential indeterminacy and fix the values of the coefficients α_i in equation (2.51). Careful choices can give smooth and nodeless pseudo-orbitals but care should always be taken against

excessive contribution from core orbitals which is described as "variational collapse" of the valence pseudo-orbital to the core.

2.7.3 Local representation of the effective core potential

It can be shown that without loss of generality the angular part of atomic Hartree-Fock orbitals can be restricted to be a spherical harmonic [44]. By taking this into account it is shown in appendix A how we can obtain a Hartree-Fock equation for the radial only part of the orbital for a single valence electron. This is relatively straightforward because the core consists of complete electron groups. The angular part of the valence pseudo-orbital can be a certain real spherical harmonic $Z_{\beta\gamma}(\theta,\phi)$ and therefore only core orbitals with the same angular part will contribute in the expansion of equation (2.51). This means that α_i has to be zero for all core orbitals whose angular part is not $Z_{\beta\gamma}(\theta,\phi)$. A consequence of this is that pseudo-orbitals with angular momentum larger than the largest angular momentum of the core will be pure valence orbitals since all α_is will be zero for them. In other words the result of the action of the generalised Phillips-Kleinman operator on such an orbital is zero.

A radial effective core potential equation for the radial part of the pseudo-orbital $(1/r)R_{\alpha\beta}^{pseudo}(r)$ can therefore be written in a similar fashion to the Hartree-Fock equation for the radial part of the orbital for a single valence electron atom. The parameters α and β are the principal quantum number and the angular momentum quantum number of the pseudo-orbital respectively. The radial equation includes the radial Hartree-Fock potential for the valence electron plus terms due to the generalised Phillips-Kleinman potential $\hat{V}_P$, which is related only to the core orbitals. These terms do not appear when the angular momentum of the valence orbital is higher than the highest angular momentum of the core, in which case we get exactly the same eigenvalue equation as in appendix A. In general, the eigenvalue equation for the radial part of the pseudo-orbital of a single valence electron atom is

$$\left[\hat{h}(r)+\hat{U}^{CORE}(r)\right]\frac{1}{r}R_{\alpha\beta}^{pseudo}(r)=\epsilon_{\alpha\beta}\frac{1}{r}R_{\alpha\beta}^{pseudo}(r) \tag{2.58}$$

where $\hat{h}(r)$ contains the point charge Coulomb attraction of the core and the radial

form of the kinetic energy operators. The operator $\hat{U}^{CORE}(r)$ as defined by (2.58) is the *effective core potential*. It represents the radial part of the Coulomb and exchange operators due to core orbitals as well as the radial part of the generalised Phillips-Kleinman operator.

There is difficulty in using the above equation in practice because both the core-exchange and generalised Phillips-Kleinman operators are nonlocal. Their nonlocal form necessitates the evaluation of two-electron integrals between core and valence orbitals. This defeats our objective which is the elimination of the core orbitals from the problem. However, we can overcome this difficulty by using an equivalent local form for $\hat{U}^{CORE}(r)$. The price we have to pay for the local operator is that its functional form must be different for every single valence orbital. We therefore have to replace the one nonlocal potential with a set of local potentials, defined in equations (2.59) and (2.60). These equations are obtained by solving equation (2.58) directly for $\hat{U}^{CORE}(r)$ for every pseudo-orbital. The result is the following two sets of local operators

$$\hat{U}_{\beta}^{CORE}(r) = \frac{\hat{U}^{CORE}(r)(\frac{1}{r}R_{\alpha\beta}^{pseudo})}{\frac{1}{r}R_{\alpha\beta}^{pseudo}} = \epsilon_{\alpha\beta} - \frac{r\hat{h}(\frac{1}{r}R_{\alpha\beta}^{pseudo})}{R_{\alpha\beta}^{pseudo}} , \qquad \beta < L \qquad (2.59)$$

and

$$\hat{U}_{\beta}^{CORE}(r) = \frac{\hat{U}^{CORE}(r)(\frac{1}{r}R_{\alpha\beta})}{\frac{1}{r}R_{\alpha\beta}} = \epsilon_{\alpha\beta} - \frac{r\hat{h}(\frac{1}{r}R_{\alpha\beta})}{R_{\alpha\beta}} , \qquad \beta \geq L \qquad (2.60)$$

where L is defined to be greater by one than the maximum angular momentum quantum number encountered in the core orbitals. Notice the simplification that the dependence of the local effective core potentials on the principal quantum number α of the valence orbital has been neglected. This approximation can be rigorously justified for the case of Hartree-Fock equivalent pseudopotentials [44] in terms of the close spacing of the eigenvalues of valence orbitals with different principal quantum numbers and the same angular momentum quantum numbers. It is assumed to be valid for the local Generalised Phillips-Kleinman (2.59) and Hartree-Fock (2.60) potentials too. It is clear now from equations (2.59) and (2.60) that the radial functions of the pseudo-orbitals should be nodeless. A node (zero value) of $\frac{1}{r}R_{\alpha\beta}^{pseudo}$

at a point r_s would result in a singularity [45] of (2.59)

$$\epsilon_{\alpha\beta} - \frac{r\hat{h}(\frac{1}{r}R^{pseudo}_{\alpha\beta})}{R^{pseudo}_{\alpha\beta}(r_s)} = \epsilon_{\alpha\beta} + \frac{Z}{r} + r\frac{\nabla^2_r(\frac{1}{r}R^{pseudo}_{\alpha\beta})}{2R^{pseudo}_{\alpha\beta}} - \frac{\beta(\beta+1)}{2r^2} \tag{2.61}$$

since $\nabla^2_r(r^{-1}R^{pseudo}_{\alpha\beta})$, defined according to (A.4), would not in general be zero at r_s. A singularity in the effective potential is something we wish to avoid since it is bound to lead to numerical problems in our calculations. Therefore, a feature common in all pseudo-orbitals is that they have no radial nodes. Singularities in the potentials (2.60) can be avoided by using always the $(1/r)R_{(\beta+1)\beta}(r)$ Hartree-Fock orbitals that have no radial nodes by definition.

Furthermore it is observed in practice that the ECPs of equation (2.59) differ significantly from each other while the ECP's of equation (2.60) are similar to each other. This is attributed to the absence of the Phillips-Kleinman term from the latter. All these local ECP's can be combined together in one only ECP with semi-local form with the help of angular momentum projection operators

$$\hat{U}^{CORE}(r,\theta,\phi) = \sum_{l=0}^{\infty}\sum_{m=-l}^{l} \hat{U}^{CORE}_l(r)|Z_{lm}\rangle\langle Z_{lm}| \tag{2.62}$$

Since all potentials of equation (2.60) are similar, we can approximate them by a single, average term $\hat{U}^{CORE}_L(r)$, and take into account the closure property of the spherical harmonics Z_{lm} set of functions to get

$$\hat{U}^{CORE}(r,\theta,\phi) = \hat{U}^{CORE}_L(r) + \sum_{l=0}^{L-1}\sum_{m=-l}^{l} |Z_{lm}\rangle[\hat{U}^{CORE}_l(r) - \hat{U}^{CORE}_L(r)]\langle Z_{lm}|$$

which is the final expression for effective core potentials, in wide use today. The semilocal form of this expression does not hinder its applicability because it is based only on spherical harmonics and not on any set of core orbitals.

2.7.4 ECPs for atoms with many valence electrons

The majority of atoms have more than one valence electron and therefore ECPs for these atoms have to be derived as well. Even in the cases of one valence electron it is sometimes expedient to treat electrons belonging to complete groups, of principal quantum number smaller by one than the valence, as valence electrons.

This approach has proved to be more accurate since the outer shells of the core can participate in bonding to a great extent and are therefore affected by the chemical environment.

The simplest way to obtain an ECP for a valence electron for an atom with N_v valence electrons is by applying the Weeks and Rice method to the single valence electron of the positive ion of the atom with charge $N_v - 1$. Such a derivation however neglects the Coulomb and exchange interactions between the valence electrons. These interactions cause the neutral atom valence orbitals to have significantly different shapes from the positive ion orbitals. This can be thought of as extra shielding from the core due to the presence of the other valence electrons. Indeed, many authors have observed that ECPs derived from positive ions yield satisfactory results only for the ion from which they were derived [46]. Such ECPs have proved rather inaccurate for neutral atoms. The situation is improved if the rest of the valence electrons are taken into account during the derivation of each pseudo-orbital and there are a variety of ways available in the literature to do so.

The general approach [37, 47] is to obtain Hartree-Fock core and valence orbitals for the neutral atom. Then valence pseudo-orbitals can be constructed as for the case of one valence electron. The localised effective potentials are then obtained by a slight modification of equation (2.59)

$$\hat{U}_{\beta}^{CORE}(r) = \epsilon_{\alpha\beta} - \frac{r(\hat{h} + \hat{W}_{val}^{PS})(\frac{1}{r}R_{\alpha\beta}^{pseudo})}{R_{\alpha\beta}^{pseudo}} \tag{2.63}$$

where now the added operator $\hat{W}_{val}^{PS}$ represents the Coulomb and exchange interactions of the pseudo-orbital with the rest of the valence orbitals.

2.7.5 Determination of ECPs and incorporation of relativistic effects

According to our discussion so far, the construction of ECPs requires first the construction of valence pseudo-orbitals. This in turn means the determination of the coefficiens α_i of equation (2.51). Smooth nodeless pseudo-orbitals can be obtained by minimization of the kinetic energy $\langle\psi_v|\hat{T}|\psi_v\rangle$ of the pseudo-orbital [43]. Functionals of ψ_v more elaborate than the expectation value of the kinetic energy can be

conceived whose variation yields pseudo-orbitals with improved features [37]. However, this approach will never yield valence pseudo-orbitals which exactly match the valence orbitals in the valence region since by definition some of the α_is have to be nonzero. This inexact coincidence of the pseudo-orbitals with the valence orbitals in the valence region has been characterised as a major source of inaccuracy for the pseudopotentials. In order to amend this, equation (2.51) has to be abandoned. There exist then various extensions to the theory of Weeks and Rice that produce pseudo-orbitals matching exactly the valence orbitals in the valence region [48, 47]. In fact such a *shape-consistent* method has been employed in the derivation of the ECPs of Hay and Wadt[49, 50, 51]. We use these particular ECPs widely in calculations with MAGIC.

So far we have presented the principles of a theory of ECPs which is based on ab initio considerations and a rigorous theoretical framework. The approximations involved in each stage of the derivation can be clearly distinguished. However, as is the case with exchange-correlation density functionals, empirical approaches which fit some functional form to either experimental data or high accuracy ab-initio results have proved very successful. The *energy-adjusted* pseudopotentials are such a case [46]. The following ansatz is the functional form which is used to represent the potential

$$\hat{U}^{CORE}(r,\theta,\phi) = \frac{N_c}{r} + \sum_{l=0}^{L}\sum_{m=-l}^{l}\left(\sum_{k} A_{lk}e^{-\zeta_{lk}r^2}\right)|Z_{lm}\rangle\langle Z_{lm}| \qquad (2.64)$$

where N_c is the number of electrons allocated to the core. The parameters A_{lk} and ζ_{lk} are determined by fitting to excitation and ionization energies or low lying states of the neutral atom and singly positive ion. These quantities have the advantage that they are quantum chemical observables, in contrast to orbitals which do not have any such direct interpretation. Here too, it has been shown that fitting to a neutral, many electron atom yields more accurate potentials than the one-electron ion. Of course, once energy-adjusted potentials are constructed one can use them to obtain valence pseudo-orbitals. These pseudo-orbitals are of secondary importance as they only serve the purpose of leading to an appropriate basis set for use in conjuction with the pseudopotentials in molecular calculations. We use frequently for our

calculations with MAGIC the energy-adjusted pseudopotentials of the Stuttgart group, [52, 53, 54]. This is a comprehensive range of accurate ECPs that covers essentially all of the periodic table.

The representation of the interaction of the core electrons by an ECP does not necessarily have to be based on the Hartree-Fock model. Pseudopotentials can be derived using higher levels of theory. For heavy atoms in particular, the most important contributions from relativistic effects can be incorporated without any increase in the cost or complexity of the calculation. To this end, the Darwin and mass-velocity terms are usually included in a one component formalism (similar to the Hartree-Fock equations) which is used to obtain the pseudo-orbitals or energies from which ECPs are derived. Hay and Wadt used the relativistic formalism of Kahn, Cowan and Hay [55] for their pseudopotentials while the Stuttgart relativistic pseudopotentials are derived using the formalism of Wood and Boring[56]. The resulting *quasirelativistic* pseudopotentials are an effective and simple way to include relativistic effects in a calculation even when no explicit relativistic terms are used for the description of the valence electrons. It is fortunate for this reason that relativistic effects affect mainly the core orbitals and valence orbitals are affected implicitly through interaction with core orbitals.

We present now some simple results we obtained with the ECPs already mentioned in order to demonstrate how they compare with all-electron calculations. First in Table 2.1 we present the optimised geometries of coinage metal hydrides. The optimisation was carried out until all components of the gradient were less than 10^{-3} which is the standard threshold for geometry optimisations in the code. The Triple Zeta Valence plus Polarization (TZVP) basis set [58] was used for the hydrogen atom and the all electron calculation on CuH. ECPs and the corresponding valence basis sets were used on the metal atoms. We have used ECPs with small cores. The core of the gold atom contained 60 electrons which corresponds to the element Nd, the core of the Ag atom contained 28 electrons (Ni) and the core of Cu contained 10 electrons (Ne). For the calculations on Au and Ag without ECPs we used basis sets of comparable quality to the TZVP bases. Two sets of calculations were performed, one with the exchange-only functional derived from the uniform

Table 2.1: Optimised geometries (Å) of coinage metal hydrides with various treatments of the core of the metal atom. The experimental values [57] are given in parentheses under the name of each molecule.

Molecule	ECP	r_e (LDAX)	r_e (BLYP)
AuH	Stut. Rel. [53]	1.549	1.550
(1.524)	Hay Rel. [49]	1.537	1.547
	Stut. HF [53]	1.722	1.746
	No ECP	1.700	1.711
AgH	Stut. Rel. [53]	1.604	1.616
(1.618)	Hay Rel. [49]	1.589	1.623
	Stut. HF [53]	1.665	1.682
	No ECP	1.670	1.687
CuH	Stut. Rel. [52]	1.455	1.490
(1.463)	Hay [49]	1.468	1.490
	Stut. HF [52]	1.476	1.480
	No ECP	1.460	1.464

Table 2.2: Optimised bond length (Å) of UF_6 with various kinds of ECPs for the uranium atom. The experimental value is given in parentheses under the name of the molecule.

Molecule	ECP	r_e (LDAX)	r_e (BLYP)
UF_6	Stut. Rel. [54]	2.010	2.034
(2.000)	Hay. Rel. [61]	2.024	2.047
	Stut. HF [54]	2.048	2.083

electron gas (LDAX) [16] and the other with the Becke88 exchange [59] and the Lee Yang and Parr [60] correlation functional (BLYP).

From Table 2.1 which also includes experimental geometries, we can observe some trends that are typical for these types of calculations. The BLYP functional leads to slightly longer bonds as a result of the correlation effects it includes. Then the quasirelativistic ECPs produce far better bond lengths than the *nonrelativistic* Hartree-Fock ECPs or the all-electron calculations which involve no relativistic effects. Apparently the quasirelativistic ECPs do incorporate relativistic effects to an appreciable extent. They seem to be capable of predicting the bond lengths of the hydrides as well as Hartree-Fock theory does for organic molecules. There is however no clear trend on the effect of the functional and the correlation effects due to the BLYP functional certainly do not improve the geometries. In particular, the maximum error for the LDAX functional, 0.029 Å, occurs with the Hay quasirelativistic ECP of AgH and the maximum error of the BLYP functional is 0.027 Å for both the Stuttgart and Hay quasirelativistic ECPs on CuH. As expected, for the methods that do not include any relativistic corrections the largest errors occur for the molecule containing the heavier element, AuH. They are 0.198 Å for the LDAX functional and 0.222 Å for the BLYP functional. So in this case the neglect of relativistic corrections increases the errors in bond lengths by an order of magnitute.

Another example is the uranium hexafluoride UF_6 molecule. In Table 2.2 geometry optimisation results are presented, obtained in a manner similar to the calculations we performed for the coinage metal hydrides. Here the effects of rela-

tivity are not so pronounced, leading only to a two-fold increase in error when they are neglected. This is because there is significant contribution from the fluorine orbitals to the bond, more than there is from the hydride s orbitals.

Quasirelativistic ECPs for the core and a simple DFT treatment of valence electrons is the lowest and computationally less demanding level of theory that MAGIC can use for calculations on molecules containing heavy elements. It remains to be seen whether and to what extent such methodology could produce results of value to chemists. Geometries are one of the easiest properties of molecules to calculate and it seems that MAGIC can successfully predict them.

2.8 ECP implementation in MAGIC

2.8.1 ECP integrals

We will now concentrate on the practical aspects of using ECPs in a DFT calculation, especially on the calculation of the required integrals. In general, the ECPs we use represent the interaction of the core electrons with the valence electrons by a potential operator of the following semi-local form [37]:

$$U^B(r,\theta,\phi) = U_L^B(r) + \sum_{l=0}^{L-1}\sum_{m=-l}^{l} |lm;B\rangle[U_l^B(r) - U_L^B(r)]\langle lm;B| \qquad (2.65)$$

This form is valid for both the shape-consistent and energy-adjusted ECPs of subsection 2.7.5. For the shape-consistent ECPs, L is larger by one than the maximum angular momentum quantum number encountered in the core. In the case of energy-adjusted ECPs, L is greated by two than the maximum angular momentum encountered in the core and $U_L^B(r) = N_c/r$. The ECP is expressed in terms of spherical polar coordinates (r,θ,ϕ). In our discussion of ECP integral evaluation we will assume that the ECP will always be located on atom B that coincides with the origin of coordinates and therefore $\mathbf{r}$ will be equal to $\mathbf{r}_B$, the distance from atom B. As one would expect, U_l^B and U_L^B approach zero asymptotically at large distance from B. The functions $|lm;B\rangle$ are real spherical harmonics Z_{lm} centred on

B, according to the definition

$$Z_{lm}(\theta,\phi) = \left(\frac{(2l+1)}{2\pi}\frac{(l-|m|)!}{(l+|m|)!}\right)^{\frac{1}{2}} \begin{cases} \cos(|m|\phi)P_l^{|m|}(\cos\theta) & m>0 \\ \frac{1}{\sqrt{2}}P_l^{|0|}(\cos\theta) & m=0 \\ \sin(|m|\phi)P_l^{|m|}(\cos\theta) & m<0 \end{cases} \tag{2.66}$$

For ECPs derived from pseudo-orbitals the core potential operators are expressed in analytical form by fitting the numerical potentials to linear combinations of Gaussian functions:

$$U_L^B(r) = \frac{N_c}{r} + \sum_k d_{kL} r^{n_{kL}} e^{-\zeta_{kL} r^2} \tag{2.67}$$

$$U_l^B(r) - U_L^B(r) = \sum_k d_{kl} r^{n_{kl}} e^{-\zeta_{kl} r^2} \tag{2.68}$$

where N_c is the number of core electrons. Energy-adjusted ECPs are expressed in terms of Gaussian functions from the outset and equations (2.67) and (2.68) still hold with the exception of the sum in (2.67). In all ECP's derived to date, the powers n_{kL} and n_{kl} are restricted to the values 0, -1 and -2, although the method developed here assumes no such restriction. We will try to follow the notation of earlier works on core potential integral evaluation [37, 38, 40]. The basis sets we use consist of contracted Cartesian Gaussian functions. The general form of an unnormalised primitive Cartesian Gaussian function on centre A (see also section 1.4) is

$$g_A = x_A^{a_x} y_A^{a_y} z_A^{a_z} \exp(-\alpha \mathbf{r}_A^2) \tag{2.69}$$

The matrix elements of the pseudopotential operators (2.67) and (2.68) with the functions g_A and g_C, according to (2.65), require the evaluation of two distinct types of integrals (referred to as type 1 and type 2 respectively).

$$\chi_{AC} = \int g_A \, r^{n_{kL}} \exp(-\zeta_{kL} r^2) g_C \, d\mathbf{r} \tag{2.70}$$

and

$$\gamma_{AC} = \int_0^\infty \langle g_A | lm; B \rangle(r) \; r^{n_{kl}+2} \exp(-\zeta_{kl} r^2) \; \langle g_C | lm; B \rangle(r) \; dr \tag{2.71}$$

where

$$\langle g_A | lm; B \rangle(r) = \int g_A(\mathbf{r}; \alpha, a_x, a_y, a_z, \mathbf{A}) Z_{lm}(\theta,\phi) d\Omega \tag{2.72}$$

is an integral over solid angle. A few methods for the analytical calculation in spherical polar coordinates around the centre B are available for the above integrals [38, 40]. All these methods have the common starting point of expanding the integrals in spherical polar coordinates. This separates them into sums of angular and radial integrals. Methods differ in the analytical approaches they follow to evaluate these angular and radial integrals. The angular integrals are relatively easy to evaluate and they require minimal computational effort with all the methods. On the other hand the radial integrals, especially those emerging from the type 2 integral, that involves the projection operators, lead to rather complicated expressions whose evaluation is responsible for the majority of the computational effort. Indeed, even though the ECP matrix is two-dimensional and needs to be calculated only once during an SCF calculation, it becomes a serious bottleneck as soon as we encounter molecules of the size of 10 atoms or more. This is what we observed with an implementation in MAGIC of a variant of one of the existing methods [62]. In order to alleviate this problem, a novel, faster approach for the type 2 integral has been devised. It is demonstrated in the remainder of this chapter.

2.8.2 Calculation of the type 2 integral

The author's approach towards the evaluation of the type 2 integral consists of performing the angular integrations analytically and the radial integration by quadrature on a one-dimensional grid of points. Previous efforts [37, 38, 40] have focused on the analytical evaluation of the radial integrals

$$\int_0^\infty e^{-\xi r^2} i_l(br) i_m(cr) r^n dr \tag{2.73}$$

that emerge after the full expansion of equation (2.71) in spherical polar coordinates. We would expect the evaluation of this integral by quadrature to be inefficient compared to the analytical approach. On the other hand, quadrature makes possible the calculation of integrals which cannot be done analytically. We can therefore use it to evaluate directly the integral of equation (2.71) as a whole. This leads to an efficient method for evaluating the type 2 integral. This would not be possible without the presence of the angular projection operators that allow the isolation of

the basis functions from each other, as far as the angular integration is concerned.

First, the terms $\langle g_A|lm;B\rangle(r)$ are evaluated analytically at every point of the radial grid. The points r of the radial grid extend from the centre B of the ECP which is the centre of the coordinates. The following formula is used for this purpose, which can be derived by expressing the Gaussian function g_A in terms of functions located on the ECP centre [37, 38]

$$\langle g_A|lm;B\rangle(r) = 4\pi \sum_{k_x=0}^{a_x}\sum_{k_y=0}^{a_y}\sum_{k_z=0}^{a_z} \begin{pmatrix} a_x \\ k_x \end{pmatrix}\begin{pmatrix} a_y \\ k_y \end{pmatrix}\begin{pmatrix} a_z \\ k_z \end{pmatrix}$$

$$\overline{BA}_x^{a_x-k_x}\overline{BA}_y^{a_y-k_y}\overline{BA}_z^{a_z-k_z}\sum_{\lambda=0}^{l+\nu} r^{k_x+k_y+k_z}[e^{-\alpha(\overline{AB}^2+r^2)}i_\lambda(2\alpha\overline{AB}r)]$$

$$\sum_{\mu=-\lambda}^{\lambda} Z_{\lambda\mu}(\hat{AB})\int Z_{\lambda\mu}(\hat{\mathbf{r}})Z_{lm}(\hat{\mathbf{r}})\hat{x}^{k_x}\hat{y}^{k_y}\hat{z}^{k_z}d\Omega \qquad (2.74)$$

where $\nu = a_x + a_y + a_z$ is the angular momentum of g_A, $\overline{BA}$ is the distance from the centre B of the ECP to the basis function centre A and $\hat{AB}$ is the unit vector from B to A.

The angular integrals in the above equation were initially evaluated using Lebedev quadrature [22, 23, 24, 25]. The Lebedev quadrature grids and weights are designed to integrate exactly spherical harmonics up to a certain order L, i.e. if $\lambda+l+k_x+k_y+k_z \leq L$ the angular integrals in (2.74) should be calculated exactly. We have used quadratures with 302, 590 and 974 points for which L is 29, 41 and 53 respectively. By looking in the parameter tables for ECPs and basis sets it can be seen that the quadrature with 302 points would suffice for all combinations of existing ECPs and basis sets. So would of course the rest of the schemes with 590 and 974 points. However, we noticed that upon varying the scheme used, the results we obtained varied in the 6th or 7th decimal digit. This is a consequence of the small accuracy with which the Lebedev parameters are known. The same observation has been made by Treutler et. al. [63] in the context of molecular numerical integration grids for DFT integrals. They have used a "brute force" optimization procedure and the original results of Lebedev as input to refine the parameters up to 17 decimals for the grid with 434 points and L =35. We have chosen rather to abandon the

numerical evaluation of these angular integrals and to calculate them analytically. A group of subroutines written especially for this purpose were used [62]. They evaluate these integrals as linear combinations of angular overlap integrals of three real spherical harmonics.

The term $e^{-\alpha(\overline{AB}^2+r^2)}i_\lambda(2\alpha\overline{AB}r)$ has to be evaluated as the exponential of the sum of its logarithms for retaining precision. This can be understood by considering that the asymptotic values of the Gaussian term, the Bessel term and their product with increasing r, are zero, infinity and zero respectively. It often happens then that with some of the r values used in the quadrature the Gaussian term becomes zero within machine precision and its product with a finite number such as the Bessel function value is bound to be zero. This of course is not the true value of the product, which is still by no means negligible, but is an artefact of finite (double in our case) arithmetic precision. The use of logarithms eliminates this error. The spherical modified Bessel function of the first kind i_λ is computed by a standard implementation [64] and its asymptotic form is used for large values of its argument [65].

The computation of γ_{AC} is completed by summing the $\langle g_A|lm;B\rangle(r)$ and $r^{n_{kl}}\exp(-\zeta_{kl}r^2)$ terms over the radial grid

$$\gamma_{AC}=\sum_{i=1}^{n_r}\langle g_A|lm;B\rangle(r_i)\,\langle g_C|lm;B\rangle(r_i)\,r_i^{n_{kl}}\exp(-\zeta_{kl}r_i^2)\,w_i \qquad (2.75)$$

where n_r is the number of radial quadrature points and w_i are the corresponding weights.

A point worth noting is that the calculation of the $\langle g_A|lm;B\rangle(r_i)$ (which is the computationaly intensive step) scales linearly with the size of the system (number of basis functions N_{BF}). Of course, the radial quadrature part scales quadratically, but it has a small prefactor so its contribution is negligible for all systems we have tested. If the quadratic part starts to dominate in large systems, linear scaling could still be achieved, if necessary, by screening of integrals that can be predicted to be negligibly small.

For the calculation of derivatives of γ_{AC} with this mixed Analytical-Numerical

(AN) method, we have selected to avoid differentiating directly the ECP operator. Instead, we use the principle of translational invariance as has been demonstrated by Cui et al. [66] for other ECP integral methods.

We tested the mixed analytical-numerical method by comparing with an implementation of a variant [62] of the method of McMurchie and Davidson [38]. This was the original ECP implementation in MAGIC. It was ensured that the variant code yielded accurate results, however it was not optimised for speed. We found that the AN method is considerably faster than the variant which requires a prohibitively large amount of time for molecules larger than 4-5 atoms. A wide range of molecular geometries was used in the tests and they seem to have no effect on the AN method. For example, correct results are obtained for UO_2^{2+} (U ECP from [61], DZP basis on O) when varying the U-O distance from 0.01 to 10.0 a_0. These tests reassure us about the reliability of the AN method but they cannot exclude the possibility of failure in some "ridiculous" case.

Table 2.3 presents some timings for the calculation of ECP integrals with the McMurchie-Davidson variant and the new AN method. A variety of molecules, basis sets and ECPs were used. The time reported is for the calculation of both the first and the second integral on one R10000 processor on a Silicon Graphics Origin 2000 computer. These results prove the necessity for a new algorithm, much faster than the McMurchie-Davidson variant. All the subroutines of MAGIC were designed with robustness as well as speed in mind and they are fast enough to make calculations on large inorganic systems feasible. Therefore the McMurchie-Davidson variant would constitute a serious bottleneck for all our calculations as it requires in many cases more time to calculate the ECP integrals than the time necessary to run the SCF calculation or even more time than that available in the longest queue of a usual workstation. The AN method has eliminated this problem, reducing the time necessary for the evaluation of ECP integrals to a few seconds, or minutes, for the most difficult cases.

Table 2.3: Timings in seconds for the evaluation of both χ_{AC} and γ_{AC} with the variant of the McMurchie-Davidson (MD) method and the Analytical-Numerical (AN) scheme. N_{BF} is the number of basis functions and N_{ECP} is the number of ECP centres present on each molecule (on metal atoms, except in the case of C_{60} where all carbon atoms contain ECPs).

Molecule	Basis	N_{BF}	ECP	N_{ECP}	MD	AN
AuH	6311G*	45	[53]	1	2	1
AuH	6311G*	20	[51]	1	1	0
AuH	cc-pV6Z	144	[53]	1	581	26
AuH	cc-pV6Z	119	[51]	1	581	26
RbCl	DZP	54	[67]	1	109	3
RbCl	DZP	32	[50]	1	165	1
UO_2^{2+}	SVP	135	[54]	1	153	14
UO_2^{2+}	SVP	74	[61]	1	213	21
UF_6	DZ	165	[54]	1	837	23
UF_6	DZ	104	[61]	1	3251	29
UF_6-UF_6	DZ	208	[61]	2	87895	319
$K[PtCl_3(C_2H_4)]$	STO3G	106	[53]	2	3262	16
$K[PtCl_3(C_2H_4)]$	STO3G	106	[51]	2	2648	11
$Rh_4(CO)_{12}$	DZ	280	[51]	4	>4 days	1715
π-$C_7H_7Mo(CO)_3^+$	TZVP	328	[67]	1	92427	45
Cs(18c6)	TZ	353	[67]	1	118325	77
C_{60}	PVDZ	840	[67]	60	>4 days	12261

2.8.3 Radial Quadrature

As far as the radial quadrature is concerned, the Log3 scheme of Mura et al. [21] was found to be particularly efficient. In order to obtain the points, we start with a number n_r of equally spaced points x_i on the interval $(0, 1)$

$$x_i = \frac{i}{n_r + 1} \tag{2.76}$$

then these points are mapped to points r_i on the interval $(0, +\infty)$ by

$$r_i = -\xi \ln(1 - x_i^3) \tag{2.77}$$

where ξ is an empirically determined parameter and has the value 5 or 7, according to the type of atom [21]. The weights are given by

$$w_i = \frac{3\xi^3 x_i^2 \ln^2(1 - x_i^3)}{(1 - x_i^3)(n_r + 1)} \tag{2.78}$$

The form of equations (2.77) and (2.78) allows for the use of an integration technique that converges the values of the integrals to a certain predefined precision. We can gradually increase the number of points without having to recalculate the value of the integrand at the points we have already used in the previous step.

In particular, we can first evaluate the integrals with a number of radial points $n_r^{(1)}$ and weights given by equation (2.78). If we then choose to use $n_r^{(2)} = 2n_r^{(1)} + 1$ radial points for evaluating the integrals at improved precision, we observe that every second point

$$r_j^{(2)}, \quad j = 2, 4, \ldots, (n_r^{(2)} - 1) \tag{2.79}$$

coincides with a point of the first set $n_r^{(1)}$ and its corresponding weight $w_j^{(2)}$ is half of the weight $w_i^{(1)}$ of $r_i^{(1)}$. Therefore calculating an integral with all the $n_r^{(2)}$ quadrature points is equivalent to calculating it using only the subset

$$r_k^{(2)}, \quad k = 1, 3, \ldots, n_r^{(2)} \tag{2.80}$$

and adding to the result half of the value calculated in the previous step with the $n_r^{(1)}$ points.

Using this algorithm we can increase the number of quadrature points consecutively, and check the convergence of the integrals at each step. We use only the

extra points added in each step, therefore avoiding carrying out the integration from the beginning with all the points. In the current implementation, we start with 31 points and the results typically converge to the $10th$ decimal by the time we reach 2047 points or 4097 points for a few cases.

The performance of the Log3 scheme was found to be consistently better than that of the Euler-Maclaurin radial quadrature scheme [28] which was also examined. This scheme maps points to the $(0, +\infty)$ interval according to

$$r_i = \frac{x_i^2}{(1 - x_i)^2} \tag{2.81}$$

The Euler-Maclaurin scheme is not as efficient for our purpose, requiring on average an order of magnitude more points in order to produce the same results as the Log3 scheme. This trend was common in all examples tried. As an illustration, the number of points required by each type of grid for a variety of molecules, ECPs and basis sets is shown in Table 2.4.

Both quadrature schemes are routinely used in DFT calculations for the evaluation of the exchange-correlation potential matrix elements. The reason for the better performance of the Log3 scheme could be attributed to its specific design for integration of Gaussian functions in contrast to the Euler-Maclaurin scheme which is supposed to be of more general applicability.

Having decided upon the type of quadrature and integration technique to be used, there remains the implementational question of memory usage as the number of basis functions and quadrature points increases. The values of $\langle g_A|lm;B\rangle(r_i)$ are calculated, contracted to $\langle G_A|lm;B\rangle(r_i)$ and stored in an array of size $N_{BF} \times n_r^{(k)}$ where N_{BF} is the number of basis functions. Furthermore the values of $e^{-\alpha(\overline{AB}^2+r^2)}i_\lambda(2\alpha\overline{AB}r)$ are also precalculated and stored in an array of size $N_{exp} \times (L + \nu_{max}) \times n_r^{(k)}$, where N_{exp} is the total number of primitive Cartesian Gaussian exponents and ν_{max} is the highest orbital angular momentum in the basis set. The sizes of these arrays can become substantial for large molecules when the number of basis functions approaches or exceeds 1000 and they are obviously affected by the increasing number of quadrature points in the iterations for converging the integrals. This dissipation of memory can be avoided by performing the radial integration us-

Table 2.4: Comparison of the performance of the Log3 and Euler-Maclaurin radial grids. Each molecule contains only one ECP centre (the metal atom) with the accompanying valence basis set. The integrals were converged to the 10th decimal digit.

Molecule	Basis	ECP	Log3 points	Euler points
RbCl	631G2DP	Wadt et al. [50]	4095	16383
AuH_2O^+	DZ	Wadt et al. [51]	4095	32767
UO_2^{2+}	DZP	Hay et al. [61]	2047	65535
UF_6	DZ	Hay et al. [61]	1023	65535
AgH	PVTZ	Hay et al. [49]	255	32767
$Pt(C_2H_4)Cl_3^-$	DZ	Wadt et al. [51]	127	65535
RbCl	631G2DP	[67]	127	255
AuH_2O^+	DZ	Andrae et al. [53]	127	511
UO_2^{2+}	DZP	Küchle et al. [54]	127	255
UF_6	DZ	Küchle et al. [54]	127	255
AgH	PVTZ	Andrae et al. [53]	127	511
$Pt(C_2H_4)Cl_3^-$	DZ	Andrae et al. [53]	127	511

ing *batches* of radial points. In such a batch formalism, subsets of n_{batch} of the radial points are used in each step of the integration, until all the $n_r^{(k)}$ radial points are exhausted. Thus, $n_r^{(k)}$ is replaced by n_{batch} in the sizes of the relevant arrays. In the present implementation the value of n_{batch} was set to 64. The use of batches of points makes the memory demands of the program more or less the same as those of the usual one-electron integrals.

It is appropriate here to make a further comment on the accuracy of the AN method. We can observe from equation (2.74) that every $\langle g_A|lm;B\rangle(r_i)$ term involves several spherical modified Bessel functions of the first kind i_l multiplied by a steeply decreasing exponential term. Even though we have ensured that accuracy is maintained by using logarithms, one could still claim that we have not succeded in our goal. This would however affect our results when we switch from Log3 to Euler-Maclaurin quadrature because the distribution of points and weights in the two cases is substantially different. However the integrals obtained using the two quadratures are identical up to the number of decimals we decided to converge them, though they require a much larger number of quadrature points for the Euler-Maclaurin case. This fact is a proof that no numerical errors, due to the finite precision of the computer, affect our results.

2.8.4 Illustrative results

We wish to demonstrate the capabilities of the AN method with calculations on some large, commonly encountered molecules. For this purpose, some single point energies of molecules containing various heavy elements with ECPs are given in Table 2.5. Single point energies are a means of verifying the code and provide a point of reference for others who may try the AN method.

The uranium and rhodium atoms were represented by ECPs with the corresponding basis sets from references [61] and [49] respectively. The geometries of the rhodium clusters were taken from crystal structures with the aid of the Quest program of the Cambridge Crystallographic Database[68], while the geometries of the 18crown6 and the uranyl were obtained from a molecular mechanics geometry optimisation using Cerius^2 [12]. The LDAX exchange functional [16] was used

throughout and no correlation functional was included. Standard double zeta basis sets on the atoms not bearing ECP's were used.

Table 2.5: Single point LDAX(exchange) energies

Molecule	Energy (E_h)
$Rh_4(CO)_{12}$	-1428.3449
$Rh_8(CO)_{19}C$	-2337.8623
$UO_2(18crown6)^{2+}$	-1104.7779
UO_2^{2+} + 18crown6	-1104.2977

Carbonyl clusters of metals are common examples of molecules with metal-metal bonds [69]. There are numerous experimental studies on these systems due to their complexity of structure, variety of unusual reactions, resemblance to bulk metals and possible use in catalysis [70, 71]. The understanding of their electronic structure is also a field of active research [72]. There are no localised orbitals and the chemical concept of a bond between two atoms due to an electron pair cannot be used. Their structures are explained often in terms of electron counting rules which have been derived from rudimentary LCAO arguments. There are no general trends and correlations with the other great class of clusters, the halide clusters whose properties are rationalised by different arguments. Our aim is to optimise the geometries of representative types of clusters at the DFT level of theory with the most important relativistic contributions accounted for through the use of ECPs. We then hope to derive conclusions concerning the stability and electronic structure of these compounds.

Ligands which bind uranium, plutonium and other actinides are of prime importance in the nuclear industry. For example, ligands such as tributyl phosphate (TBP) are used in the separation by extraction of uranium and plutonium from nuclear fission products. Also, special ligands for removing actinides from the blood in cases of contamination exist [73]. There is potential for improving the efficiency of such separative processes by designing ligands with better selectivity. Experimental investigation of such systems is quite expensive and time consuming because of the

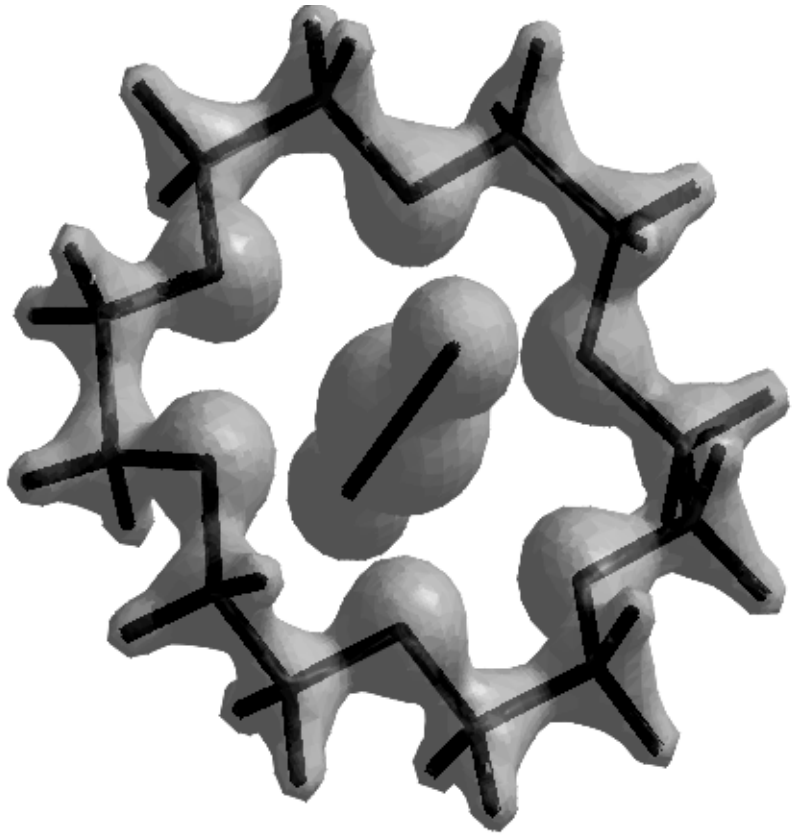

Figure 2.1: Plot of a density isosurface of $UO_2(18crown6)^{2+}$. The U core is represented by an ECP and therefore its core electron density is not included in the plot.

hazards involved. A code like MAGIC is expected to provide chemically useful information on such systems. As a starting model we have decided to investigate the interaction of a uranyl cation with the 18crown6 ether. Results by other workers using the Molecular Dynamics approach [74] claim that the complex is stable in the gaseous phase. In the gaseous phase, we find a dissociation energy of $0.4802E_h$ (301.3 kcal/mol) which indicates quite a strongly bound complex (see Table 2.5). A plot of a density isosurface of the complex is given in Figure 2.1.

Even in cases where relativistic effects are negligible, such as third row atoms, ECPs are a common choice because they reduce substantially the cost of a calculation with very small error. As a demonstration of this fact, the geometry of a

Table 2.6: Selected bond lengths (Å) and angles (°) of the optimised structures of P_7 with Molecular Mechanics (MM), All-Electron (AE) LSDA and ECP LSDA calculations.

Bond/Angle	MM	AE LSDA	ECP LSDA
P1-P2	1.780	2.219	2.061
P1-P4	1.780	2.245	2.044
P4-P6	1.780	2.246	2.041
P6-P5	1.780	2.216	2.059
P1-P4-P3	90.0	91.9	93.4
P2-P3-P7	90.0	106.0	110.3
P1-P2-P3	90.0	93.5	92.3

cluster of seven phosphorus atoms, P_7, was optimised with and without the use of ECPs. The unrestricted Kohn-Sham formalism with one unpaired electron was used, within the Local Spin Density Approximation (LSDA) for exchange and correlation which consists of the uniform electron gas exchange functional [16] and the VWN correlation functional by Vosko, Wilk and Nusair [75]. For the all-electron calculation the SVP basis of Ahlrichs et. al. [76] was used while in the ECP calculation the 10 core electron ECP of Bergner et al. [77] was used. The bases for the valence orbitals were double zeta plus polarisation in both cases and therefore of comparable quality. The starting geometry was obtained by a Molecular Mechanics (MM) optimisation with the Cerius^2 package [12] using the universal force field of Rappé et. al. [78]. The ECP calculation was significantly cheaper, with only 35 electrons and 98 basis functions in comparison to 105 electrons and 133 basis functions for the all-electron calculation. The optimised geometries are shown in Figure 2.2. Selected bond lengths and angles are given in Table 2.6.

It can be observed that the ECP results compare well with the all-electron results and the difference is of the order of magnitude of errors resulting from the inexact description of electron correlation. Part of the difference can be attributed to the ECP parameters which have been derived from Hartree-Fock (HF) calculations. They are therefore supposed to include the effects of HF core orbitals, which

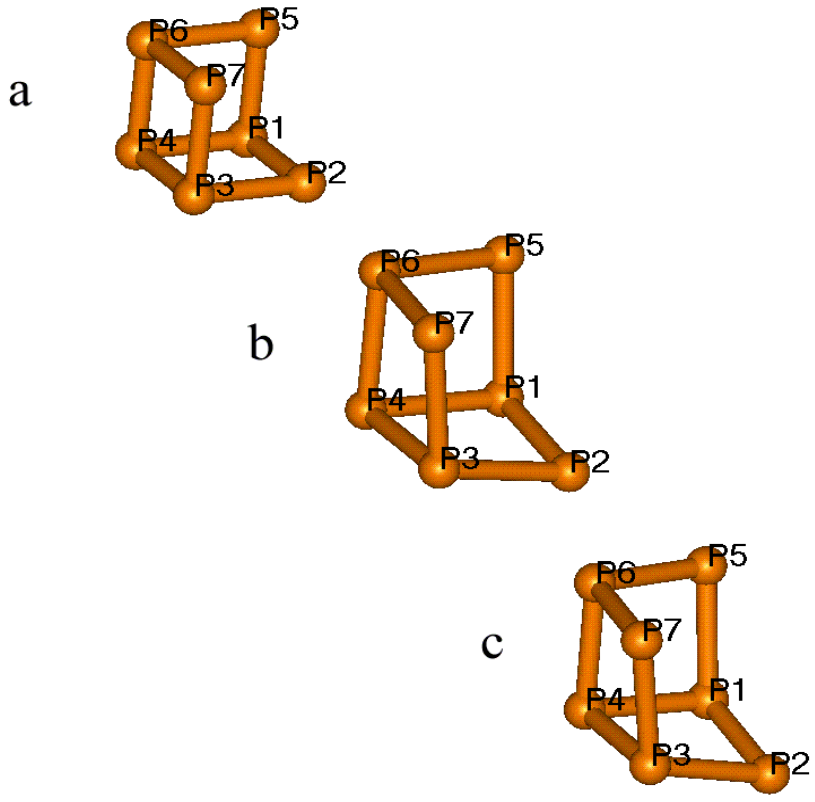

Figure 2.2: Optimised geometries of a P_7 cluster with different methods. (a) Molecular mechanics. (b) All-electron LSDA DFT. (c) ECP LSDA DFT.

should be somewhat different from the effects of DFT core orbitals. The all-electron and ECP bond lengths in Table 2.6 are comparable with the bond lengths of the orthorhombic, rhombohedral and cubic allotropes of black phosphorous which are 2.23 Å, 2.13 Å and 2.38 Å respectively [69]. Both all-electron and ECP geometry results differ quantitatively and qualitatively from the molecular mechanics results that predict a cubic structure for P_7 without any distortion. The magnitude of the dipole moment of the optimised cluster is 0.55 D in the all-electron case and 0.74 D in the ECP case.

2.8.5 Conclusions about the AN method

An efficient approach which combines analytical angular with numerical radial integration is suggested for calculating the ECP integrals that involve projection operators. It is much simpler in concept and implementation than purely analytical integration methods. The implementation of the method has been done in the MAGIC program and is used for calculations on large molecules.

2.8.6 The DFT molecular energy in calculations using ECPs

What we have achieved with the use of ECPs is to separate the core energy which is the largest part of the energy of the molecule from the valence energy which is a very small fraction. The ECPs take care of the core-valence interaction energy within the independent particle model approximation, and the DFT calculates the energy of the valence electrons, including valence-valence correlation effects. The self-energy of the electrons of each atomic core is supposed to be independent of the chemical environment of the atom, a constant according to the basic assumption of ECPs, and therefore we neglect it as it contains no chemically useful information. What is left then is the inclusion of the interaction of the core electrons of one ECP bearing atom with those of another, or with the nuclear charge of an atom without an ECP. It is not difficult to show that this term can be approximated by an electrostatic repulsion between point charges with magnitude equal to the number of valence electrons on each core [37]. The expression for the total KS-DFT energy

is therefore:

$$E[\rho_v] = \sum_v \langle \phi_v | \hat{h}^{eff} | \phi_v \rangle + E_J[\rho_v] + E_{xc}[\rho_v] + \sum_{A<B} \frac{(Z_A - N_A)(Z_B - N_B)}{|\mathbf{A} - \mathbf{B}|} \quad (2.82)$$

The first term contains the independent particle kinetic energy, nuclear attraction and effects of the core, all represented by the $\hat{h}^{eff}$ operator. The functions ϕ_v are the valence orbitals, the only orbitals that exist in an ECP calculation. The remaining terms are the self-interaction (Coulomb) energy $E_J[\rho_v]$ of the valence density ρ_v, the exchange-correlation term $E_{xc}[\rho_v]$ and the (approximate) interaction between the electrons of one core with those of another. N_A is the number of core electrons of atom A and is set to zero if this atom does not contain an ECP.

Chapter 3

Coulomb Energy Evaluation

3.1 Introduction

3.1.1 Density Functional Theory for large systems

Density Functional Theory (DFT) has been established as a practical method for including electron correlation effects in calculations on chemically important molecular systems. While research into finding improved functionals continues, there are a large number of reasonably accurate functionals available. Many studies of chemical properties have been carried out using those functionals. To this end, an efficient computer program is essential as the amount of computation necessary is large. In the regime of the size of molecules which are of practical interest to many experimental chemists, the number of integrals necessary for a DFT calculation is simply too large to store in core memory or on disk. *Direct SCF* algorithms, first introduced by Almlöf et al. [79], are the only possibility. This breakthrough in computational chemistry was made possible by reducing the prohibitive and unnatural cost of such a calculation, which appeared to be proportional to N_{BF}^4, where N_{BF} is the number of basis functions, a quantity proportional to the size of the molecular system. In the Direct methodology, the integrals are calculated afresh in every SCF cycle and tests are used to skip the evaluation of integrals which are predicted to make zero contribution to the Fock matrix. As a result, the cost of the calculation scales quadratically for sufficiently large systems. Refinements to this

procedure were developed by Ahlrichs and coworkers [80, 81]. The direct SCF developments were originally applied in Hartree-Fock calculations. They are however readily transferable to Kohn-Sham theory and in fact easier to implement due to the lack of exchange integrals.

In Kohn-Sham theory the contributions to the electronic interaction energy are expressed as functionals of the electronic density. These are the exchange-correlation term E_{XC} and the Coulomb term E_J

$$E_{XC}[\rho] = \int f(\rho, \nabla\rho, \ldots) dv \tag{3.1}$$

$$E_J[\rho] = \frac{1}{2} \int \int \rho(\mathbf{r}_1) \frac{1}{r_{12}} \rho(\mathbf{r}_2) dv_1 dv_2 \tag{3.2}$$

The evaluation of E_{XC} is typically carried out with numerical integration. Its computational cost is a small percent of the whole cost of a DFT calculation for medium sized molecules ($\sim$ 50 atoms) and it has been shown that it can be made to scale linearly with N_{BF} [82]. It is the evaluation of the Coulomb term which dominates the computational procedure as soon as molecules of reasonable size are encountered. Methods for calculating this term which scale linearly asymptotically have been invented [83, 84]. However, their breakeven point with conventional methods has been demonstrated to be of the order of hundreds of basis functions and this for cases of molecules of light atoms with extended geometries, such as linear hydrocarbons, graphite sheets and water clusters. It is therefore reasonable to expect that in large complexes containing heavy atoms or three dimensional metal clusters the breakeven point will be located at a prohibitively large number of basis functions. This renders current linear scaling methods unsuitable for practical, every day calculations on such compounds. The complexity of the implementation of such methods, without any optimum "recipe" available in the literature, is another drawback. Quantum Chemistry programs such as MAGIC [85] are mainly intended for the study of inorganic compounds containing heavy elements [86]. Methods for reducing the cost of the calculation by having a small prefactor even though they still scale quadratically would lead to significant benefits in this case.

3.1.2 Representation of the density by an auxiliary basis set

A quadratically scaling method for calculating the Coulomb energy which is faster than the conventional approach is the *fitted density approximation*. It was used in different forms in the early work of Baerends [87] and Dunlap [88]. It is based on the observation that the basis we use to describe the molecular orbitals is more flexible than required to describe the density. This can be more clearly understood if we consider that the basis set is required to describe all molecular orbitals. These are usually quite different from each other and contain features not present in the density (eg. sign changes, different levels of localisation). If $\{\chi_i\}_{i=1}^{N_{BF}}$ is the set of basis functions we use to express the orbitals, the density is represented as a quadratic form in the basis in terms of the density matrix $\mathbf{D}$:

$$\rho(\mathbf{r}) = \sum_{i=1}^{N_{BF}} \sum_{j=1}^{N_{BF}} \chi_i(\mathbf{r})\chi_j(\mathbf{r})D_{ji} \tag{3.3}$$

When the basis consists of Gaussian functions, then according to the product rule, $\chi_i(\mathbf{r})\chi_j(\mathbf{r}) = \chi_t(\mathbf{r})$, where $\chi_t(\mathbf{r})$ is a linear combination of a few Gaussian functions, centred on the line joining the centres of $\chi_i(\mathbf{r})$ and $\chi_j(\mathbf{r})$ [89]. Consequently, the above expression for the density can equivalently be written as

$$\rho(\mathbf{r}) = \sum_{t=1}^{N_{BF}(N_{BF}+1)/2} \chi_t(\mathbf{r})q'_t \tag{3.4}$$

where $q'_{i(i-1)/2+j} = (2 - \delta_{ij})D_{ij}$. As the space of the $\chi_t(\mathbf{r})$ functions is nearly degenerate [90, 91], it is desirable to obtain an accurate representation of the density in terms of a new basis set, especially tailored for this purpose. This new basis set $\{f_t\}_{t=1}^{N_{AUX}}$ is commonly called the auxiliary basis set. The density is approximated by the auxiliary basis set as

$$\rho(\mathbf{r}) \simeq \rho_{AUX}(\mathbf{r}) = \sum_{t=1}^{N_{AUX}} f_t(\mathbf{r})q_t \tag{3.5}$$

where the expansion coefficients, or "charges" q_t [92, 93] are determined in some optimum way. The approximate density is subsequently used to calculate the Coulomb energy

$$E_J[\rho] \simeq \frac{1}{2} \int \int \rho_{AUX}(\mathbf{r}_1)\frac{1}{r_{12}}\rho_{AUX}(\mathbf{r}_2)dv_1dv_2 \tag{3.6}$$

The above result would equal the exact Coulomb energy only if the auxiliary set was a complete basis with an infinite number of functions or the set of $N_{BF}(N_{BF}+1)/2$ functions arising from all the distinct products of pairs of the original basis functions. None of these choices would result in any computational savings however. To have any significant savings, N_{AUX} has to be proportional to N_{BF}. Indeed, Eichkorn et al. [94, 95] have constructed auxiliary basis sets for every element (excluding the lanthanides and the actinides) which satisfy the requirement

$$N_{AUX} < 3N_{BF} \tag{3.7}$$

and it is claimed that this leads to an increase of the speed of calculation of E_J by an order of magnitude. The absolute error introduced by these auxiliary sets is expected to be smaller than the errors arising from the incompleteness of the basis sets and the inexact treatment of correlation. In fact, the relative error, which is important for chemical properties, is expected to be even less and should not hinder attempts to improve our results in an effort to achieve "chemical accuracy" of 1 mE_h [96].

The MAGIC quantum chemistry program, intended for performing relativistic calculations on large systems containing heavy atoms [97, 98], is able to calculate the Coulomb energy either by an auxiliary basis fitted density, or with the "exact" density. In agreement with the above, it has been observed that the fitting density approximation is markedly faster than the exact calculation. We find however that there are very few auxiliary basis sets available in the literature [94, 95, 99] and the method's accuracy has not been tested extensively. A great part of this chapter is devoted to testing the robustness of some of the most widely used auxiliary basis sets with respect to the size of the basis set. We wish to examine their performance for smaller and larger basis sets than the ones they were meant to be used with and see if we can establish criteria for judging the quality of the representation of the fitted density without comparing with the "exact" calculation. In general, every basis set is not accompanied by a corresponding auxiliary set. Therefore, even though the auxiliary fit method is efficient, it may not be of much practical value without general-purpose auxiliary sets, accurate for a range of basis sets.

In section 3.2 a brief comparison of density fitting procedures and the underlying theory including the procedure implemented in MAGIC, is given. In section 3.3 the calculations performed, in order to answer the questions we have posed, are described. Section 3.4 is a discussion and rationalisation of the results obtained. This investigation ends in section 3.5 where we reach some conclusions regarding the transferability of auxiliary basis sets and suggest ways of predicting how well they will perform with a particular basis set and molecule.

3.2 Density fitting procedures

We summarize briefly and compare the most common density fitting procedures in the literature. The notation of earlier works in the field is followed. Both the basis set and the auxiliary basis set consist of nonorthogonal functions. The first step in fitting procedures is to orthonormalise the auxiliary basis set. Symmetric orthonormalisation is used for this purpose. This leads to two broad classes depending on the kind of metric used.

3.2.1 Inner product: Overlap integral

The overlap integral

$$S_{ts} = \int f_t^*(1) f_s(1) dv_1 = \langle f_t | f_s \rangle \tag{3.8}$$

is used as a metric. Then symmetric orthonormalisation

$$\mathbf{f}' = \mathbf{f}\mathbf{S}^{-\frac{1}{2}} \tag{3.9}$$

yields the auxiliary basis set $\{f_t'\}_{t=1}^{N_{AUX}}$ which is orthonormal in the linear vector space with metric $\mathbf{S}$. The density can be fitted now by simply projecting it onto the orthonormal auxiliary basis.

$$\rho \simeq \tilde{\rho} = \mathbf{f}'\langle \mathbf{f}'|\rho\rangle = \mathbf{f}\,\mathbf{S}^{-\frac{1}{2}}\langle \mathbf{f}\,\mathbf{S}^{-\frac{1}{2}}|\rho\rangle = \mathbf{f}\,\mathbf{S}^{-1}\langle \mathbf{f}|\rho\rangle = \mathbf{f}\tilde{\mathbf{q}} \tag{3.10}$$

The Coulomb energy can therefore be represented by

$$2E_J \simeq (\tilde{\rho}|\tilde{\rho}) \quad = \quad (\mathbf{f}\mathbf{S}^{-1}\langle \mathbf{f}|\rho\rangle | \mathbf{f}\mathbf{S}^{-1}\langle \mathbf{f}|\rho\rangle)$$

$$\begin{aligned} &= \langle\rho|\mathbf{f}\rangle\mathbf{S}^{-1}(\mathbf{f}|\mathbf{f})\mathbf{S}^{-1}\langle\mathbf{f}|\rho\rangle \\ &= \langle\rho|\mathbf{f}\rangle\mathbf{S}^{-1}\mathbf{V}\mathbf{S}^{-1}\langle\mathbf{f}|\rho\rangle \end{aligned} \tag{3.11}$$

where $\mathbf{V}$ is the matrix of two-centre two-electron integrals in the auxiliary basis, see equation (3.13) below. Equation (3.11) was originally derived by minimising the mean square deviation of the fitted density [87]:

$$\int |\rho(\mathbf{r}) - \tilde{\rho}(\mathbf{r})|^2 dv \tag{3.12}$$

3.2.2 Inner product: Electrostatic interaction integral

The electrostatic interaction integral

$$V_{ts} = \int\int f_t^*(1)\frac{1}{r_{12}}f_s(2)dv_1dv_2 = (f_t|f_s) \tag{3.13}$$

can serve as another definition of inner product and be used as a metric. Symmetric orthonormalisation in a similar fashion as before

$$\mathbf{f''} = \mathbf{f}\mathbf{V}^{-\frac{1}{2}} \tag{3.14}$$

yields the auxiliary basis set $\{f_t''\}_{t=1}^{N_{AUX}}$ which is orthonormal in the linear vector space with metric $\mathbf{V}$. The density is again expanded in the orthonormal auxiliary basis

$$\tilde{\tilde{\rho}} = \mathbf{f''}(\mathbf{f''}|\rho) = \mathbf{f}\mathbf{V}^{-\frac{1}{2}}(\mathbf{f}\mathbf{V}^{-\frac{1}{2}}|\rho) = \mathbf{f}\mathbf{V}^{-1}(\mathbf{f}|\rho) = \mathbf{f}\tilde{\tilde{\mathbf{q}}} \tag{3.15}$$

The expression for the Coulomb energy in this case is

$$\begin{aligned} 2E_J \simeq (\tilde{\tilde{\rho}}|\tilde{\tilde{\rho}}) &= (\mathbf{f}\mathbf{V}^{-1}(\mathbf{f}|\rho)|\mathbf{f}\mathbf{V}^{-1}(\mathbf{f}|\rho)) \\ &= (\rho|\mathbf{f})\mathbf{V}^{-1}(\mathbf{f}|\mathbf{f})\mathbf{V}^{-1}(\mathbf{f}|\rho) \\ &= (\rho|\mathbf{f})\mathbf{V}^{-1}\mathbf{V}\mathbf{V}^{-1}(\mathbf{f}|\rho) \\ &= (\rho|\mathbf{f})\mathbf{V}^{-1}(\mathbf{f}|\rho) \end{aligned} \tag{3.16}$$

By noting that $(\rho|\tilde{\tilde{\rho}}) = (\tilde{\tilde{\rho}}|\tilde{\tilde{\rho}})$, a variational principle can be written which shows that the error in Coulomb energy due to auxiliary basis set incompleteness is negative

$$2E_J \geq (\tilde{\tilde{\rho}}|\tilde{\tilde{\rho}}) \tag{3.17}$$

The result of equation (3.16) was originally derived by minimising the Coulomb energy of the residual of the fitted density [88]:

$$\frac{1}{2}\int\int \frac{(\rho(\mathbf{r}_1)-\tilde{\tilde{\rho}}(\mathbf{r}_1))(\rho(\mathbf{r}_2)-\tilde{\tilde{\rho}}(\mathbf{r}_2))}{|\mathbf{r}_1-\mathbf{r}_2|}dv_1dv_2 \tag{3.18}$$

3.2.3 Combination of the two methods

If the two ways of fitting the density are combined the following expression results.

$$2E_J \simeq (\tilde{\rho}|\tilde{\tilde{\rho}}) = \langle\rho|\mathbf{f}\rangle\mathbf{S}^{-1}(\mathbf{f}|\rho) \tag{3.19}$$

As will be seen in the next subsection, this expression is a compromise in computational cost between equations (3.11) and (3.16). When used in a direct SCF scheme it requires the evaluation of three-index two-electron integrals and three-index overlap integrals in every SCF cycle.

3.2.4 Comparison of the three approximations

In order to use equation (3.11) in a direct SCF calculation, one would have first to calculate the $\mathbf{S}^{-1}\mathbf{V}\mathbf{S}^{-1}\langle\mathbf{f}|\rho\rangle$ column vector and then contract it with the $\langle\rho|\mathbf{f}\rangle$ row. These two steps require the calculation of three-index overlap integrals twice per SCF cycle. In a similar way we can show that for equation (3.16) it is necessary to calculate three-index-two electron integrals twice per SCF cycle. The three schemes therefore have substantially different computational costs. They also differ substantially in their performance in fitting the density. By intuition, we would expect the use of the electron repulsion integral as a metric to yield better results since the reason we are fitting the density is to approximate such an integral. Or in other words, minimising directly the Coulomb energy of the density residual should lead to better results as far as energy is concerned. This assumption was verified by Vahtras et al. [100] through a series of simple tests. They found that for every auxiliary basis set they tried equation (3.16) (the "V approximation") was far more accurate than (3.11) (the "SVS approximation") while the results due to (3.19) (the "S approximation") were in between. The variational principle of equation (3.17) is an added benefit of the V approximation that is also referred as the RI-J approximation (Resolution of the Identity for the Coulomb energy). It applies strictly for

ρ being the density of the RI-J calculation. However under the assumption that the density $\rho_{\text{“exact”}}$ of the non-fitted calculation is almost equal to ρ one can deduce that the RI-J error in energy should be negative. When this subtle generalisation is valid, it leads to some cancellation of systematic errors in energy differences. As a consequence, the V approximation has become the most widely used today. Some results of accuracy as a function of auxiliary basis set size have been given by Van Alsenoy [101] for the S approximation with the added constraints of preserving charge and dipole moment. However the auxiliary basis sets used were far from optimised and explicit corrections to the Coulomb energy in terms of four index electron repulsion integrals had to be included.

[We should note at this point that in the case of hybrid exchange-correlation density functionals the auxiliary basis set approximation is not as efficient since four-index integrals are necessary for the exchange energy and have to be calculated as well.]

The program approximates the Coulomb energy using the V approximation. This method was chosen because of its accuracy. Furthermore, calculation of the gradient (section 5.2) or higher derivatives is not much more complicated than the conventional approach [102].

3.3 Calculations and results

The computational efficiency as well as the quality of the V approximation depend on the auxiliary basis. There is little justification for using RI-J DFT unless the auxiliary basis is optimised for both speed and accuracy. This is achieved by requiring the auxiliary sets to represent the density of the isolated atom in such a way as the error which results in the atomic energy is below a certain threshold. It is important to note however that the optimization procedure of the auxiliary basis is carried out for a particular kind of basis. There is therefore no *a priori* guarantee that they are going to perform equally well for basis sets other than the one for which they were optimised. On the other hand, the construction of an auxiliary basis is not a trivial task and is certainly not one that can be performed on a daily

basis for each basis set we encounter. Consequently, the practice of considering the available auxiliary basis sets more or less as "universal" has prevailed. They are thus used with little regard to the basis set selected. We wish to examine the validity of this assumption for a variety of basis sets and molecules. Furthermore we wish to gain some insight into the quality of the RI-J approximation for a particular auxiliary basis set as a function of the basis set and the type of molecule.

For this study, it was decided to use the auxiliary basis sets of Ahlrichs et. al. [94, 95] which were designed specifically for basis sets of SVP and TZVP quality by the same group [76, 58]. These auxiliary sets are available for almost all the elements, apart from the actinides and lanthanides and are meant to produce an error of less than 0.2 mE_h per atom. We decided to treat these auxiliary basis sets as standard "universal" auxiliary basis sets.

Six types of basis sets were selected [103] which we describe in order of increasing size. First was the STO3G minimal basis set of Pople [104, 105]. Calculations with a minimal basis are essentially semiempirical as a result of its incompleteness and lack of polarization functions. The second basis set that we use is the Double Zeta (DZ) basis of Dunning et. al. [106, 107]. This is certainly an improvement over the STO3G but still lacks polarisation functions. Next in the series come the SVP and TZVP bases of Ahlrichs et al., the ones for which the auxiliary basis sets were designed. These were therefore expected to perform better than the rest of the basis sets. These sets are fully optimised (exponents + contraction coefficients) and describe well both the core area with large contractions and especially the valence area. The fifth basis set we tried is the cc-pVTZ basis of Dunning et al. [108, 109]. This basis, like the TZVP, deals with the core orbitals with large fixed contractions and puts the emphasis on the valence region which is mainly responsible for most molecular properties, especially the ones related to the energetics of bond breaking and bond forming. It is substantially larger than the TZVP and contains polarisation functions with angular momentum up to and including d for Hydrogen and f for second and third row atoms. The sixth and final basis that we employed was the cc-pVQZ, again by Dunning et al. [108, 109]. This basis further extends cc-pVTZ with its four zeta description of the valence region and is probably sufficient

for the most demanding of DFT calculations. It contains polarisation functions up to and including f for Hydrogen and g for first and second row atoms.

In order to determine the effect of the functional, if any, on the accuracy of the RI-J method, we ran some of the calculations with the Local Density Approximation exchange-only (LDAX) functional [16] and some with the Becke 88 gradient corrected exchange functional [59] plus the correlation contribution by Lee, Yang and Parr [60] (BLYP). The LDAX functional is equivalent to the Xα exchange functional whose adjustable parameter α can be determined according to different criteria [110, 111]. The value $\alpha = 2/3$ was selected which comes from the uniform-electron-gas approximation for the exchange energy [16].

As we are interested in ways of evaluating the quality of the RI-J approximation we assess here the usefulness of the Weighted Root Mean Square deviation of the fitted Density (WRMSD) from the "exact" density for this purpose. The WRMSD test computes the following quantity at the end of an RI-J calculation:

$$\sqrt{\sum_{i}^{N_{GRID}} w_i |\rho(\mathbf{r}_i) - \rho_{AUX}(\mathbf{r}_i)|^2} \tag{3.20}$$

where ρ and ρ_{AUX} are given by equations (3.3) and (3.5) respectively. Both of them are computed with the density matrix $\mathbf{D}$ and the charges $\mathbf{q}$ of the RI-J calculation. The points $\mathbf{r}_i$ and the weights w_i come from the molecular quadrature grid that MAGIC uses to calculate the DFT exchange-correlation energy and matrix elements (section 1.5). We note that these grids are extensive with 9060 grid points for every first row element, increasing to 15100 points per atom for actinide elements. It would be reasonable to expect that the WRMSD test should produce a good indication of the quality of the RI-J approximation for results using the same molecule with different basis sets.

MAGIC is able to perform both "exact" and RI-J (V approximation) DFT calculations. We have selected a wide variety of molecules on which we have run both types of calculations. Some of them are inorganic compounds and for their metal atoms we have used ECPs (section 2.7) to represent the interaction of the core electrons with the valence. Therefore, for the metal atoms, the valence basis set which accompanies their ECP is always used regardless of what basis is used for

the rest of the atoms in the molecule. We use this practice very often in applications because ECPs are a cheap and simple way of taking into account the most important of the relativistic effects. We selected the ECPs of the Stuttgart group [52, 54] as they have small cores and large valence basis sets for maximum accuracy and also because our auxiliary sets are optimised especially for them.

The results we obtained for each molecule are given in Tables 3.1 and 3.2. The geometry of RbCl was obtained from a Molecular Mechanics (MM) optimisation and the BLYP functional was used. The geometry of $K[PtCl_3(C_2H_4)]$ was optimised by MAGIC using the SVP basis set and the LDAX functional was used throughout. The geometries of CH_2FCOO^- and $CH_3C_6H_5$ were optimised by MM and the BLYP and LDAX functionals were used respectively. NO_2, B_2H_6 and $TiCl_4$ were optimised by MAGIC with an SVP basis and the BLYP, LDAX and BLYP functionals were used respectively. The geometry of $(H_3PAu)_2S$ was adopted from similar molecules in the literature [112] and the BLYP functional was used. Finally, the LDAX functional was used for both H_3COSiH_3 and $CH_3NH_3^+$ whose geometries were obtained by MM. The number of auxiliary functions and the number of basis functions for each basis set for each molecule are given. For each case we performed an "exact" calculation with four-index two-electron integrals and an RI-J calculation and we present the error in total molecular energy, the error in atomization energy and the WRMSD. Atomisation energy is the difference of the total energy of the molecule from the sum of the energies of the neutral isolated atoms comprising the molecule, both calculated either with or without the RI-J approximation.

Having obtained the above mentioned results on the RI-J approximation for different molecules and basis sets, we performed calculations with the same basis set but on molecules of increasing size. The purpose here was to gain some insight into the effect of the RI-J approximation as the molecules become larger. We therefore ran calculations on crown ethers, starting with 3c1 (C_2H_4O) , to 6c2, all the way up to 21c7. The LDAX functional and the SVP basis set were used. Table 3.3 contains the results of these calculations, which are again the errors in the energies and atomization energies and the WRMSD. The energy error and atomization energy error are plotted as functions of the number of monomer units (3c1) in Figure 3.1.

Table 3.1: Errors in total energy (E) and atomisation energy (EA) and WRMSD values (equation (3.20)) for the RI-J method. The number of auxiliary basis functions for each molecule is given in parentheses under its name. Also given are the functional and the method for obtaining the geometry (eg. BLYP//MM means that the BLYP functional was used and the geometry was obtained by molecular mechanics).

Molecule	Basis Set	N_{BF}	$E-E_{RI\text{-}J}$ (mE_h)	$EA_{RI\text{-}J}-EA$ (mE_h)	WRMSD ($\times 10^7$)
RbCl	STO3G	39	8.110	0.249	3.33
(74)	DZ	48	0.602	0.533	1.09
BLYP//MM	SVP	49	0.567	0.546	0.99
	TZVP	53	0.643	0.611	1.01
	cc-pVTZ	69	0.736	0.705	1.01
	cc-pVQZ	104	0.892	0.801	1.27
$K[PtCl_3(C_2H_4)]$	STO3G	106	55.259	1.304	9.83
(439)	DZ	147	31.943	0.034	8.12
LDAX//LDAX(SVP)	SVP	172	31.753	0.101	8.09
	TZVP	198	31.856	0.186	8.12
	cc-pVTZ	312	32.018	0.342	8.12
	cc-pVQZ	567	32.276	0.281	8.20
CH_2FCOO^-	STO3G	27	2.288	3.567	2.40
(256)	DZ	54	0.301	0.267	1.72
BLYP//MM	SVP	85	0.400	0.374	2.08
	TZVP	112	0.464	0.444	2.06
	cc-pVTZ	205	0.484	0.451	2.12
	cc-pVQZ	420	0.522	0.499	2.21
$CH_3C_6H_5$	STO3G	43	2.155	6.308	1.83
(428)	DZ	86	0.255	0.205	1.56
LDAX//MM	SVP	145	0.463	0.428	2.13
	TZVP	188	0.552	0.520	2.18
	cc-pVTZ	365	0.666	0.633	2.38
	cc-pVQZ[1]	525	0.672	0.627	2.39
NO_2	STO3G	15	1.494	19.128	2.35
(132)	DZ	30	0.207	0.193	1.58
BLYP//BLYP(SVP)	SVP	45	0.277	0.256	1.94
	TZVP	60	0.313	0.302	1.80
	cc-pVTZ	105	0.308	0.292	1.81
	cc-pVQZ	201	0.340	0.329	1.86

[1]The cc-pVTZ basis set was used on the C atoms.

Table 3.2: Errors in total energy (E) and atomisation energy (EA) and WRMSD values (equation (3.20)) for the RI-J method. The number of auxiliary basis functions for each molecule is given in parentheses under its name. Also given are the functional and the method for obtaining the geometry (eg. BLYP//MM means that the BLYP functional was used and the geometry was obtained by molecular mechanics).

Molecule	Basis Set	N_{BF}	$E-E_{RI\text{-}J}$ (mE_h)	$EA_{RI\text{-}J}-EA$ (mE_h)	WRMSD ($\times 10^7$)
B_2H_6	STO3G	16	0.556	5.507	1.32
(178)	DZ	32	0.049	0.017	0.80
LDAX//LDAX(SVP)	SVP	60	0.049	0.042	0.78
	TZVP	76	0.058	0.044	0.89
	cc-pVTZ	160	0.074	0.057	1.01
	cc-pVQZ	350	0.088	0.062	1.06
$TiCl_4$	STO3G	85	34.405	−0.519	10.39
(294)	DZ	121	4.082	0.323	6.75
BLYP//BLYP(SVP)	SVP	125	3.895	0.328	6.55
	TZVP	141	3.944	0.336	6.61
	cc-pVTZ	205	3.949	0.345	6.62
	cc-pVQZ	345	4.228	0.383	6.91
$(H_3PAu)_2S$	STO3G	111	25.078	−2.727	7.90
(439)	DZ	144	0.227	0.092	1.13
BLYP//exp	SVP	165	0.209	0.139	1.03
	TZVP	183	0.242	0.149	1.14
	cc-pVTZ	285	0.285	0.185	1.14
	cc-pVQZ	510	0.718	0.427	1.54
H_3COSiH_3	STO3G	25	10.158	4.754	7.64
(229)	DZ	50	0.333	0.241	1.58
LDAX//MM	SVP	79	0.342	0.312	1.82
	TZVP	99	0.385	0.348	1.92
	cc-pVTZ	199	0.402	0.358	1.93
	cc-pVQZ	424	0.590	0.419	2.18
$CH_3NH_3^+$	STO3G	16	0.714	0.947	1.55
(178)	DZ	32	0.100	0.067	1.18
LDAX//MM	SVP	60	0.152	0.134	1.62
	TZVP	76	0.178	0.161	1.64
	cc-pVTZ	160	0.197	0.179	1.71
	cc-pVQZ	350	0.216	0.187	1.77

Table 3.3: The RI-J approximation for crown ethers of increasing size. The values of WRMSD (equation (3.20)) and the errors in total energy (E) and atomization energy (EA) are given. 3c1 is 3-crown-1 (C_2H_4O) and contains 65 auxiliary basis functions.

Molecule	N_{BF}	$E-E_{RI\text{-}J}$ (mE_h)	$EA_{RI\text{-}J}-EA$ (mE_h)	WRMSD$\times 10^7$
3c1	65	0.429	0.412	2.33
6c2	130	1.071	1.038	2.95
9c3	195	1.456	1.405	2.98
12c4	260	1.885	1.818	3.08
15c5	325	2.239	2.155	2.98
18c6	390	2.738	2.636	2.97
21c7	455	3.257	3.139	2.81

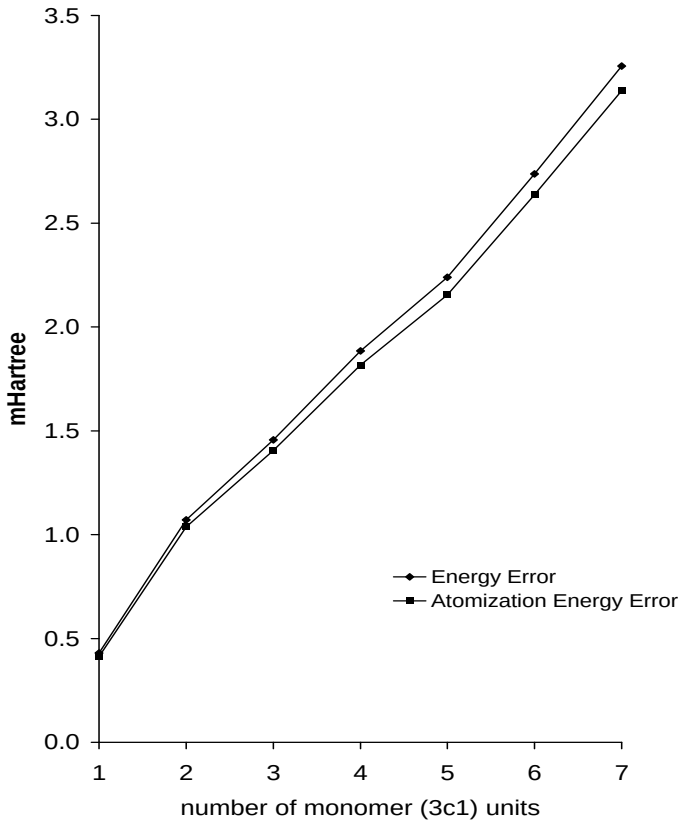

Figure 3.1: Error in energy and in atomisation energy for the RI-J approximation as a function of increasing crown ether size.

3.4 Discussion

Even though the list of molecules studied is by no means exhaustive, it contains many cases similar to those encountered in chemical applications with DFT. Equilibrium, or near equilibrium geometries, where DFT is most commonly used, were selected. We focus on energies since our auxiliary basis sets are optimised for them and therefore they are a direct indication of how well the RI-J approximation works. Furthermore, atomization energies are useful for comparisons of stability between different molecules and do not depend on errors in the description of the core region. Many molecular properties have this characteristic.

From Tables 3.1 and 3.2 we can observe that the RI-J energy is lower than the

non-fitted energy in accordance with the generalisation of the variational principle of equation (3.17). The atomisation energies of the RI-J calculations are larger than the four index results, probably because the RI-J energies of the isolated atoms are calculated more accurately than the energies of the molecules. Only in $TiCl_4$ and $(H_3PAu)_2S$, both with the STO3G basis, is the four index atomization energy higher than the RI-J atomization energy.

Our next observation is that the target accuracy of less than $1mE_h$ has been achieved for the atomisation energies for the SVP and TZVP basis sets for which our auxiliary basis functions were designed. In most molecules this is true for the total energy which gives errors of comparable magnitude. However, in $K[PtCl_3(C_2H_4)]$ and $TiCl_4$, which include third row or lower elements, the errors in energy are much larger and way above our threshold. These errors can be attributed to the density of the core electrons and cancel in the atomization energies as they are not affected by the chemical environment of the atoms.

We now look at how the rest of our basis sets performed. Surprisingly, STO3G which is much smaller than SVP and TZVP and in some cases has almost an order of magnitude less functions than the auxiliary basis, performs rather poorly. It seems that the auxiliary basis does not have the flexibility to follow its inadequate description of the density, which is substantially different from the density of a near-complete basis. This causes errors in the core region description for RbCl, $K[PtCl_3(C_2H_4)]$ and $TiCl_4$, in the valence region for NO_2 and B_2H_6 and in both core and valence for CH_2FCOO^-, $CH_3C_6H_5$, $(H_3PAu)_2S$ and H_3COSiH_3. Only in $CH_3NH_3^+$ does it seem to perform well, probably as a result of its positive charge which contracts its electron density, but still worse than the rest of the basis sets.

DZ performs in most cases almost equally well or a little better than the SVP and TZVP bases. This should probably be the general trend for a basis set smaller than the ones for which the auxiliary basis set was optimised but larger than minimal.

The cc-pVTZ and cc-pVQZ basis sets perform surprisingly well. They afford comparable errors to the SVP and TZVP basis sets even though they have almost the same number or more (for the cc-pVQZ case) functions than the auxiliary basis. This shows that the auxiliary basis sets are quite robust towards the complete basis

set limit and can probably be considered as "universal" auxiliary basis sets as long as the basis set has plenty of flexibility.

In evaluating now the usefulness of the WRMSD as a means of deciding the suitablility of the auxiliary basis for a particular calculation we observe the following. First of all the WRMSD is not an absolute measure of the quality of a calculation but it has to be compared to some reference, "good" calculation for the molecule in question. For example, in the $(H_3PAu)_2S$ molecule, if our reference result is the one with the SVP basis, one can observe that DZ, TZVP and cc-pVTZ are equally good, with similar values of WRMSD. On the other hand, cc-pVQZ is not as accurate and yields a slightly larger value of WRMSD, while STO3G is much worse and this causes WRMSD to increase substantially. This rationale holds for the rest of the results apart from STO3G $CH_3C_6H_5$. Overall, the WRMSD seems to be fairly sensitive to changes in errors. Its usefulness lies in the fact that it can give (most of the time) some indication about the quality of the RI-J approximation with a particular basis set if no four-index program is available. However, it requires an extra calculation with the reference basis set and gives no *a priori* indication of the magnitute of the error caused by an unsuitable basis set.

Table 3.3 presents the variation of the energy error, atomisation energy error and WRMSD with increasing molecular size for the SVP basis set. We observe that the WRMSD is almost constant, as should be expected for the same basis set and class of molecules. The error in energy and atomization energy however grows proportionally with the size of the molecule as shown more clearly in Figure 3.1. This was to be expected since the auxiliary basis sets are expected to produce errors of less than 0.2mE_h per atom. It is worrying however to observe that the target of 1mE_h is missed even for the atomization energy of 6c2. Since the RI-J method is meant for much larger molecules than this, we must hope that this increasing error with molecular size will not render the chemical information we can obtain from a large molecule useless, although this has to be tested. At least it is possible to take advantage of this regular increase of the error with molecule size and use it in a more direct approach to predict the performance of a particular basis set for an auxiliary basis: RI-J and four-index calculations on a molecule much smaller than

the one of interest should provide an error from which we can estimate the error on the large molecule by extrapolation.

In all the RI-J calculations it was observed that the convergence of the SCF procedure was either as good as the four-index case or better for some cases in the sense that it required less iterations. There seems to be no observable trend in RI-J accuracy related to the type of functional we used. BLYP which is a gradient corrected functional is not more demanding in terms of auxiliary basis set requirements than LDAX. The present calculations also raise the question of the accuracy of the RI-J approximation for molecules containing transition metals. However, the examples presented here are not sufficient for this purpose. Nevertheless, we can note that complexes with quasi spherical metals such as Au and Rb are more accurately described than complexes containing transition metals with partly filled d orbitals such as Ti and Pt.

3.5 Some conclusions regarding the RI-J approximation

We have tested extensively the accuracy of existing auxiliary basis sets for a variety of molecules and basis sets. We have found that when used in conjunction with smaller basis sets than the ones they were designed for they perform equally well except in the case of minimal basis sets. Furthermore, they performed very well in conjunction with increasingly larger basis sets, producing errors of the same order of magnitude as their standard basis sets. The robustness of the auxiliary basis sets towards the complete basis set limit is a particularly interesting result. Increasing size of basis set leads to a very steep increase in the cost of a calculation and an accurate RI-J approximation with current, readily available, auxiliary sets makes possible much larger calculations.

The WRMSD test was introduced as a means of predicting how well a combination of basis set and auxiliary set for a particular molecule will perform. It is useful when there is no capability for an "exact" four-index calculation; however it requires a reference RI-J result. For the auxiliary bases tested in this work this

reference result is a calculation with the SVP or TZVP basis set. When four-index calculations are feasible, we suggest a much more direct test for the suitablity of an auxiliary basis set. An RI-J and a four-index calculation on a molecule similar to the one in question, but much smaller, give an error which can reliably predict the error of the RI-J calculation for the large molecule. As Table 3.3 shows the error of an RI-J calculation grows linearly with the size of the molecule. This should always be taken into account.

The RI-J method appears to be the only practical way for DFT calculations on the type of large inorganic molecules we are interested in. Our present findings form a basis for ensuring that we achieve the accuracy we desire each time we use the RI-J method. This will prove particularly useful, especially as there is currently a gap in the literature on optimised auxiliary basis sets suitable for the valence basis sets of effective core potentials for lanthanides and actinides and also for all-electron basis sets of these elements. Finally, the option of an algorithm for optimising an auxiliary basis set on the fly for each new basis set encountered is a possibility well worth exploring.

3.6 Calculation of the charges

The determination of the charges $\tilde{\tilde{\mathbf{q}}}$ of equation (3.15) should be carried out carefully as the $\mathbf{V}$ matrix can very often be nearly singular.

Eichkorn et al. [94] have solved this problem by adding a small positive number δ to the diagonal elements of $\mathbf{V}$. This results in raising all the eigenvalues of $\mathbf{V}$ by δ, which is supposed to be a small number but greater than the computer precision. Then a set of charges can be obtained without fear of rounding errors.

$$\tilde{\tilde{\mathbf{q}}}_0 = (\mathbf{V} + \delta)^{-1}(\mathbf{f}|\rho) \tag{3.21}$$

However these charges are not exactly correct since we have manipulated the $\mathbf{V}$ matrix to make it more stable. The charges used in the calculation are obtained in a second step where $\tilde{\tilde{\mathbf{q}}}_0$ are corrected by subtracting from them the contribution of

the residual

$$\tilde{\tilde{\mathbf{q}}}_1 = \tilde{\tilde{\mathbf{q}}}_0 - (\mathbf{V}+\delta)^{-1}\mathbf{R} = \tilde{\tilde{\mathbf{q}}}_0 + (\mathbf{V}+\delta)^{-1}[(\mathbf{f}|\rho) - \mathbf{V}\tilde{\tilde{\mathbf{q}}}_0] \tag{3.22}$$

It is claimed that the charges $\tilde{\tilde{\mathbf{q}}}_1$ obtained with the above procedure are both accurate and stable with respect to rounding errors. The parameter δ has been chosen to be equal to 10^{-9} for the particular implementation of the authors. An alternative approach to this scheme would be to simply neglect the eigenvalues of $\mathbf{V}$ which are lower than some threshold value δ and then construct a numerically stable $\mathbf{V}^{-1}$ [64]. This *singular value decomposition* is a straightforward way of removing contamination from near nullspace solutions.

The drawback of the above schemes for determining the charges is that they depend on the choice of the parameter δ. The optimum value of this parameter is a function of the precision of the computer in use. It must therefore be redefined every time the code is ported to a different platform. In order to eliminate this dependence we have chosen to solve the system of linear equations $\mathbf{V}\tilde{\tilde{\mathbf{q}}} = (\mathbf{f}|\rho)$ with a BLAS subroutine which is designed for systems of linear equations with $\mathbf{V}$ being symmetric and indefinite. Such mathematical library subroutines are common to all workstations and are optimised for efficiency and numerical stability. Finally a subroutine for improving iteratively the solutions of the BLAS subroutine is called. The charges obtained are checked by examining the Maximum Absolute Relative Residual (MARR).

$$MARR = \max_i \quad \frac{|(\mathbf{V}\tilde{\tilde{\mathbf{q}}})_i - (f_i|\rho)|}{|(f_i|\rho)|} \tag{3.23}$$

The value of MARR is usually $\sim 10^{-11}$ or less for auxiliary basis sets stable towards linear dependence and can range up to $\sim 10^{-4}$ before near linear dependence starts to dominate the solution of the linear system (even with the specialised solution schemes) and affect SCF convergence.

3.7 Unoptimised auxiliary basis sets

Our investigations so far have been focused on the use of existing auxiliary basis sets. However the question arises as to what we can do in cases where there are no auxiliary basis sets available in the literature. We often encounter this problem, such as in the case of calculations on molecules containing actinides and lanthanides with and without ECPs, or second and third row transition metals without ECPs. As we have mentioned already, the optimisation of auxiliary basis sets is a complicated nonlinear problem.

3.7.1 A standard auxiliary basis set construction method

It is instructive to outline here the procedure that Ahlrichs et al. [94, 95] have followed in order to create the most complete selection of auxiliary basis sets available in the literature, that we have used for our studies. Based on preliminary results, they decided to represent the exponents η_i of each particular angular momentum by the expression

$$\eta_{i+1} = \eta_i \beta \left(1 + \gamma \frac{i^2}{(n+1)^2} \right), \quad i = 0, 1, \ldots, n-1 \tag{3.24}$$

where it is assumed that there will be n exponents for each angular momentum. The ansatz of equation (3.24) is an extension of the formula for even-tempered basis sets [113]. The optimisation of an auxiliary basis set is a much easier task using this ansatz as only three parameters (η_0, β, γ) need to be optimised, as opposed to the much more difficult task of optimising freely all the exponents. A simulated annealing technique was used in order to optimise simultanously the parameters for all angular momenta in two steps. In the first step the exponents of the functions of s, d, etc. symmetry were determined from atomic calculations by maximising the Coulomb energy with respect to the parameters. Because the atoms have spherical, or spherically averaged densities, only the even functions participated in the fit and therefore the parameters for the odd functions p, f, etc. could not be determined from atomic calculations. These were determined in a second step by calculations on the hydrides of the atoms. Hartree-Fock theory was used as it does not depend on the choice of a functional. Apart from exponents, the calculations on the

atoms produced charges that were used as contraction coefficients to provide a light segmented contraction of the auxiliary basis sets.

3.7.2 How to obtain a working auxiliary basis

Without endeavouring to fully optimise auxiliary basis sets, we seek a practical, *working* solution that allows us to perform calculations involving types of atoms for which auxiliary basis sets are not available. We have found that one can devise or "hand-optimise" auxiliary basis sets without significant effort. These are obviously going to be much larger than their optimised equivalents but hopefully equally accurate. The accuracy of such auxiliary basis sets can be checked with the criteria we have developed.

The choice of the exponents has to be done in a trial and error fashion. In order to make our task simpler we have decided to represent the exponents of each angular momentum by an even tempered formula (geometric sequence)

$$\eta_{i+1} = \eta_i \beta, \quad i = 0, 1, \ldots, n-1 \tag{3.25}$$

where n is the number of exponents for a particular angular momentum. Thus, only two parameters per angular momentum are needed. We were kindly provided with the following set of parameters by Ahlrichs [114].

type	η_0	β	n
s	0.06	1.8	16
p	0.20	2.2	7
d	0.20	2.2	6
f	0.20	2.4	5
g	0.20	2.4	4
h	0.30	2.4	3
i	0.60	2.4	3

These parameters produce an auxiliary basis with many closely spaced exponents distributed over a large range of values. Due to this large flexibility, this uncontracted auxiliary basis set is considered capable of describing the valence density of

all actinide elements with ECPs. We have found however that even with the precautions we take for solving the system of linear equations for the charges (3.15), instabilities arise which often affect badly SCF convergence. This increased randomness in the determination of the charges is illustrated by the lowest eigenvalue of the $\mathbf{V}$ matrix for a single atom containing this auxiliary set which is equal to 4.06×10^{-14}, close to the precision threshold of most computers.

To alleviate this problem we have contracted this auxiliary basis using as contraction coefficients for the even functions (s,d,g,i) the charges from an LDAX calculation on UF_6 with octahedral geometry. Contraction coefficients for the odd functions (p,f,g) were obtained from the charges from an LDAX calculation on UF_2 with a 90° bond angle. The SVP basis was used on the fluorine atoms and the Stuttgart group quasirelativistic ECP with 60 core electrons on uranium. This resulted in reducing the lowest eigenvalue of the $\mathbf{V}$ matrix to 2.14×10^{-10}, a value that maintains stable convergence behaviour. The contraction of the actinide auxiliary basis set is [16s;7p;6d;5f;4g;3h;3i](1s,1s,2s,4s,8s;1p,1p,1p,2p,2p;1d,1d,1d,3d;1f,1f,3f; 1g,3g;1h,2h;1i,1i,1i) where the number of primitive exponents for each angular symmetry is in square brackets and the contraction pattern is in parentheses.

It is expected that this contraction will be compatible with many uranium compounds. As a demonstration, the following Table contains the energies of some uranium complexes calculated with the uncontracted uranium auxiliary basis, the contracted version of it and without the RI-J approximation.

Molecule	UO_2^{2+}	UBr_6	US
"Exact"	-621.871281	-551.722916	-449.466415
Uncontracted	-621.871335	-551.722966	-449.466933
Contracted	-621.871589	-551.723997	-449.467086

It can be seen that both the uncontracted and contracted auxiliary bases achieve millihartree accuracy. However, convergence with the uncontracted auxiliary basis was problematic, requiring an excessive number of iterations. On the other hand, no convergence difficulties were encountered with the contracted uranium auxiliary basis or without the RI-J approximation. Switching from the uncontracted to the

contracted auxiliary basis causes an increase in the error as expected but does not change its order of magnitute. It is probably reasonable to suggest that the contracted auxiliary should be used in place of the uncontracted one as it is almost as accurate and does not affect convergence. The LDAX functional was used for UO_2^{2+} and UBr_6 and the BLYP functional for US. The Ahlrichs auxiliary bases were used on nometallic atoms. The SVP basis was used on the oxygen atoms and the DZP basis on the sulphur. The bromine atoms were described by an ECP with 28 core electrons and the accompanying valence basis set. The uranium ECP of UO_2^{2+} and UBr_6 represented 60 core electrons while the one on US represented 78 core electrons.

Another way to obtain a working auxiliary basis set is to modify or extend one that is already available. For example, there is no auxiliary basis available for an all-electron gold atom, but there is one for the valence density of a gold atom with an ECP. We can augment this valence auxiliary basis to create a new one, suitable for an all-electron calculation. For this purpose, we add functions from the existing all-electron auxiliary basis set for copper, as it belongs to the same group of the periodic table as gold. Only the functions (contracted and primitive), which contain exponents larger than the exponents of the gold valence auxiliary basis, for each angular momentum are added, since the goal is to improve the ability to describe the core density. However this is not enough for an adequate description of the core density of gold because its nuclear charge (79 a.u.) is much larger than that of copper (29 a.u.). We need functions of spherical symmetry with considerably larger exponents, for the density in the vicinity of the nucleus. Hence, we add s primitive Gaussian functions with even tempered exponents according to equation (3.25), with parameter values $\eta_0 = 38.56104604754$, $\beta = 1.8$ and $n = 19$.

The resulting auxiliary basis set for gold consists of 152 distinct functions (angular momentum components included in the count) and the primitives it contains are: [38s;5p;7d;6f;4g]. The lowest eigenvalue of its $\mathbf{V}$ array is 2.73×10^{-11}. For an indicative test, we have performed LDAX calculations on the AuH molecule with a basis set of double zeta plus polarisation quality. The energy we obtained was -17849.878015 E_h as compared to the "exact" energy of -17849.877991 E_h without

the RI-J approximation. The role of the even tempered s core functions we added is very important. This is illustrated by the large error that results by neglecting them, in which case the energy obtained is -17857.624717 E_h.

There is not much point to examine any further auxiliary basis sets derived with the empirical procedures described above, since they are far from optimised. The aim of our discussion was to demonstrate that it is possible to construct auxiliary basis sets for cases where properly optimised ones are not available. The resulting working auxiliary sets should be used with caution but it is possible to ensure, by testing them beforehand, that they will be adequate for the needs of the application in hand.

3.8 The RI-J approximation with Slater type basis functions

It was mentioned in section 1.4 that Gaussian basis sets are used almost exclusively for calculations on polyatomic molecules. Some of the alternative options that have been examined over the years are numerical basis sets, plane-wave basis sets and Slater basis sets. A primitive spherical Slater function [115] centred at point **A** is represented by the following formula:

$$s_{A_i}(\mathbf{r};\alpha_i,n,l,m,\mathbf{A}) = r^{n-1}\exp(-\alpha_i r)\,Z_{lm}(\theta,\phi) \tag{3.26}$$

Slater functions are claimed to be superior to Gaussians because their short range (cusp on nucleus) and long range (decay rate) behaviour can be adjusted to be exact if their exponents are chosen appropriately. This is a benefit over Gaussian functions as they do not possess a nuclear cusp and decay too fast. It is known that asymptotically with increasing basis set size only half as many Slater functions are required to achieve accuracy comparable to the accuracy of a certain number of Gaussians [20]. On the other hand, the basic difficulty with Slater functions is that integrals involving more than one centre cannot, in general, be expressed in closed form and approximations are necessary. Molecular quadrature is probably the best option for evaluating the integrals, but even then, the situation becomes very

complicated when it comes to the evaluation of the two-electron integrals as they are six-dimensional. However, the electrostatic potential due to a single primitive spherical Slater function can be readily expressed in an analytic form [116]. This result can be used to make three-centre two-electron integrals three-dimensional.

Based on this fact, a version of MAGIC was modified to use primitive spherical Slater basis functions within the RI-J approximation [116]. The molecular quadrature grid of section 1.5, with a variety of radial grids, was used for evaluating all the integrals. The overall performance of this scheme was poor compared to the standard Gaussian function code. Because the quadrature grid was not optimised for Slater functions, a very large number of points was necessary in order to evaluate the two-electron integrals to sufficient accuracy with a consequent increase in computational cost. It was concluded that Slater basis functions could not become competitive to the Gaussian basis functions within the RI-J approximation.

Probably the only way that Slater functions can become competitive to Gaussians is when they are employed in DFT calculations where the density for approximating the Coulomb energy has been fitted according to the SVS approximation (section 3.2.4). The bulk of the work in the SVS approximation goes into the evaluation of three-centre overlap integrals and this can be done in an efficient way with an appropriate quadrature grid [117]. The ADF program [118] can perform DFT calculations on molecules using Slater functions with the "discrete variational" [87] variant of the SVS method which fits separately densities of diatomics. Slater functions preclude Hartree-Fock or DFT calculations with hybrid functionals, because they require exact exchange energy which in turn requires evaluation of four-centre two-electon integrals.

3.9 Two-electron integral evaluation

Since the first quantum chemistry programs became available, 3-4 decades ago, it was recognised that the calculation of two-electron integrals is naturally the most computationally demanding step in a calculation. As a consequence, the derivation of efficient algorithms for the evaluation of these integrals is a major area of

research which is still active. The capacity for improvement was limited in early computations that used Slater basis functions because multicentre integrals have to be expressed as infinite series and no closed forms are available. The first breakthrough was due to S. F. Boys [19] who decided to use Cartesian Gaussian basis functions. In his scheme he gave a closed form for the two-electron integral involving only s-type functions. He expressed all other integrals in terms of this basic integral by taking advantage of the fact that the derivative of a Gaussian function is a sum of Gaussian functions. More efficient methods have been invented since then, based on different closed form formulae. One of these methods employs Rys quadrature to evaluate the integrals. This method has been implemented, taking into account some recent modifications for increased efficiency. In what follows we describe the relevant theory on which the code is based and then show how the Rys quadrature method can be used as a starting point to derive other methods in the literature.

The starting point is to express the interelectronic repulsion operator r_{12}^{-1} as a Gaussian transform, as we did with the nuclear attraction operator in equation (2.32) of section 2.6. Then a change of variables as in equation (2.33) is applied to yield

$$\frac{1}{r_{12}} = \frac{2}{\sqrt{\pi}} \int_0^\infty \exp[-u^2(\mathbf{r}_1 - \mathbf{r}_2)^2] du \tag{3.27}$$

The general form of an integral involving four primitive Gaussian functions is

$$\begin{aligned}
[g_A g_B | g_C g_D] &= \int\int g_A(\mathbf{r}_1; \alpha, a_x, a_y, a_z, \mathbf{A})\, g_B(\mathbf{r}_1; \beta, b_x, b_y, b_z, \mathbf{B}) \\
&\times \frac{1}{r_{12}} g_C(\mathbf{r}_2; \gamma, c_x, c_y, c_z, \mathbf{C})\, g_D(\mathbf{r}_2; \delta, d_x, d_y, d_z, \mathbf{D}) d\mathbf{r}_1 d\mathbf{r}_2 \\
&= \frac{2}{\pi^{\frac{1}{2}}} \int_0^\infty [g_A g_B | \exp(-u^2 r_{12}^2) | g_C g_D] du \\
&= \frac{2}{\pi^{\frac{1}{2}}} \int_0^\infty I'_x I'_y I'_z du
\end{aligned} \tag{3.28}$$

where the transformed interelectronic repulsion operator inside the integral sign can be expressed as a product of terms depending only in x, y or z coordinates. Thus the integrand is split into three factors. Let us examine the I'_x factor

$$I'_x = \int\int (x_1 - A_x)^{a_x} (x_1 - B_x)^{b_x} (x_2 - C_x)^{c_x} (x_2 - D_x)^{d_x} \exp(-Q_x) dx_1 dx_2$$

where

$$\begin{aligned}\exp(-Q_x) &= \exp\Big(-\alpha(x_1-A_x)^2-\beta(x_1-B_x)^2-\gamma(x_2-C_x)^2 \\ &- \delta(x_2-D_x)^2-u^2(x_1-x_2)^2\Big) \end{aligned} \tag{3.29}$$

We now define the following quantities

$$L_x=\frac{\alpha A_x+\beta B_x}{\alpha+\beta}, \qquad R_x=\frac{\gamma C_x+\delta D_x}{\gamma+\delta} \tag{3.30}$$

$$\Lambda=\alpha+\beta, \qquad P=\gamma+\delta \tag{3.31}$$

$$\rho=\frac{\Lambda P}{\Lambda+P} \tag{3.32}$$

$$U_x=\rho(L_x-P_x)^2 \tag{3.33}$$

$$k_{abx}=\exp\left(-\frac{\alpha\beta}{\alpha+\beta}(A_x-B_x)^2\right), \quad k_{cdx}=\exp\left(-\frac{\gamma\delta}{\gamma+\delta}(C_x-D_x)^2\right) \tag{3.34}$$

In terms of the above definitions, $\exp(-Q_x)$ becomes

$$\exp(-Q_x)=k_{abx}k_{cdx}\exp\Big(-\Lambda(x_1-L_x)^2-P(x_2-R_x)^2-u^2(x_1-x_2)^2\Big)$$

where the first two terms in the right hand side product are constants depending on the Gaussian function parameters (exponents + positions). Let us make a change of variables from u to t.

$$u=\sqrt{\rho}\frac{t}{\sqrt{1-t^2}} \qquad du=\frac{\sqrt{\rho}}{(1-t^2)^{\frac{3}{2}}}dt \tag{3.35}$$

This changes the range of integration in (3.28) from $[0,+\infty)$ for u to $[0,1]$ for t. We also define the *2D integrals*

$$I_x=I_x[a_x,b_x|c_x,d_x](t)=\frac{e^{U_xt^2}}{k_{abx}k_{cdx}\sqrt{1-t^2}}\sqrt{\frac{\Lambda}{\pi}}\sqrt{\frac{P}{\pi}}I'_x \tag{3.36}$$

Now equation 3.28 becomes

$$[g_Ag_B|g_Cg_D]=q\int_0^1 I_xI_yI_z\exp(-(U_x+U_y+U_z)t^2)dt \tag{3.37}$$

where

$$q=2\sqrt{\frac{\rho}{\pi}}k_{ab}k_{cd}\left(\frac{\pi}{\Lambda}\right)^{\frac{3}{2}}\left(\frac{\pi}{P}\right)^{\frac{3}{2}} \tag{3.38}$$

depends only on the exponents and the positions of the primitive Gaussian functions participating in the integral, with $k_{ab}=k_{abx}k_{aby}k_{abz}$ and $k_{cd}=k_{cdx}k_{cdy}k_{cdz}$. By

extending the line of thought of section 2.6 for examining the $M_x(t)$ integrals, it can be shown [119] that,

$$P(t) = I_x I_y I_z \tag{3.39}$$

is an even polynomial in t of degree $n_{pol} = 2(\lambda_A + \lambda_B + \lambda_C + \lambda_D)$. Therefore the above integral can be evaluated by Rys quadrature using the positive roots and corresponding weights of $R_{N_{Rys}}(t, U_x + U_y + U_z)$ where

$$N_{Rys} = \left[\frac{n_{pol}}{4}\right] + 1 \tag{3.40}$$

The subroutines we use to generate the Rys roots and weights are due to the authors of the Rys quadrature method [119, 31, 32]. They take as arguments the number of roots N_{Rys} and the value $U_x + U_y + U_z$ and return the values of v^2 and the quadrature weights. Then the values of the squared quadrature points t^2 are calculated according to (see also subsection 2.5.3)

$$t^2 = \frac{v^2}{1 + v^2} \tag{3.41}$$

as these are the only values we will need subsequently because we are dealing only with even polynomials of t.

The next step is to generate the I_x, I_y and I_z integrals for each value of t^2. Even though they can be expressed in closed form, their straighforward calculation is not computationally efficient. The most efficient approach is through recursion relations.

In order to facilitate the following discussion we will introduce a simplified notation for Gaussian basis functions and two-electron integrals. We will use the vector of angular momentum indices $\mathbf{a} = (a_x, a_y, a_z)$ to represent the function g_A. For example if g_A is a p function, $\lambda_A = 1$ its angular momentum components are

$$(x - A_x)e^{-\alpha(\mathbf{r}-\mathbf{A})^2}, \quad (y - A_y)e^{-\alpha(\mathbf{r}-\mathbf{A})^2} \quad \text{and} \quad (z - A_z)e^{-\alpha(\mathbf{r}-\mathbf{A})^2} \tag{3.42}$$

and $\mathbf{a}$ can be $(1,0,0)$, or $(0,1,0)$ or $(0,0,1)$ respectively. In a similar manner the two-electron integral of equation (3.28) can be represented as

$$[\mathbf{ab}|\mathbf{cd}] \tag{3.43}$$

and the set of integrals formed by all allowed values of **a**, **b**, **c** and **d** will be called a *batch of integrals*. The expression (3.43) will be used to represent both a single integral and a batch of integrals, depending on the context.

In the recursive scheme implemented for the four-index two-electron integrals, in order to calculate the batch of equation (3.43) we need the following batches of integrals

$$[\mathbf{e0}|\mathbf{f0}], \quad \mathbf{f} = \max(\mathbf{c},\mathbf{d}),\ldots,\mathbf{c}+\mathbf{d}, \quad \mathbf{e} = \max(\mathbf{a},\mathbf{b}),\ldots,\mathbf{a}+\mathbf{b} \tag{3.44}$$

which are called *uncontracted source integrals*. The addition of **c** and **d** represents a vector whose angular momentum is equal to the sum of their angular momenta.

3.9.1 Generation of the 2D integrals

We start by calculating by recursion the 2D integrals necessary for the generation of the uncontracted source integrals. These recursion relations were discovered by Rys et al. [119] by integrating partial derivatives of the integrands of the 2D integrals. We will demonstrate the recursion for the 2D integrals related to the x-coordinate. The starting value is $I_x[0,0|0,0](t)$ and it is easy to show that it is independent of t and equal to 1. Then the angular momentum of the first index of the left hand side and of the first index of the right hand side are increased by alternating application of the two recursion formulae

$$\begin{aligned} I_x[e_x+1,0|f_x,0](t) &= \left((L_x-A_x)+\frac{\rho t^2}{\Lambda}(R_x-L_x)\right) I_x[e_x,0|f_x,0](t) \\ &+ \frac{e_x}{2\Lambda}\left(1-\frac{\rho t^2}{\Lambda}\right) I_x[e_x-1,0|f_x,0](t) \\ &+ \frac{f_x \rho t^2}{2\Lambda P} I_x[e_x,0|f_x-1,0](t) \end{aligned} \tag{3.45}$$

and

$$\begin{aligned} I_x[e_x,0|f_x+1,0](t) &= \left((R_x-C_x)+\frac{\rho t^2}{P}(L_x-R_x)\right) I_x[e_x,0|f_x,0](t) \\ &+ \frac{f_x}{2P}\left(1-\frac{\rho t^2}{P}\right) I_x[e_x,0|f_x-1,0](t) \\ &+ \frac{f_x \rho t^2}{2\Lambda P} I_x[e_x-1,0|f_x,0](t) \end{aligned} \tag{3.46}$$

where terms with negative indices are substituted by zero. A simple way to generate the necessary batches of uncontracted source integrals is to use equation (3.45) successively to generate

$$I_x[1,0|0,0](t), I_x[2,0|0,0](t), \ldots I_x[\lambda_A+\lambda_B,0|0,0](t) \tag{3.47}$$

Then equation (3.46) is used to generate $I_x[0,0|1,0](t)$ and another pass through equation (3.45) will yield

$$I_x[1,0|1,0](t), I_x[2,0|1,0](t), \ldots I_x[\lambda_A+\lambda_B,0|1,0](t) \tag{3.48}$$

Continuation of this procedure generates all integrals from $I_x[0,0|0,0](t)$ up to and including $I_x[\lambda_A+\lambda_B,0|\lambda_C+\lambda_D,0](t)$ which are kept in memory for the next stage.

3.9.2 Construction of the primitive source integrals

Once all the 2D integrals for all the values of t^2 have been calculated and stored, they are combined to generate the primitive source integrals. Each member of a batch of primitive source integrals is calculated using Rys quadrature.

$$[\mathbf{e0}|\mathbf{f0}] = q \sum_{i=1}^{N_{Rys}} I_x[e_x,0|f_x,0](t_i)\ I_y[e_y,0|f_y,0](t_i)\ I_z[e_z,0|f_z,0](t_i)\ W_i \tag{3.49}$$

where q is defined in equation (3.38). The above equation is used several times in the process of generating one batch of uncontracted two-electron integrals and makes a substantial contribution to the overall computational cost of the two-electron integrals.

In order to minimise this cost, the number of multiplications performed in equation (3.49) must be reduced. To this end, the same number of Rys quadrature points for evaluating all the batches of primitive source integrals of equation (3.44) must be used, even though some batches could be evaluated with less than the N_{Rys} roots of equation (3.40). This ensures that the same 2D integrals are used for all uncontracted primitive source batches. One improvement possible then is to premultiply every $I_z[e_z,0|f_z,0](t_i)$ with W_i and use the result $I_z^* = I_z W_i$ in place of I_z, disposing of the W_i. This provides some computational benefits in our code because the same I_z^* are used to calculate different batches of primitive source integrals. A further

improvement for efficiency which we have implemented is the *reduced multiplication scheme* of Lindh et al. [120]. The scheme suggests the storage in memory and reutilisation of the $I_x[e_x, 0|f_x, 0](t_i)\, I_y[e_y, 0|f_y, 0](t_i)$ products. The gain in arithmetic operations is achieved through increase in memory requirements since all the products satisfying the relations

$$0 \leq e_x + e_y \leq \lambda_A + \lambda_B \quad \text{and} \quad 0 \leq f_x + f_y \leq \lambda_C + \lambda_D \tag{3.50}$$

for every t_i, have to be kept in memory. This is however not a problem with modern computers. The point that needs most attention is the implementation as this scheme introduces additional code complexity. The code has to be well-structured and consist of small, specialised subroutines if any improvement in performance is to be observed in practice.

The recursions of section 3.9.1 and the quadrature of equation (3.49) are programmed by explicit formulas for the [**00**|**00**], [**10**|**00**], [**00**|**10**], [**10**|**10**], [**20**|**00**] and [**00**|**20**] types of uncontracted primitive source integrals. The explicit evaluation is cheaper than the recursions and produces observable computational savings, especially since the majority of basis functions are usually of s (**0**), p (**1**) and d (**2**) type.

3.9.3 Contraction of the primitive source integrals

The next step is the contraction of the batches of primitive source integrals in order to produce batches of *contracted source integrals*.

$$(\mathbf{e0}|\mathbf{f0}) = \sum_{i=1}^{K_A} \sum_{j=1}^{K_B} \sum_{k=1}^{K_C} \sum_{l=1}^{K_D} c'_i c'_j c'_k c'_l [\mathbf{e}_i \mathbf{0}_j | \mathbf{f}_k \mathbf{0}_l] \tag{3.51}$$

Here c'_i is the contraction coefficent c_i multiplied by the normalisation coefficient n'_{A_i} of equation (1.23). In practice the contraction is achieved by accumulating the primitive source integral batches, as they are generated, into the array which is meant to contain the contracted source integral batches.

3.9.4 Generation of the batch of contracted integrals

This is the final step for obtaining the contracted integrals batch and is carried out by recursion. The recurrence relation we use was first reported by Rys et. al. [119] for application to the 2D integrals. It was called the *transfer equation*. Later, Head-Gordon et. al. [121] observed that it is independent of the radial part of the basis functions and hence can be applied after contraction of the integral batches has taken place. The resulting recursion was named the *horizontal recurrence relation*

$$(\mathbf{j}(\mathbf{k}+\mathbf{1}_\xi)|\mathbf{mn}) = ((\mathbf{j}+\mathbf{1}_\xi)\mathbf{k}|\mathbf{mn}) + (J_\xi - K_\xi)(\mathbf{jk}|\mathbf{mn}) \tag{3.52}$$

where $\xi = x, y$ or z and it is implied that the J_ξ ($= A_x$ in our discussion so far) coordinate is a component of the position vector of the centre of $\mathbf{j}$ and similarly for K_ξ ($= B_x$). Since the right hand side of the contracted batches does not change, it can be omitted to simplify the notation

$$(\mathbf{j}(\mathbf{k}+\mathbf{1}_\xi)| = ((\mathbf{j}+\mathbf{1}_\xi)\mathbf{k}| + (J_\xi - K_\xi)(\mathbf{jk}| \tag{3.53}$$

The calculation of the contracted batch is completed by application of the horizontal recurrence relation to the ket side of the contracted source batches.

$$|\mathbf{m}(\mathbf{n}+\mathbf{1}_\xi)) = |(\mathbf{m}+\mathbf{1}_\xi)\mathbf{n}) + (M_\xi - N_\xi)|\mathbf{mn}) \tag{3.54}$$

Equations (3.53) and (3.54) look deceptively simple. Their implementation is very complicated as each recursion is in three dimensions (x, y, z) simultaneously. Formally, twelve-dimensional arrays are needed to store each batch of integrals. This would be very inefficient in terms of memory management since the majority of the elements of such an array would remain unused because for every triplet of indices, only the elements whose indices add up to the angular momentum of a basis function will be used. In order to overcome this problem, the code stores batches in two-dimensional arrays where the elements (integrals) are always stored in a definite order so that all the memory allocated is utilised while the integrals of a batch can still be accessed easily for performing the recursions. The indexing scheme is based on a general order that is followed thoughout the integral subroutines of MAGIC for counting the components of Cartesian Gaussian functions, for every angular momentum. For example, the following loop structure

do $a_z = 0, \lambda_A$

do $a_y = 0, \lambda_A - a_z$

$a_x = \lambda_A - a_z - a_y$

$\vdots$

more code

$\vdots$

enddo

enddo

counts the components of a Cartesian Gaussian function of any angular momentum. For example, the ordering of the 15 components of a g function ($\lambda = 4$) is x^4, x^3y, x^2y^2, xy^3, y^4, x^3z, x^2yz, xy^2z, y^3z, x^2z^2, xyz^2, y^2z^2, xz^3, yz^3 and z^4. Conversely, given a component of a Cartesian Gaussian basis function, the implementation uses the following formula

$$a_z(a_x + a_y + a_z + 2) + a_y + 1 - \frac{a_z(a_z + 1)}{2} \tag{3.55}$$

to determine its order (position) in the indexing scheme. For the example just mentioned (3.55) is equal to 1 for x^4, 2 for x^3y, 3 for x^2y^2, etc.

Even with this indexing scheme, strictly speaking, the product **ab** defines a two-dimensional array. This in turn, means that a four-dimensional array is needed in order to store a batch. This is avoided by introducing a further indexing scheme for the product of Gaussian functions where the two-dimensional array **ab** is perceived and expressed as a one-dimensional row vector constructed by joining together the consecutive rows of the two-dimensional array. Thus every batch of integrals is always stored in a two-dimensional array.

There is some arbitrariness regarding the application of equations (3.53) and (3.54) when basis functions of f type or higher angular momentum are involved. The most efficient paths to follow for this tree search problem have been investigated by Ryu et al. [122]. The biggest savings they achieved in floating point operations were 44% for batches containing exclusively i functions ($\lambda = 6$) and much less for

other types of batches. Functions of such high angular momentum are rare in most basis sets, and are usually located on only one atom. As a result they appear in only a small percentage of the two-electron integral batches. It was therefore decided not to follow the Ryu scheme which would introduce a substantial amount of unnecessary complexity in the code. Rather, the horizontal recursion relations are programmed in the easiest way to understand. Intermediate batches of contracted source integrals are generated according to the indexing schemes we have presented.

Finally, in order to minimise the number of times the horizontal recursion relation is used, we produce the batches so that the right hand side of the bra and ket sides have the lowest angular momentum possible and then we shift them over if the batch we wished to generate was the other way round. For example, if $\lambda_A = 0$, $\lambda_B = 1$, $\lambda_C = 1$ and $\lambda_D = 1$ the batch $(\mathbf{ba}|\mathbf{cd})$ is calculated and then its elements are swapped around to get the desired $(\mathbf{ab}|\mathbf{cd})$ batch. Swapping elements of arrays takes no time compared to the savings resulting from less applications of the horizontal recursions. The calculation of a contracted batch is completed by multiplying each of its elements by the appropriate normalisation constants N'_A, N'_B, N'_C and N'_D, defined in equation (1.24).

In the case of the three-index two-electron integrals used in the RI-J approximation the horizontal recursion needs to be applied only to the ket side of each batch. Therefore the savings achieved from the application of the horizontal recursion at the contracted stage are not as significant. Hence it was chosen to apply the transfer equation to the 2D integrals. This choice involves much simpler one-dimensional recursion relations such as the following for the x coordinate

$$I_x^{TI}[j_x,(k_x+1)|m_x](t) = I_x^{TI}[(j_x+1),k_x|m_x](t) + (J_x - K_x)I_x^{TI}[j_x,k_x|m_x](t)$$

where the definition of I_x^{TI} follows from equation (3.36), by assuming g_D does not exist. The I_x^{TI} are then used directly to generate the batches of uncontracted integrals and then they are contracted. The need for batches of source integrals and the horizontal recurrence relation has been eliminated. As a result the code involved is considerably simpler and straightforward and can be optimised better for performance. So even though the theoretical count of floating point operations

is higher, the code is fast because it is highly optimised.

3.9.5 Common points between modern two-electron integral evaluation methods

It is now known that most modern methods for evaluating two-electron integrals are equivalent. By this we mean that if we select arbitrarily one of the methods as the fundamental method, we can derive from it the other methods. This principle however is not transferable to the implementation which has to be tailored to one particular method in order to be efficient. In this subsection we will regard the Rys quadrature method as the fundamental method and indicate how the theory of the other available methods can be derived from it.

In the McMurchie and Davidson method [89] the following functions ("auxiliary functions") which can expressed in terms of the incomplete gamma function [33]

$$F_m(x) = \int_0^1 t^{2m} e^{-xt^2} dt = \frac{1}{2x^{m+\frac{1}{2}}} \gamma(m + \frac{1}{2}, x) \tag{3.56}$$

are the essential starting quantities for the application of a series of recurrence relations. Looking back to subsection 2.5.2 it is obvious that $F_m(x)$ can be calculated with Rys quadrature. In practice however, this would not lead to an efficient algorithm because in the implementations of the McMurchie and Davidson method much effort has been put on algorithms dedicated to this purpose [123]. The optimised implementation of such algorithms is a laborious computer science task, justifying authors to regard the resulting code as "a secret of great commercial importance" [124].

Another method is by using the 3-dimensional *vertical recurrence relation* suggested by Head-Gordon and Pople [121], as a simplification of the recurrence relation on which the earlier method of Obara and Saika was based [125]. Lindh et al. [120] showed how to derive the vertical recurrence relation from the recurrence relations for the 2D integrals of the Rys method. In particular, we can take equation (3.45) for a Rys point t_i and multiply both sides with

$$t_i^{2m} I_y[e_y, 0|f_y, 0](t_i) I_z[e_z, 0|f_z, 0](t_i) w_i \tag{3.57}$$

If we then sum up over all points t_i necessary for the integration of an even polynomial of degree $n_{pol} + 2m$, we obtain the vertical recurence relation for the x-component of the bra side

$$\begin{aligned}[(\mathbf{e}+\mathbf{1}_x)\mathbf{0}|\mathbf{f0}]^{(m)} &= (L_x - A_x)[\mathbf{e0}|\mathbf{f0}]^{(m)} + \frac{\rho}{\Lambda}(R_x - L_x)[\mathbf{e0}|\mathbf{f0}]^{(m+1)} \\ &+ \frac{e_x}{2\Lambda}\left([(\mathbf{e}-\mathbf{1}_x)\mathbf{0}|\mathbf{f0}]^{(m)} - \frac{\rho}{\Lambda}[(\mathbf{e}-\mathbf{1}_x)\mathbf{0}|\mathbf{f0}]^{(m+1)}\right) \\ &+ \frac{f_x\rho}{2\Lambda P}[\mathbf{e0}|(\mathbf{f}-\mathbf{1}_x)\mathbf{0}]^{(m+1)} \end{aligned} \tag{3.58}$$

where the *auxiliary electron repulsion integrals* are defined as

$$[\mathbf{e0}|\mathbf{f0}]^{(m)} = \int_0^1 t^{2m} P(t) \exp(-(U_x + U_y + U_z)t^2) dt \tag{3.59}$$

and are, in theory, possible to evaluate by Rys quadrature. Lindh et. al. [120] went even further by spliting the five-term vertical recurrence relation to two simpler four-term recurrence relations, for added efficiency and simplicity.

Finally we should mention that Gill et al. [126, 127] have combined some of the above methods together into the "PRISM" algorithm which is supposed to be more efficient than any method alone. This happens because the PRISM algorithm selects the method best suited to a particular molecule and basis set. However, as one would expect, the complexity associated with implementing a PRISM algorithm is substantially higher than implementing each one method alone.

The paper by Taketa et al. [128] gives closed form analytic expresions for the two-electron integrals of primitive Cartesian Gaussian functions. Due to their high complexity these expressions have little practical value.

3.10 Quadratic scaling in Coulomb energy evaluation

Direct SCF methods are possible because they skip the evaluation of two-electron integrals which are predicted to make negligible contributions to the quantities involved in the SCF calculation. There is no definite measure of "negligible contributions" but usually a threshold that can be determined empirically and should be satisfactory for most calculations. Integral algorithms calculate integrals in *batches*, therefore direct SCF schemes skip batches of integrals.

3.10.1 Upper bound for a batch of integrals

The magnitude of the maximum element of a batch of integrals will be represented by

$$(IJ|KL) = (KL|IJ) \tag{3.60}$$

for four-index two-electron integrals and by

$$(F|IJ) = (IJ|F) \tag{3.61}$$

for three-index two-electron integrals. The symbol I represents a particular shell of contracted Cartesian Gaussian basis functions, i.e. the set of all angular momentum components of a contracted Cartesian Gaussian function. The effort to calculate the numbers $(IJ|KL)$ and $(F|IJ)$ still scales unfavourably with the size of the system, so they have to be approximated by upper bounds. As an upper bound we use the Schwarz inequality which was first employed for this purpose by Ahlrichs et al. [80]

$$(IJ|KL) \leq \sqrt{(IJ|IJ)}\sqrt{(KL|KL)} = EST(IJ, KL) \tag{3.62}$$

and

$$(T|IJ) \leq \sqrt{(T|T)}\sqrt{(IJ|IJ)} = EST(T, IJ) \tag{3.63}$$

The quantities $\sqrt{(IJ|IJ)}$ and $\sqrt{(T|T)}$ constitute a convenient, separable upper bound as they are elements of a matrix and a vector respectively and can be very easily stored on disk.

3.10.2 Tests for rejecting batches of integrals

The two-electron implementation of MAGIC takes advantage of tests for rejecting batches of integrals based on their contribution to the Fock matrix. These tests are much simpler to implement in a DFT formalism since one does not have to predict the contribution of two-electron integrals to the exchange, as is the case with Hartree-Fock calculations.

For the case of the RI-J approximation there are two sets of tests. The first time the three-index two-electron integrals are calculated, an upper bound on their

contribution to the charges is used for neglecting batches

$$V_T^{-1} EST(T, IJ) D_{IJ} < THR1 \tag{3.64}$$

where V_T^{-1} is a compressed form of the $\mathbf{V}^{-1}$ matrix according to the following relation

$$V_T^{-1} = \max_{\substack{s\epsilon(1,...N_{AUX}) \\ t\epsilon T}} |V_{st}^{-1}| \tag{3.65}$$

where T denotes a shell of auxiliary functions. In a similar manner D_{IJ} is a compressed density matrix.

$$D_{IJ} = \max_{i\epsilon I, j\epsilon J} |D_{ij}| \tag{3.66}$$

We can observe that all the quantities in equation (3.64) have insignificant computational and storage requirements. Integral batches $(\mathbf{t}|\mathbf{ij})$ are rejected then when the left hand side of (3.64) is less than the threshold value $THR1$.

The second time the three-index two-electron integrals are calculated an upper bound based on their contribution to the Molecular Orbital (MO) Fock matrix elements between occupied and virtual orbitals is used. Almolf et al. [79] argue that this upper bound to neglect integrals should be adequate. Also it should not affect convergence since the elements of the Fock matrix between occupied and virtual orbitals are the ones that determine the amount of virtual orbitals that will be mixed to the occupied orbitals in each SCF cycle. The test for skipping integrals now is

$$q_T EST(T, IJ) C_{IJ} < THR2 \tag{3.67}$$

with the following definitions.

$$\begin{aligned} C_{IJ} &= \max_{i\epsilon I, j\epsilon J} \quad (o_i u_j + o_j u_i) \\ o_i &= \max_{a\ \epsilon\ occ} \quad |c_{ia}| \\ u_i &= \max_{b\ \epsilon\ virt} \quad |c_{ib}| \\ q_T &= \max_{t\epsilon T} \quad |q_t| \end{aligned} \tag{3.68}$$

The subsripts a and b denote occupied and virtual orbitals respectively, c_{ij} are the orbital expansion coefficients in terms of the basis set and T is a particular shell of auxiliary functions. Again, the calculation of the batch $(\mathbf{t}|\mathbf{ij})$ is skipped if the left hand side of equation (3.67) is less than the value of $THR2$.

One further development implemented in MAGIC is the *recursive Fock matrix build*. This technique becomes more efficient towards the last few iterations of an SCF calculation. It is based on the obvious fact that close to convergence there is none, or very little change to some of the charges between two consecutive SCF iterations. Therefore for all SCF cycles apart from the first the Fock matrix can be built as an increment to the Fock matrix of the previous iteration

$$F_{ij}^{(m)} = F_{ij}^{(m-1)} + (ij|\mathbf{f})(\mathbf{q}^{(m)} - \mathbf{q}^{(m-1)}) \tag{3.69}$$

where the superscripts in parentheses denote the number of the SCF cycle. The same principle can be applied to save work from the calculation of the charges.

$$\mathbf{q}^{(m)} = \mathbf{q}^{(m-1)} + \mathbf{V}^{-1}(\mathbf{f}|\rho^{(m)} - \rho^{(m-1)}) \tag{3.70}$$

As an indication of the efficiency of the recursive Fock matrix build, it is worth mentioning that the time spent in the evaluation of the Coulomb energy in the last SCF iteration is roughly half of the time spent for the same task in the first SCF iteration.

The tests for skipping integrals are combined together with the recursive Fock matrix build by replacing D_{IJ} with $D_{IJ}^{(m)} - D_{IJ}^{(m-1)}$ in equation (3.64) and q_T with $q_T^{(m)} - q_T^{(m-1)}$ in equation (3.67).

The implementation of the tests for rejecting integrals in the four-index two-electron code of MAGIC is slightly different as it is designed to skip integrals based on their contribution to elements of the Fock matrix in the basis set representation. Therefore the tests for the batch of integrals $(\mathbf{ij}|\mathbf{kl})$ are now simply

$$EST(IJ,KL)(D_{KL}^{(m)} - D_{KL}^{(m-1)}) < THR2 \tag{3.71}$$

and

$$EST(IJ,KL)(D_{IJ}^{(m)} - D_{IJ}^{(m-1)}) < THR2 \tag{3.72}$$

and they are of comparable efficiency to the tests for the RI-J method of calculating the Coulomb part of the Fock matrix.

A series of RI-J calculations on crown ethers of increasing size were performed in order to determine the highest possible values of $THR1$ and $THR2$ that do not compromise accuracy. Crown ethers 3c1 (C_2H_4O) up to 21c7 ($C_{14}H_{28}O_7$) were employed for this investigation. The LDAX functional and DZ basis were used. $THR1$ and $THR2$ were varied independently and $THR1 = THR2 = 10^{-11}$ were selected as optimum threshold values. The resulting error in energy for this value of the thresholds is shown below:

Molecule	Error (E_h)
3c1	3.805×10^{-6}
6c2	3.912×10^{-6}
9c3	-2.704×10^{-4}
12c4	-3.780×10^{-6}
15c5	-6.402×10^{-5}
18c6	-3.365×10^{-5}
21c7	-1.139×10^{-5}

The maximum error in energy, with respect to the energy obtained without integral cutoffs, with these thresholds is -2.709×10^{-4} E_h for the 9c3 ($C_6H_{12}O_3$) molecule. Further testing of these threshold values was performed with a set of 85 molecules covering a wide range of functionals and basis sets and resulted in values of mean, RMS and maximum error of 1.0 $\times10^{-6}$, 2.0 $\times10^{-6}$ and 1.2 $\times10^{-5}$ E_h respectively.

These threshold values were derived for the RI-J approximation but they have proved equally efficient and accurate for the four-index case.

Although they have been tested extensively, it is important to note that these thresholds are not guaranteed to be successful in every case and the user should be aware of it. For example, in rare cases we have observed that they may lead to convergence difficulties even though they produce accurate energies. Such artefacts disappear by setting the thresholds to lower values.

As mentioned earlier, the RI-J approximation is faster than the "exact" calculation by roughly one order of magnitude. For example, let us consider the first SCF iteration for the H_3COSiH_3 molecule with the LDAX functional, the TZVP basis set [58] and the corresponding auxiliary basis set of Ahlrichs et al. [94, 95]. In this particular case, with $THR1 = THR2 = 10^{-11}$, the time it takes to calculate the Coulomb energy "exactly" is 79.4 s while the time it takes to calculate it with the RI-J approximation is 8.8 s, all on one 200MHz R10000 processor of a Silicon Graphics Origin 2000 computer. This fact is dictated by the difference in the amount of computation in the two cases and holds without exception for all calculations. The requirements in computer resources of the three- and four-index code are comparable because they both calculate the Coulomb contribution in a direct SCF fashion and use only as much memory as is necessary for the generation of one batch of integrals at a time.

Chapter 4

Convergence of SCF calculations

4.1 Introduction

The solution of the SCF equations for a single determinant wavefunction, where the orbitals are expressed as linear combinations of basis functions with the Roothaan formalism [2], is a complicated non-linear problem. The simple iterative solution of the Roothaan equations is successful only for very few small cases. For basis sets larger than minimal or molecules with three atoms or more the sequence of diagonalisations and updates of the Fock matrix leads to divergent or oscillatory behaviour. The early work by Cízek and Paldus [129] on the stability of Hartree-Fock solutions is classic. There are numerous schemes in the literature which have been devised to amend the shortcomings of plain diagonalisation and assist convergence. These schemes increase substantially our ability to converge SCF calculations but by no means provide a method that will always converge. Therefore, failure to converge with one method does not necessarily mean that a solution does not exist and indeed very often convergence is achieved by changing the parameters of the convergence assisting methods. In this chapter we describe the most common and successful convergence assistance techniques that have been implemented in MAGIC as well as our experiences with some new methods that are still under development.

4.2 Direct inversion in the iterative subspace

The Direct Inversion in the Iterative Subspace (DIIS) is a method of extrapolation which aims to speed up SCF convergence by constructing an improved approximation to the solution which is a linear combination of all previous approximations. By solution we mean either the orbital coefficient matrix, or the density matrix, or the Fock matrix, or in general any set of parameters that is sufficient to define the density resulting from an SCF calculation.

In the implementation of DIIS it was chosen to use the Fock matrix $\mathbf{F}$ in the basis set representation as the set of parameters that defines an SCF solution. The original idea of DIIS is due to Pulay [130] and is based on the assumption that at each SCF iteration we can define a quantity called the *error vector*. The error vector $\mathbf{e}_i$ at the ith SCF iteration is supposed to represent the deviation of our current approximation $\mathbf{F}_i$ from the SCF solution $\mathbf{F}_{SCF}$.

$$\mathbf{F}_i = \mathbf{F}_{SCF} + \mathbf{e}_i \tag{4.1}$$

If this assumption is true, then a linear combination of available error vectors could be constructed that approaches the zero vector in the least squares sense

$$\sum_{j=1}^{N_{err}} c_j \mathbf{e}_j \simeq 0 \tag{4.2}$$

where N_{err} is the number of error vectors that we chose to participate in the sum of equation (4.2). In general, if the error vectors are linearly independent, equation (4.2) will be exact only when the dimension of the error vector space exceeds the dimension of the parameter space. That is only when $N_{err} > N_{BF}(N_{BF}+1)/2$ where N_{BF} is the number of basis functions. Furthermore, if we impose the constraint that the expansion coefficients add up to unity

$$\sum_{j=1}^{N_{err}} c_j = 1 \tag{4.3}$$

we can easily show that the SCF solution is equal to

$$\mathbf{F}_{SCF} = \sum_{j=1}^{N_{err}} c_j \mathbf{F}_j \tag{4.4}$$

Therefore the DIIS method attempts to find $\mathbf{F}_{SCF}$ as an extrapolation from previous $\mathbf{F}_j$. We calculate the error vector as follows

$$\mathbf{e}_i = \mathbf{F}_i\mathbf{D}_i\mathbf{S} - \mathbf{S}\mathbf{D}_i\mathbf{F}_i \tag{4.5}$$

where $\mathbf{S}$ is the overlap matrix. It can be easily shown that this quantity becomes zero when self consistency is reached. SCF convergence is achieved when the element of $\mathbf{e}_i$ with the largest magnitude

$$\delta_i^{DIIS} = \max_{r,s} |(\mathbf{e}_i)_{rs}| \tag{4.6}$$

is less than the convergence threshold value we have set. The default value of the convergence threshold is 10^{-6}.

We follow a variation by Sellers [131] to the original DIIS scheme. This variation has been termed C^2-DIIS and has been demonstrated to have improved stability properties. At each SCF iteration we compute and store the corresponding error vector. We then construct the DIIS matrix $\mathbf{B}$ with elements

$$B_{ij} = \mathbf{e}_i \cdot \mathbf{e}_j = \sum_{k=1}^{N_{BF}} \sum_{l=1}^{k} (\mathbf{e}_i)_{kl}(\mathbf{e}_j)_{kl} \tag{4.7}$$

and diagonalise it. If its smallest eigenvalue is greater than 5 we do not attempt to perform a DIIS extrapolation. Otherwise we select the eigenvector corresponding to the smallest eigenvalue subject to the conditions that this eigenvalue is greater than zero and that the largest element of the eigenvector is less than 100. This process is repeated until we find an eigenvector $\mathbf{q}$ which satisfies these conditions. If no such eigenvector is found no extrapolation takes place and the DIIS will start from the beginning in the next SCF iteration. If the search has been successful, $\mathbf{q}$ is normalised to one in order to produce the coefficients of equation (4.4).

$$c_j = \frac{q_j}{\sum_{i=1}^{N_{err}} q_i} \tag{4.8}$$

Our presentation of DIIS was in the context of the restricted closed shell SCF formalism. The extension to unrestricted SCF is straighforward and does not involve any new concepts.

4.3 Level shifting

The "Level shifting" method of Saunders et al. [132] has proved to be quite a successful tool for assisting convergence and is implemented in MAGIC.

We will outline the method for the restricted closed shell case as the generalisation to unrestricted determinants is straightforward. Let $\mathbf{F}^{mo}$ be the Fock matrix in the molecular orbital basis and $\mathbf{F}^{ao}$ be the Fock matrix in the atomic orbital (basis functions) basis. The number of basis functions is N_{BF}, the number of occupied orbitals is N_{occ} and the number of virtual orbitals is N_{virt}.

At the nth iteration of the SCF procedure the Fock operator $\hat{F}_n$ will be constructed from the current set of molecular orbitals which we represent as

$$\{|i\rangle\}_{i=1}^{N_{BF}} = \{|a\rangle\}_{a=1}^{N_{occ}}, \{|r\rangle\}_{r=N_{occ}+1}^{N_{BF}} \tag{4.9}$$

where the indices i, j, k will be used to denote any orbital, the indices a, b, c will denote occupied orbitals and the indices r, s, t will denote virtual orbitals. These orbitals are orthonormal and form a complete basis in the space of the N_{BF} basis functions. Using the closure property of the orbitals we can write the Fock operator as

$$\hat{F}_n = \sum_{a=1}^{N_{occ}} \sum_{b=1}^{N_{occ}} |a\rangle\langle a|\hat{F}_n|b\rangle\langle b| + \sum_{r=N_{occ}+1}^{N_{BF}} \sum_{s=N_{occ}+1}^{N_{BF}} |r\rangle\langle r|\hat{F}_n|s\rangle\langle s| \tag{4.10}$$

$$+ \sum_{a=1}^{N_{occ}} \sum_{r=N_{occ}+1}^{N_{BF}} \Big[|a\rangle\langle a|\hat{F}_n|r\rangle\langle r| + |r\rangle\langle r|\hat{F}_n|a\rangle\langle a|\Big] = \hat{F}_n^{oo} + \hat{F}_n^{vv} + \hat{F}_n^{ov+vo} \tag{4.11}$$

Without loss of generality we can assume that the orbitals $|k\rangle$ are pseudocanonical [133], i.e. that

$$\hat{F}_n^{oo}|a\rangle = \epsilon_a|a\rangle, \quad \hat{F}_n^{oo}|r\rangle = 0 \tag{4.12}$$

$$\hat{F}_n^{vv}|r\rangle = \epsilon_r|r\rangle, \quad \hat{F}_n^{vv}|a\rangle = 0 \tag{4.13}$$

Pseudocanonical orbitals can always be constructed by a unitary transformation of the occupied orbitals with themselves and the virtual orbitals with themselves as this has no effect on the wavefunction.

The next step is to modify the $\hat{F}^{vv}$ operator by including a large positive number β to form the $\hat{F}^{vv+\beta}$ operator

$$\hat{F}_n^{vv+\beta} = \sum_{r=N_{occ}+1}^{N_{BF}} \sum_{s=N_{occ}+1}^{N_{BF}} |r\rangle\langle r|\hat{F}_n + \beta|s\rangle\langle s| \tag{4.14}$$

This results in the following modification of equation (4.13)

$$\hat{F}_n^{vv+\beta}|r\rangle = (\epsilon_r + \beta)|r\rangle, \quad \hat{F}_n^{vv+\beta}|a\rangle = 0 \tag{4.15}$$

The eigenvalues of the virtual orbitals are shifted upwards by β. The value of β is supposed to be large enough to raise the eigenvalues of the virtual orbitals higher than any occupied orbital eigenvalue even if this was not the case initially.

To show the effect of shifting the eigenvalues of the virtual orbitals on the convergence properties of the wavefunction we will apply Rayleigh-Schrödinger perturbation theory. We wish to determine the orbitals that will emerge from the diagonalisation of $\hat{F}_n^{\beta} = \hat{F}_n^{oo} + \hat{F}_n^{vv+\beta} + \hat{F}_n^{ov+vo}$ in the $|i\rangle$ basis. The zeroth order Hamiltonian is

$$\hat{H}^{(0)} = \hat{F}_n^{oo} + \hat{F}_n^{vv+\beta} \tag{4.16}$$

with the molecular orbitals $|i\rangle$ being its eigenfunctions and zeroth order solutions. The perturbation is

$$\hat{H}^{(1)} = \hat{F}_n^{ov+vo} \tag{4.17}$$

From a standard text of quantum chemistry [134] we can find that the first order correction to the occupied orbitals should be as follows:

$$\begin{aligned} |a\rangle^{(1)} &= \sum_{b\neq a} \frac{\langle b|\hat{H}^{(1)}|a\rangle}{\epsilon_a - \epsilon_b}|b\rangle + \sum_{r=N_{occ}+1}^{N_{BF}} \frac{\langle r|\hat{H}^{(1)}|a\rangle}{\epsilon_a - (\epsilon_r + \beta)}|r\rangle \\ &= 0 + \sum_{r=N_{occ}+1}^{N_{BF}} \frac{\langle r|\hat{F}_n|a\rangle}{\epsilon_a - (\epsilon_r + \beta)}|r\rangle = \sum_{r=N_{occ}+1}^{N_{BF}} \Delta_{ra}|r\rangle \end{aligned} \tag{4.18}$$

It can be seen that to first order only virtual orbitals are mixed into the occupied ones. If β is large enough, Δ_{ra} will be small enough to make second and higher order contributions negligible. For the same reason we take into account only the linear terms that contribute to changes in the electronic energy.

$$\Delta E = E_{n+1} - E_n \simeq \sum_{r=N_{occ}+1}^{N_{BF}} \sum_{a=1}^{N_{occ}} \Delta_{ra}\langle r|\hat{F}_n|a\rangle \tag{4.19}$$

We observe that this expression is always negative. However ΔE can be very small and make convergence too slow. The choice of the value of β is crucial for this. In our implementation we start with $\beta = 4$ and when DIIS is switched on we either set it to zero, or alter its value according to the following ansatz

$$\beta_n = \exp\left(-\left(\frac{n+1}{\delta_n^{DIIS}}\right)^{0.7}\right) \tag{4.20}$$

where β_n is the value of β for the nth iteration. This ansatz for β_n is justified by practical experience, not theory. We can observe that β_n decreases quickly with increasing SCF iteration number n and decreasing convergence parameter magnitude δ_n^{DIIS}. When the error vector magnitude becomes less than or equal to 10^{-5} we set β equal to zero to make sure that the eigenvalues of the virtual orbitals are not shifted at convergence.

In our implementation we simply add in every iteration the matrix

$$\mathbf{SC}\left(\begin{array}{c|c} \mathbf{0}^{oo} & \mathbf{0}^{ov} \\ \hline \mathbf{0}^{vo} & \mathbf{I}^{vv}\beta_n \end{array}\right)\mathbf{C}^{\dagger}\mathbf{S} \tag{4.21}$$

to the $\mathbf{F}^{ao}$ matrix, where $\mathbf{S}$ is the overlap matrix and $\mathbf{C}$ is the coefficient matrix for all the molecular orbitals.

4.4 Initial approximation for the density

An initial approximation, or guess for the density matrix $\mathbf{D}$ is necessary for starting an SCF calculation. The self consistent solution is equivalent to the constrained minimisation of the energy in the space of the elements of $\mathbf{D}$ or the coefficients for the expansion of the occupied orbitals in terms of the basis set. An iterative procedure produces a sequence of points in this space which we desire to be convergent. The starting point of the sequence determines to a great extent the convergence properties. It is obvious that the closer the starting point is to the solution, the better are the chances for the sequence to converge.

Probably the simplest type of initial approximation to the density is the one that can be obtained by the diagonalisation of the core Hamiltonian $\hat{H}^{core}$. The

core Hamiltonian for one electron in the potential of N_{nuc} nuclei is defined by

$$\hat{H}^{core} = -\frac{1}{2}\nabla^2 - \sum_{A=1}^{N_{nuc}} \frac{Z_A}{|\mathbf{r} - \mathbf{A}|} \tag{4.22}$$

where Z_A is the charge of nucleus A in atomic units and $\mathbf{A}$ is its position. The orbitals that emerge from this procedure are certainly not close to the converged SCF orbitals. Their drawback is that they do not include any effects due to the interaction of electrons with each other. We have observed that this kind of initial guess often leads to divergence, especially when it is used with molecules containing atoms of the fourth period or lower where the electrons experience an effective nuclear charge much smaller than the real one due to shielding from other electrons.

An improved initial guess which we have implemented is the Independent Atomic Densities Initial Aproximation (IADIA). Within this scheme, calculations are performed for every different atom and basis set of the molecule. The density matrices computed for each atom are then combined together and stored as diagonal blocks in a large block-diagonal matrix. For a chosed shell molecule for example the block diagonal density matrix would be

$$\mathbf{D}^{block} = \begin{pmatrix} \mathbf{D}_A & \mathbf{0} & \\ \mathbf{0} & \mathbf{D}_B & \\ & & \ddots \end{pmatrix} \tag{4.23}$$

where $\mathbf{D}_A$ is the sum of the alpha and beta density matrices for atom A. Since we are using a single determinant formalism to calculate the atomic densities we have to use fractional occupation numbers for the incomplete groups in order to produce space isotropic atomic densities. Therefore, for the oxygen atom for example, we perform an unrestricted calculation where we assume five occupied alpha and five occupied beta orbitals. The occupation numbers of the alpha orbitals are all equal to one as is the occupation of the first two beta orbitals ($1s\beta, 2s\beta$) while the occupation of the remaining three beta orbitals ($2p\beta$) is $\frac{1}{3}$. In setting up fractional occupation numbers for the atomic orbitals we assume that they are always occupied according to the following order:

$$\begin{aligned} &1s < 2s < 2p < 3s < 3p < 4s < 3d < 4p < 5s < 4d < 5p \\ &< 6s < 4f < 5d < 6p < 7s < 5f < 6d < 7p \end{aligned} \tag{4.24}$$

Even if this order is not absolutely correct for every element, it has negligible effect on the quality of the guess. For atoms whose core is represented by an effective core potential we assume the same filling order starting from the orbitals not present in the core. The atomic SCF calculations are carried out using a core Hamiltonian guess and this can lead to convergence problems, especially for the heavier elements. A method which usually overcomes this problem is the gradual introduction of the Coulomb part of the Fock operator, which is by far the largest contribution added to the core Hamiltonian operator. This is achieved by scaling the Coulomb operator through the first 10 SCF iterations for atoms with atomic number larger than 20. Thus the Coulomb part of the Fock operator is scaled by 0.1 for the the first SCF iteration, 0.2 for the second SCF iteration, etc. Unfortunately this method is not very successful for molecules.

A fundamental property of a density matrix is idempotency which is equivalent to orthonormality of the orbitals. We want our IADIA density to be idempotent. This can be achieved by solving the following generalised eigenvalue problem

$$\mathbf{D}^{block}\mathbf{S}\mathbf{C} = \mathbf{C}\eta' \tag{4.25}$$

where $\mathbf{S}$ is the overlap matrix for the molecule. The result is a set of orbital coefficients $\mathbf{C}$ and fractional occupation numbers η'. Next we set the N_{occ} largest values of η' equal to 2 and zero the rest to obtain a column vector of integer occupation numbers η. The idempotent IADIA density is then

$$\mathbf{D}^{IADIA} = \mathbf{C}\eta\mathbf{C}^{\dagger} \tag{4.26}$$

Here too, the extension to unrestricted determinants is straighforward.

4.5 Density Matrix Search methods

4.5.1 Density matrix formulation of the SCF procedure

It has been known since the pioneering work of McWeeny [135] that a Hartree-Fock (HF) calculation can be performed without using any orbitals but using the density matrix instead. The HF energy and all properties can be written as functions of

the density matrix elements and orbitals need not appear in the iterative solution of the SCF equations.

In order to facilitate our discussion we will represent the trace of the product of two matrices **A** and **B** as a dot product

$$\mathbf{A}^\dagger \cdot \mathbf{B} = \mathrm{Tr}(\mathbf{AB}) = \sum_{ij} A_{ij} B_{ji} \tag{4.27}$$

where we perceive **B** as a column vector constructed by stacking the columns of the matrix **B** on top of each other in order to form one large column. We see $\mathbf{A}^\dagger$ as a row vector constructed by stacking the rows of the matrix $\mathbf{A}^\dagger$ together to form one large row vector. We assume that we will be dealing only with real matrices, so $\mathbf{A}^\dagger$ is the transpose of **A**.

Using this notation we can write the HF energy expression for a restricted closed shell calculation as

$$E(\mathbf{D}) = \mathbf{D}^\dagger \cdot (\mathbf{H} + \mathbf{F}) = 2\mathbf{D}^\dagger \cdot (\mathbf{H} + \mathbf{II} \cdot \mathbf{D}) \tag{4.28}$$

where **D** is the density matrix for the electrons with alpha spin. For the restricted closed shell case it is equal to one half of the total electron density matrix since electrons with alpha and beta spin occupy the same orbitals. **H** is the core Hamiltonian matrix and **II** is the two-electron integral supermatrix, *all expressed in terms of an orthonormal basis set.* The elements of **II** are

$$II_{ijkl} = (ij|kl) - \frac{1}{2}(il|kj) \tag{4.29}$$

In his original work, McWeeny showed that a HF calculation could be performed with a Density Matrix Search (DMS) method. Starting from an initial guess density matrix $\mathbf{D_0}$ we can iteratively converge to the same result as a conventional calculation with Fock matrix diagonalisation by minimising the following function with a steepest descent procedure.

$$\Omega_1(\mathbf{D}) = \mathbf{F}^\dagger \cdot \mathbf{D} = \sum_{a=1}^{N_{occ}} \epsilon_a \ , \tag{4.30}$$

The value of Ω_1 is equal to the sum of the occupied orbital energies for every density matrix **D** that can be shown to be made of N_{occ} occupied orthonormal

spatial orbitals. The gradient of the function at each step of the procedure is simply $\mathbf{F}$ (not taking into account the dependence of $\mathbf{F}$ on $\mathbf{D}$). At each steepest descent step $\mathbf{F}$ is updated by the new density. However, it is necessary to impose the condition of idempotency on the density matrix, $\mathbf{D}^2 = \mathbf{D}$, which is equivalent to the orthonormality of orbitals. This is achieved by repeated applications of the purification transformation

$$\mathbf{D}_n = 3\mathbf{D}_{n-1}^2 - 2\mathbf{D}_{n-1}^3 \tag{4.31}$$

until $\mathbf{D}_n$ becomes equal to $\mathbf{D}_{n-1}$ within some predetermined tolerance. This artificial application of the idempotency constraint is not always successful. As Li et al. have showed [136] the purification transformation restores the idempotency of an almost-idempotent density matrix only when its eigenvalues (which correspond to the occupation numbers of the orbitals) are in the interval $(-0.5, 1.5)$. If some iteration of the steepest descent DMS procedure produces a density matrix with eigenvalues outside this interval the purification transformation diverges rapidly and the method breaks down.

4.5.2 Impoved density matrix search methods

Since diagonalisation is inherently an N_{BF}^3 process [64], where N_{BF} is the number of basis functions, attempts to achieve linear scaling in quantum chemical calculations should avoid it. Furthermore, the solution of the SCF equations by repeated diagonalisation can lead to divergent behaviour even though a solution exists.

As an alternative to diagonalisation, DMS methods involve matrix multiplications and can be made to scale linearly provided that the matrices involved are sparse enough to be handled efficiently by sparse matrix multiplication routines whose computational cost increases linearly with system size. Convergence behaviour should be better as well, since DMS methods seek to minimise a function of many variables in a systematic way rather than repeat a process until self consistency is achieved.

Ochsenfeld et al. [137] proposed to minimise the following function

$$\Omega_2(\mathbf{D}) = 2(\tilde{\mathbf{D}}^\dagger \cdot \mathbf{H} + \tilde{\mathbf{D}}^\dagger \cdot \mathbf{II} \cdot \tilde{\mathbf{D}}) \tag{4.32}$$

where

$$\tilde{\mathbf{D}} = 3\mathbf{D}^2 - 2\mathbf{D}^3 \tag{4.33}$$

The value of this function is equal to the HF energy for any idempotent density. The function has the same form as the expression for the HF energy in terms of the density matrix (4.28) but with a purification transformation in place of the density matrix. Therefore it has some built-in idempotency-preserving capabilities and the authors claim it can be minimised with a Newton-Raphson type method in an unconstrained fashion. Idempotency and the correct number of electrons constraints are taken care of automatically by the form of the function.

We are not currently interested in calculations on molecules whose size causes the diagonalisation stage to become a computational bottle neck. However we are very much interested in methods alternative to diagonalisation from the point of view of converging SCF calculations. Difficulties arise often in the convergence of DFT calculations on heavy atom complex compounds. We want to investigate if DMS methods can yield a convergence technique which is more robust or at least complementary to diagonalisation.

We first implemented the Conjugate Gradient Density Matrix Search (CG-DMS) method for DFT calculations by Millam and Scuseria [138]. The function to be minimised is

$$\Omega_3(\mathbf{D}) = \mathbf{F}^\dagger \cdot \tilde{\mathbf{D}} + \mu(\mathbf{D}^\dagger \cdot \mathbf{I} - N_{occ}) \tag{4.34}$$

where N_{occ} is the number of occupied orbitals and the Lagrange multiplier μ is introduced to keep the number of occupied orbitals (or alpha electrons) constant. We observe that this function has some idempotency-preserving properties too as it is equivalent to the original function $\Omega_1(\mathbf{D})$ of McWeeny with a purification transformation in place of the density.

In our implementation we use the IADIA initial approximation as a starting density. Furthermore, we use the set of orbitals that emerge from it as the orthonormal basis set in terms of which the Fock and density matrices are expressed. On the other hand, Millam and Scuseria used the Cholesky decomposition of the overlap matrix to orthogonalise the basis set due to computational cost considerations for

large systems. A conjugate gradient minimization method is used to find the density which mininises the function. The gradient with respect to the elements of $\mathbf{D}$, assuming $\mathbf{F}$ does not depend on $\mathbf{D}$, is

$$\nabla\Omega_3(\mathbf{D}) = 3\mathbf{DF} + 3\mathbf{FD} - 2\mathbf{D}^2\mathbf{F} - 2\mathbf{DFD} - 2\mathbf{FD}^2 + \mu\mathbf{I} \tag{4.35}$$

The Lagrange multiplier μ is chosen so that the gradient is traceless. This is sufficient to satisfy the constraint.

$$\mu = \frac{-3\mathbf{D}^\dagger \cdot \mathbf{F} - 3\mathbf{F}^\dagger \cdot \mathbf{D} + 2(\mathbf{D}^2)^\dagger \cdot \mathbf{F} + 2(\mathbf{DF})^\dagger \cdot \mathbf{D} + 2\mathbf{D}^\dagger \cdot \mathbf{F}^2}{N_{BF}} \tag{4.36}$$

The minimization of Ω_3 is carried out with the conjugate gradient method. The conjugate gradient method minimizes a function in steps by choosing a particular direction for each step in the space of minimization variables and then carrying out a line search in order to find the minimum of the function in this direction. The directions are selected in such a way that if the function we minimise is quadratic, we are guaranteed to reach a minimum in a number of steps which is equal to the number of independent variables [139]. The CG-DMS method involves the following steps:

1. Define initial direction as the negative of the gradient at the starting density:

$$\mathbf{J}_0 = \mathbf{G}_0 = -\nabla\Omega_3(\mathbf{D}_0) \tag{4.37}$$

2. Construct a new density matrix $\mathbf{D}_{i+1} = \mathbf{D}_i + \lambda_i\mathbf{J}_i$, where λ_i is a line search coefficient and $\mathbf{J}_i$ is the line search direction for the $(i+1)$th step. The density $\mathbf{D}_{i+1}$ is not completely idempotent and therefore we need to apply the purification transformation to it. We iterate the purification transformation until the absolute value of each element of the matrix $(\mathbf{D}^2 - \mathbf{D})$ is less than 10^{-14}. The density matrices that can be obtained by diagonalisation are idempotent to a similar extent. Usually five or less purification transformations are enough to achieve idempotency below this threshold. Covergence of the CG-DMS calculation is examined at this point by calculating the rms value of the difference of the new density matrix from the density matrix of the previous step.

3. $\mathbf{G}_{i+1} = -\nabla\Omega_3(\mathbf{D}_{i+1})$

4. $\mathbf{J}_{i+1} = \mathbf{G}_{i+1} + \gamma_i \mathbf{J}_i$

5. Set i equal to $i+1$ and go to (2).

The line search in order to determine the coefficient λ_i can be performed exactly since Ω_3 has a cubic dependence on $\mathbf{D}_i$ and can therefore be expressed as a cubic polynomial in λ_i along the line search direction.

$$\Omega_3(\mathbf{D}_i + \lambda_i \mathbf{J}_i) = a\lambda_i^3 + b\lambda_i^2 + c\lambda_i + d \tag{4.38}$$

where

$$\begin{aligned} a &= -2(\mathbf{J}_i^3)^\dagger \cdot \mathbf{F}_i \\ b &= 3(\mathbf{J}_i^2)^\dagger \cdot \mathbf{F}_i - 2(\mathbf{D}_i\mathbf{J}_i^2)^\dagger \cdot \mathbf{F}_i - 2(\mathbf{J}_i\mathbf{D}_i\mathbf{J}_i)^\dagger \cdot \mathbf{F}_i - 2(\mathbf{J}_i^2\mathbf{D}_i)^\dagger \cdot \mathbf{F}_i \\ c &= \mathbf{J}_i^\dagger \cdot \nabla\Omega_3(\mathbf{D}_i) \\ d &= \Omega_3(\mathbf{D}_i) \end{aligned}$$

If we differentiate equation (4.38) with respect to λ_i and set its derivative equal to zero we obtain

$$3a\lambda_i^2 + 2b\lambda_i + c = 0 \tag{4.39}$$

Solution of this quadratic equation yields two roots. We keep the root that yields the smallest value of Ω_3.

The next step is to determine the value of γ_i. There are three different formulas possible which constitute the three different variants of the conjugate gradient method [140]. These variants are equivalent when the function to be minimised is quadratic with respect to the independent variables but differ for functions of higher order.

1. The Polak-Ribière formula:

$$\gamma_i^{PR} = \frac{(\nabla\Omega_3(\mathbf{D}_{i+1}) - \nabla\Omega_3(\mathbf{D}_i))^\dagger \cdot \nabla\Omega_3(\mathbf{D}_{i+1})}{(\nabla\Omega_3(\mathbf{D}_i))^\dagger \cdot \nabla\Omega_3(\mathbf{D}_i)} \tag{4.40}$$

2. The Fletcher-Reeves formula:

$$\gamma_i^{FR} = \frac{(\nabla\Omega_3(\mathbf{D}_{i+1}))^\dagger \cdot \nabla\Omega_3(\mathbf{D}_{i+1})}{(\nabla\Omega_3(\mathbf{D}_i))^\dagger \cdot \nabla\Omega_3(\mathbf{D}_i)} \tag{4.41}$$

Table 4.1: Number of iterations needed to converge DFT calculations to a convergence threshold of 10^{-6} with different CG-DMS variants (PR=Polak-Ribière, HS=Hestenes-Stiefel, FR=Fletcher-Reeves) and with diagonalisation (Diag).

Molecule	Basis	PR	HS	FR	Diag
H_2O	DZ	46	43	53	9
RbCl	631G2DP	157	100	174	13
UO_2^{2+}	DZP	74	71	213	26
PuO_2^{2+}	DZP	89	77	76	30
UF_4	STO3G	85	76	72	no conv.

3. The Hestenes-Stiefel formula:

$$\gamma_i^{HS} = \frac{(\nabla\Omega_3(\mathbf{D}_{i+1}) - \nabla\Omega_3(\mathbf{D}_i))^\dagger \cdot \nabla\Omega_3(\mathbf{D}_{i+1})}{(\nabla\Omega_3(\mathbf{D}_{i+1}) - \nabla\Omega_3(\mathbf{D}_i))^\dagger \cdot \mathbf{J}_i} \tag{4.42}$$

Millam and Scuseria used the Polak-Ribière variant which is the preferred method for most applications. We have chosen to examine all three variants in our implementation. Some representative results are given in Table 4.1.

The LDAX functional was used for the calculations on H_2O, RbCl and UF_4 and the BLYP functional for UO_2^{2+} and PuO_2^{2+}. Quasirelativistic ECPs were used to treat the core electrons of the metal atoms. For the calculations with diagonalisation both DIIS and level shifters were used. The results of Table 4.1 are typical of density matrix search methods. There is no clear-cut superiority of one CG-DMS variant from the other and this can be seen also from other calculations which we don't present here. DMS calculations require roughly 5 times as many iterations as diagonalisation in order to converge to the same extent. CG-DMS is not therefore our first choice for converging calculations for the types of systems we are interested in. It has however some properties that make it preferable for systems which are difficult to converge with conventional diagonalisation techniques. The energy in CG-DMS decreases monotonically through the iterations. This is always observed, in contrast with diagonalisation where the energy can often oscillate without decreasing overall. Another observation is that the energy decrease is rapid towards the early CG-DMS iterations and slows down considerably towards convergence.

Thus, we consider the CG-DMS to be a method which is useful for producing a high quality initial approximation to the density matrix rather than a technique for converging calculations to the end. We use it routinely as a means for extending the quality of the IADIA initial approximation. Twenty to fifty CG-DMS iterations produce energies which differ from the converged energy to a few millihartrees or less and can be driven to convergence by diagonalisation without divergent oscillations that might occur with other initial approximations. The clusters $Rh_4(CO)_{12}$ and $Rh_8(CO)_{19}C$ are two examples of molecules which converge with the assistance of CG-DMS but not with any of the other initial approximations we have implemented. Finally, CG-DMS used thoughout a calculation has proved effective in converging calculations that seem to be intrinsically divergent when diagonalisation is used. The UF_4 molecule of Table (4.1) is such an example.

There are however instances where the CG-DMS method breaks down. This happens when the application of the purification transformation breaks down and results in density matrices with elements whose magnitude increases rapidly through the purification iterations. We have explained under what conditions the purification transformation fails in subsection 4.5.1. Our implementation of CG-DMS does provide for the rare cases where this happens. When it detects divergence of the purification transformation it imposes idempotency by directly diagonalising the density matrix and switching the occupation numbers to 1 and 0.

A further comment about the CG-DMS is that it can be used in conjunction with the RI-J approximation for the Coulomb energy since in its minimisation procedure it neglects the dependence of the Fock matrix on the density and it updates it with the new density after each step. In contrast, minimization of the function of equation (4.32) with a Newton-Raphson scheme requires explicit use of four-index two-electron integrals. Furthemore, Ω_2 is only valid for HF calculations and cannot be adopted for DFT calculations without modification.

4.5.3 Density matrix search with explicit idempotency constraints

In an effort to improve the efficiency of density matrix search techniques we have sought to devise a scheme which is conceptually more rigorous than the ones we

have mentioned so far in the sense that it disposes completely of the purification transformation and includes the idempotency constraint in a natural way. This can be achieved simply by incorporating idempotency constraints through a matrix of Lagrange multipliers $\mathbf{\Lambda}$ to the function of equation (4.30).

$$\begin{aligned}\Omega_4(\mathbf{D}) &= \mathbf{F}^\dagger \cdot \mathbf{D} + \mathbf{\Lambda}^\dagger \cdot (\mathbf{D}^2 - \mathbf{D}) \\ &= \mathbf{H}^\dagger \cdot \mathbf{D} + 2\mathbf{D}^\dagger \cdot \mathbf{II} \cdot \mathbf{D} + \mathbf{\Lambda}^\dagger \cdot (\mathbf{D}^2 - \mathbf{D}) \\ &= \frac{1}{2}\mathbf{D}^\dagger \cdot (4\mathbf{II} + \mathbf{I} \otimes \mathbf{\Lambda} + \mathbf{\Lambda} \otimes \mathbf{I}) \cdot \mathbf{D} + (\mathbf{H} - \mathbf{\Lambda})^\dagger \cdot \mathbf{D} \qquad (4.43)\end{aligned}$$

If we were using Ω_4 to perfom a Hartree-Fock calculation $\mathbf{H}$ should be the core Hamiltonian and $\mathbf{II}$ the two-electron supermatrix as defined in equation (4.29). Then equation (4.43) is a quadratic equation in the elements of $\mathbf{D}$ and provided we knew $\mathbf{\Lambda}$, we could solve for the minimum in one step with the Newton-Raphson method. For DFT calculations $\mathbf{H}$ has to be redefined as the sum of the core Hamiltonian and the exchange-correlation contribution to the Fock matrix. The two electron supermatrix has to be redefined also to contain only the two electron integrals that contribute to the Coulomb energy.

$$II_{ijkl} = (ij|kl) \qquad (4.44)$$

The $\mathbf{H}$ matrix now depends on $\mathbf{D}$ in terms of some complicated function and Ω_4 could not be minimised in one step with a Newtod-Raphson method. We try to minimise Ω_4 using a steepest descent method where we ignore the dependence of $\mathbf{H}$ on $\mathbf{D}$ during the calculation of the gradient and the steepest descent step and update it afterwards. For this purpose the gradient is necessary

$$\nabla\Omega_4(\mathbf{D}) = (4\mathbf{II} + \mathbf{I} \otimes \mathbf{\Lambda} + \mathbf{\Lambda} \otimes \mathbf{I}) \cdot \mathbf{D} + (\mathbf{H} - \mathbf{\Lambda}) \qquad (4.45)$$

In steepest descent the direction $\mathbf{J}$ for each step is given by the negative of the gradient.

$$\mathbf{J} = -\nabla\Omega_4(\mathbf{D}) \qquad (4.46)$$

We also perform a line search to find a coefficient λ which determines the minimum value of Ω_4 along the steepest descent direction. Therefore the new density $\mathbf{D}_{new}$

at each steepest descent step will be given by

$$\mathbf{D}_{new} = \mathbf{D} + \lambda \mathbf{J} \tag{4.47}$$

where $\mathbf{D}$ is the density that was computed in the previous step, or the starting density. The line search has to be carried out at each step in conjunction with the determination of the Lagrange multipliers. There seems to be no direct way to find the Lagrange multipliers. We have devised an iterative scheme for this purpose. Assuming that we start from an idempotent density, the idempotency condition for the new density can be written and rearranged as follows

$$\begin{aligned} (\mathbf{D} + \lambda \mathbf{J})^2 &= \mathbf{D} + \lambda \mathbf{J} \\ \mathbf{J} &= \mathbf{D}\mathbf{J} + \mathbf{J}\mathbf{D} + \lambda \mathbf{J}^2 \qquad (4.48) \\ \mathbf{\Lambda} &= \mathbf{H} + \mathbf{A} \cdot \mathbf{D} + \mathbf{D}\mathbf{J} + \mathbf{J}\mathbf{D} + \lambda \mathbf{J}^2 \qquad (4.49) \end{aligned}$$

where equation (4.49) is derived by expanding the left side of equation (4.48) and $\mathbf{A} = 4\mathbf{II} + \mathbf{I} \otimes \mathbf{\Lambda} + \mathbf{\Lambda} \otimes \mathbf{I}$.

The line search coefficient λ is calculated simply by inserting the density matrix of equation (4.47) into the expression for Ω_4 and minimising with respect to to λ. The resulting expression is

$$\lambda = \frac{\mathbf{J}^\dagger \cdot (\mathbf{\Lambda} - \mathbf{H} - \mathbf{A} \cdot \mathbf{D})}{\mathbf{J}^\dagger \cdot \mathbf{A} \cdot \mathbf{J}} \tag{4.50}$$

Our idea was to determine both $\mathbf{\Lambda}$ and λ with an iterative process at every steepest descent minimization step. We proceeded as follows:

1. Start by setting $\mathbf{\Lambda}$ equal to the unit matrix.
2. Insert the current $\mathbf{\Lambda}$ into equation (4.50) to get an improved estimate for λ.
3. Insert the current λ into equation (4.49) in to get an improved estimate for $\mathbf{\Lambda}$.
4. Stop if $\mathbf{\Lambda}$ has converged, otherwise go to step 2.

Unfortunately this process either converges very slowly (thousands of iterations) or, most of the times, diverges. The behaviour depends on the molecule and basis set.

Our next attempt was to simplify the function we optimise by neglecting the dependence of the Fock matrix on the density during the steepest descent steps. Thus such a function can be written as

$$\Omega_5(\mathbf{D}) = \frac{1}{2}\mathbf{D}^\dagger \cdot (\mathbf{I} \otimes \mathbf{\Lambda} + \mathbf{\Lambda} \otimes \mathbf{I}) \cdot \mathbf{D} + (\mathbf{F} - \mathbf{\Lambda})^\dagger \cdot \mathbf{D} \tag{4.51}$$

and its gradient is

$$\nabla\Omega_5(\mathbf{D}) = (\mathbf{I} \otimes \mathbf{\Lambda} + \mathbf{\Lambda} \otimes \mathbf{I}) \cdot \mathbf{D} + \mathbf{F} - \mathbf{\Lambda} \tag{4.52}$$

The line search direction $\mathbf{J}$ is defined again as the negative of the gradient

$$\mathbf{J} = -\nabla\Omega_5(\mathbf{D}) \tag{4.53}$$

and the idempotency condition with equation (4.52) provide a formula for $\mathbf{\Lambda}$

$$\begin{aligned} \mathbf{\Lambda} &= (\mathbf{I} \otimes \mathbf{\Lambda} + \mathbf{\Lambda} \otimes \mathbf{I})^\dagger \cdot \mathbf{D} + \mathbf{F} + \mathbf{DJ} + \mathbf{JD} + \lambda\mathbf{J}^2 \\ &= \mathbf{\Lambda D} + \mathbf{D\Lambda} + \mathbf{F} + \mathbf{DJ} + \mathbf{JD} + \lambda\mathbf{J}^2 \end{aligned} \tag{4.54}$$

The line search coefficient is given as before by minimising Ω_5 with respect to λ

$$\lambda = \frac{\mathbf{J}^\dagger \cdot (\mathbf{\Lambda} - \mathbf{F} + \mathbf{D\Lambda} + \mathbf{\Lambda D})}{\mathbf{J}^\dagger \cdot (\mathbf{\Lambda J} + \mathbf{J\Lambda})} \tag{4.55}$$

It turns out that it is possible to determine $\mathbf{\Lambda}$ and λ iteratively for Ω_5 with little effort. In all cases we tried, $\mathbf{\Lambda}$ converges to a maximum error of less than 10^{-10} in less than 20 iterations if we start from the unit matrix and in less than 10 iterations if we start from the $\mathbf{\Lambda}$ of the previous steepest descent step. This in turn produces a density matrix which is idempotent to a maximum error of the order of 10^{-14}, i.e. comparable to diagonalisation. Attempts to improve the efficiency of the minimisation of Ω_5 by using a conjugate gradient method have failed, again due to difficulty or inability to converge $\mathbf{\Lambda}$.

Overall, the minimisation of Ω_5 with the steepest descent method appears to be as efficient as the minimisation of Ω_3 with the conjugate gradient method. Energy lowering is fast at the beginning but slows down considerably when approaching convergence. We view this too as a method for improving the initial approximation prior to converging with diagonalisation. Amongst the advantages of the scheme is

its independence from the purification transformation and that it can be combined with the RI-J approximation. Updating the Fock matrix after every four steepest descent steps instead of after every step slightly increases the efficiency of the method as it does for Ω_3 [141].

Probably other conceivable functions for DMS will perform in a similar way. Improvements in efficiency should be sought in combining DMS methods with some appropriate convergence acceleration technique. Millam and Scuseria suggest combining the density matrix based DIIS with their CG-DMS method. We currently have implemented only the Fock matrix based DIIS method which we described in section 4.2. We have observed that the combination of this type of DIIS with the minimisation of either Ω_3 or Ω_5 breaks down the minimization sequence and leads to divergence. Level shifters also have a devastating effect on convergence. It may well be that this does not happen with density matrix based DIIS. This is one of the possibilities we wish to explore in the future. Also construction of new extrapolation schemes suited better to DMS and combination with diagonalisation are research directions worth pursuing.

Chapter 5

Gradient and geometry optimisation

5.1 Introduction

A major success of quantum chemistry has been its ability to calculate and predict the equilibrium geometries of molecules. Within the Born-Oppenheimer approximation that all our results are derived, the total molecular energy is a function of the coordinates of the positions of the atoms. This function is a surface in many dimensions and is called the *Potential Energy Surface* (PES). The equilibrium geometry of a molecule is defined as the minimum of its potential energy surface. The PESs of molecules are usually very complicated functions with many local minima in which case we have many equilibrium geometries or stable conformations. Equilibrium geometries are only a small part of the information available from the PES. In principle, chemical reactions can be represented as paths on the potential energy surface and features such as saddle points define transition states.

We need to explore the PES in order to obtain useful information for molecules. The obvious approach of calculating the value of the PES at various points is very inefficient due to the many dimensions of the surface ($3 \times N_{at}$), where N_{at} is the number of atoms. A more efficient approach is to use first and higher derivatives of the PES that provide information about the topology of the surface around a point.

Derivatives can be calculated in two ways:

1. Numerically, by varying each coordinate separately. Each partial derivative is approximated by a finite difference from the SCF results at two or more points.

2. Analytically, by evaluation of the expression for the gradient of the SCF energy with respect to the nuclear coordinates.

The numerical approach requires at least $6 \times N_{at}$ single point energy calculations and therefore is not computationally tractable for large molecules. Furthermore, it is only approximate and the coordinate interval for the finite difference has to be chosen carefully; it has to be small enough to avoid contaminating effects of higher derivatives but large enough to avoid causing significant errors by computational roundoff [142]. On the other hand, the analytical gradient is exact. It has been observed that the computational cost of calculating the gradient analytically is only 3 - 4 times the cost of a single point SCF calculation [143]. Hence analytical derivatives are necessary for calculations on large molecules. The current version of MAGIC is able to calculate analytically first derivatives and use them to locate equilibrium geometries.

5.2 The analytic gradient of the Kohn-Sham energy

The analytic gradient formulae for a variety of ab initio methods are readily available [144]. The expression for the partial derivative of the restricted (closed shell) Kohn-Sham energy with respect to, say, nuclear coordinate A_x is [2]

$$\begin{aligned}\frac{\partial E}{\partial A_x} &= \sum_{i,j=1}^{N_{BF}} D_{ij}\frac{\partial H_{ji}^{core}}{\partial A_x} + \sum_{i,j=1}^{N_{BF}} D_{ij}\langle\chi_j|v_{xc}|\frac{\partial \chi_i}{\partial A_x}\rangle + \frac{1}{2}\sum_{i,j,k,l=1}^{N_{BF}} D_{ij}\frac{\partial (ji|lk)}{\partial A_x}D_{kl} \\ &- \sum_{i,j=1}^{N_{BF}} Q_{ij}\frac{\partial S_{ji}}{\partial A_x} + \frac{\partial U_{NN}}{\partial A_x} \qquad (5.1)\end{aligned}$$

where $(ji|lk)$ is a four-index two-electron integral with j, i, etc. being abbreviations for the basis functions χ_j, χ_i, etc. The classical electrostatic repulsion energy of the

nuclei is U_{NN} and

$$Q_{ji} = 2 \sum_{a=1}^{N_{occ}} \epsilon_a c_{ia} c_{ja} \tag{5.2}$$

where the c_{ia} are the orbital expansion coefficients and ϵ_a are the eigenvalues of the occupied orbitals. As a result of the self-consistent nature of the energy expression, equation (5.1) does not include partial derivatives of the density matrix elements. The second term in (5.1) comes from the differentiation of the exchange-correlation energy

$$\begin{aligned} \frac{\partial E_{xc}[\rho]}{\partial A_x} &= \int \frac{\delta E_{xc}[\rho]}{\delta \rho} \frac{\partial \rho}{\partial A_x} d\mathbf{r} \\ &= \sum_{i,j=1}^{N_{BF}} \frac{\partial D_{ij}}{\partial A_x} \langle \chi_j | v_{xc} | \chi_i \rangle + \sum_{i,j=1}^{N_{BF}} D_{ij} \langle \chi_j | v_{xc} | \frac{\partial \chi_i}{\partial A_x} \rangle \end{aligned} \tag{5.3}$$

where the first term in (5.3) is absorbed into the formation of Q_{ij} of equation (5.2).

In chapter 3 the RI-J approximation was presented and its potential to increase the speed of calculations by roughly an order of magnitude was discussed. The computational benefits of the RI-J approximation are also transfered to the calculation of the gradient. Therefore the gradient implementation in MAGIC is based on the RI-J approximation. This requires the substitution of the third term in the right hand side of equation (5.1) by

$$\sum_{i,j=1}^{N_{BF}} \sum_{t=1}^{N_{AUX}} D_{ij} \frac{\partial (ji|t)}{\partial A_x} q_t - \frac{1}{2} \sum_{s,t=1}^{N_{AUX}} q_s \frac{\partial (s|t)}{\partial A_x} q_t \tag{5.4}$$

with $(ji|t)$ being a three-index two-electron integral between two basis functions and one auxiliary function. A detailed derivation of the gradient formalism in the RI-J case, including extensions for second derivatives has been published by Komornicki et al. [102].

It can be seen from equations 5.1 and 5.4 that first derivatives of the one- and two-electron integrals are required. The calculation of the derivatives of the two-electron integrals is done in a direct manner. This means that each batch of derivatives of integrals is computed, included into the expression for the gradient, and then deleted from memory. As shown in equation (1.25), the derivative of a primitive Cartesian Gaussian function is simply the sum of two primitive Cartesian Gaussian functions and thus the derivatives of the two-electron integrals are expressed

as sums of two-electron integrals. Hence the implementation of the derivatives of the two-electron integrals is simply an appropriate modification of the subroutines that calculate two-electron integrals. The calculation of two-electron integrals is described in section 3.9.

The derivatives of all one-electron integrals are initially computed together, stored in the archive (disk) and then accessed in order to form the gradient of the energy. The storage of these derivatives in the archive deserves some caution. In early versions of the program they were stored in the form of lower-triangle two-dimensional arrays, one for every atomic coordinate. Each array contained $N_{BF}(N_{BF}+1)/2$ elements so the total space required for these derivatives was $3 \times N_{at} \times N_{BF}(N_{BF}+1)/2$. This is not the most efficient way of solving the problem because the required storage space grows cubically with system size and already becomes prohibitively large at molecules of the order of 50 atoms. Most of this space is filled with zeros. This is because the derivatives of one-electron integrals are zero if none of the two basis functions and the operator belong to the centre with respect to which the differentiation is carried out or if all three of them belong to the same centre. The solution to this difficulty is quite simple. Let the following be the integral to be differentiated

$$\langle \chi_i(\mathbf{A}) | \hat{O}(\mathbf{B}) | \chi_j(\mathbf{C}) \rangle \tag{5.5}$$

where the basis functions $\chi_i(\mathbf{A})$ and $\chi_j(\mathbf{C})$ depend on the coordinates of centres A and C respectively and the one-electron operator $\hat{O}(\mathbf{B})$ depends on the coordinates of centre B. All the information necessary for the gradient can be obtained from derivatives of the type

$$\langle \chi_i(\mathbf{A}) | \hat{O}(\mathbf{B}) | \frac{\partial \chi_j(\mathbf{C})}{\partial C_\xi} \rangle \ , \qquad \xi = x, y, z \tag{5.6}$$

because the translational invariance principle [66, 145] can be used to avoid differentiation of the operator. Its derivative integral can be expressed in terms of integrals containing derivatives of basis functions.

$$\langle \chi_i(\mathbf{A}) | \frac{\partial \hat{O}(\mathbf{B})}{\partial B_\xi} | \chi_j(\mathbf{C}) \rangle = -\langle \frac{\partial \chi_i(\mathbf{A})}{\partial A_\xi} | \hat{O}(\mathbf{B}) | \chi_j(\mathbf{C}) \rangle - \langle \chi_i(\mathbf{A}) | \hat{O}(\mathbf{B}) | \frac{\partial \chi_j(\mathbf{C})}{\partial C_\xi} \rangle$$

The storage requirements for the integrals of equation (5.6) are only $3 \times N_{BF}^2$, scaling quadratically with system size and furthermore none of the elements stored is zero. They are comparable to the storage requirements of usual one-electron integrals of a single point SCF calculation and constitute a small fraction of the information stored in the archive during a geometry optimisation.

Some attention is also due to the evaluation of the derivatives of the exchange-correlation potential matrix elements. These integrals are evaluated by three-dimensional molecular quadrature and errors in the gradient can result with small quadrature grids. These errors disappear in the limit of an infinite grid or if consistency is preserved by taking account of the derivatives of the grid with respect to atomic coordinates, as some authors have stated [146, 147, 148]. In all calculations described in this thesis large enough grids were used with consequent negligible errors in the gradient. Such an approach is preferable to the computational complexity of grid derivatives because it leads to overall more accurate exchange-correlation energies. The extra overhead due to the larger grid is very small due to the neglect of zero contributions, an important feature of the DFT subroutines of MAGIC.

5.3 The BFGS geometry optimiser

The optimisation of geometries is achieved through an implementation of a quasi-Newton optimisation method. This is essentially the Newton-Raphson method for locating minima of functions, using an exact gradient calculated by analytic derivatives and an approximation to the inverse Hessian. This approximation to the inverse Hessian is calculated with the Broyden, Fletcher, Goldfarb and Shanno (BFGS) update formula [149, 150, 151, 152] which improves as the number of optimiser steps increases [153, 154]. Such quasi-Newton methods have been demonstrated to be rather successful while avoiding the high computational cost of directly calculating the Hessian [2, 155]. According to the BFGS formula the inverse Hessian $\mathbf{G}_n$ at a specific molecular geometry (nth step of the geometry optimisation)

is given by the following expression:

$$\mathbf{G}_n = \left(\mathbf{I} - \frac{\mathbf{q}_n \mathbf{d}^\dagger{}_n}{\mathbf{q}^\dagger{}_n \mathbf{d}_n}\right) \mathbf{G}_{n-1} \left(\mathbf{I} - \frac{\mathbf{q}_n \mathbf{d}^\dagger{}_n}{\mathbf{q}^\dagger{}_n \mathbf{d}_n}\right)^\dagger + \frac{\mathbf{q}_n \mathbf{q}_n^\dagger}{\mathbf{q}_n^\dagger \mathbf{d}_n} \tag{5.7}$$

where the column vector $\mathbf{q}_n = \mathbf{X}_n - \mathbf{X}_{n-1}$ is the difference between the molecular geometry at step n and at the previous step. In a similar fashion, $\mathbf{d}_n = \mathbf{g}_n - \mathbf{g}_{n-1}$ contains the difference between the two consecutive gradients. $\mathbf{I}$ is the unit matrix. The new geometry at point $n+1$, is given by the Newton-Raphson equation.

$$\mathbf{X}_{n+1} = \mathbf{X}_n - \alpha \mathbf{G}_n \mathbf{g}_n \tag{5.8}$$

As an initial approximation for $\mathbf{G}_n$ the unit matrix is used. Even though the approximation to the inverse Hessian improves with increasing number of iterations, it never gets satisfactorily close to the exact inverse Hessian. This realisation, combined with the fact that the potential energy surface is not simply a quadratic function of the coordinates suggests the need for a line search. The line search determines the coefficient α of equation (5.8) that minimises the molecular energy. A variety of schemes can be used, such as schemes specially tailored for the BFGS method [153] or simply fitting the energy of the molecule as a function of α to a polynomial. These schemes are costly because they require several single point SCF calculations and sometimes gradient evaluations too. Their implementation and testing in MAGIC showed that the benefit they afford by reducing the optimiser steps is usually outweighted by the extra cost and each scheme is effective within particular classes of molecules. Furthermore, unpredictable oscillatory behaviour is rare but cannot be excluded. The approach that proved successful is to simply set α equal to 1 (the Newton-Raphson value) for all optimiser iterations apart from the first. In the first step α is set equal to 0.4 because the magnitude of the gradient is large (especially with a poor starting geometry) and the approximation to the inverse Hessian is non-existent. In such cases, a value of α equal to 1 can overshoot the equilibrium geometry and seriously slow down the subsequent steps of optimisation. As the equilibrium geometry is approached, the PES is locally approximately quadratic, the inverse Hessian approximation has improved and thus convergence with $\alpha = 1$ is rapid.

Usually during a geometry optimisation the first SCF calculation is the most expensive. The subsequent SCF calculations employ as an initial approximation for the density the converged density of the previous geometry. This is a very good initial approximation because the consecutive geometries differ only slightly. Thus, all SCF calculations at subsequent geometries converge in a small fraction of the number of SCF iterations at the initial geometry.

5.4 An example geometry optimisation

The energy gradient and geometry optimiser of MAGIC were tested extensively during and after development in order to ensure that correct results are obtained. The tests involved a variety of small molecules and combinations of all functionals currently available in MAGIC: uniform electron gas exchange (LDAX) [16], Becke '88 gradient correction to exchange (B88X) [59], Vosko-Wilk-Nussair correlation (VWN) [75] and Lee-Yang-Parr gradient corrected correlation (LYP) [60]. Both restricted and unrestricted determinant Kohn-Sham calculations were used to describe the electronic state of the PESs.

Here an example geometry optimisation on a somewhat larger molecule which has been an important discovery for the developent of organometallic chemistry is presented. Zeise's salt, $K[Pt(C_2H_4)Cl_3]$, was discovered in about 1827 and was the first π-complex to be known [69]. Although its elemental composition was elucidated very early, it took until 1950 to resolve its structure by X-ray crystallography. The key point in such complexes of unsaturated organic molecules is that the C$-$C axis of the coordinated alkene is perpendicular to one of the expected bond directions from the metal. A qualitative description of this form of bonding was given by Chatt, Dewar and Duncanson [69]. The alkene-metal bond consists of two components

1. A σ component resulting from donation of electronic density from the π bond of the alkene to metal orbitals of suitable symmetry.

2. A π component resulting from back-donation of electronic density from the metal into antibonding orbitals on the carbon atoms.

Thus the bonding has dual character and its two components are synergically related to each other, i.e. the increase or decrease of the strength of one of the components has an analogous effect on the other.

An optimisation of the geometry of $K[Pt(C_2H_4)Cl_3]$ was performed, using the LDAX functional and the closed-shell restriced determinant formalism. The initial geometry was obtained from the crystal structure of the complex [156]. The SVP basis set was used on non-metallic atoms. The metal atoms were described by quasirelativistic ECPs with 60 core electrons for Pt [53] and 10 core electrons for K [67]. The auxiliary basis sets of Ahlrichs et al. [94, 95] were used on all atoms. The total number of basis functions was 172 and the total number of auxiliary functions was 439. For the DFT integration (section 1.5) the value of LEBEDEV was set to 3 and the value of LOG3 was set to 10. The resulting quadrature grid had 480850 points. The optimisation was completed in 56 steps, and the maximum magnitute of the gradient components was equal to 0.000345 a.u. In MAGIC a geometry optimisation is considered completed by default when the maximum magnitude of the gradient components is less than 10^{-3}. This value can be altered in the input file.

Figure (5.1) shows the geometries of the complex from the crystal structure and the LDAX optimisation. Lengths of selected bonds (in Å) and selected angles (in degrees) are also given. There is reasonably good agreement between the experimental and theoretical geometry. This is especially true if we consider that finite temperature, as well as steric effects from interactions with the other molecules packed in the crystal, affect the geometry of the crystal structure. The C−C bond length in the crystal structure is 1.375 Å while for the LDAX optimised molecule it is 1.430 Å. Both of these values are larger than the C−C bond length of a free ethylene molecule which is 1.330 Å. This lengthening is consistent with the Chatt, Dewar and Duncanson model that predicts weakening of the C−C bond upon coordination.

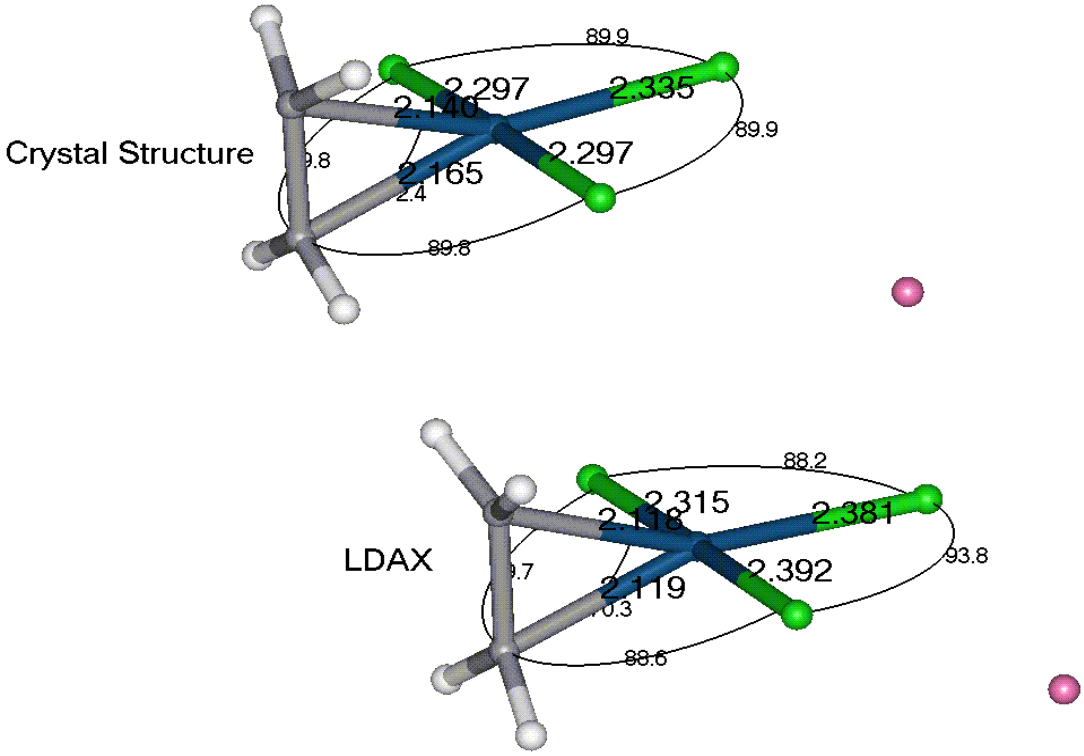

Figure 5.1: Experimental (top) and theoretical (bottom) geometry of $K[Pt(C_2H_4)Cl_3]$. Pt atoms are represented by blue spheres, Cl atoms by green spheres and K atoms by purple spheres. Bond lengths are given in Å and bond angles in degrees.

Chapter 6

Applications

Even though this thesis describes mainly methodologial developments of DFT and their implementation, it is necessary to demonstrate the functionality and usability of the MAGIC program, which is the final result. It is also satisfying for the author to demonstrate that this work has made some contibution to the understanding of chemistry from the theoretical viewpoint. The examples in this chapter are taken from the area of inorganic chemistry which is the target of application of MAGIC. Two out of the four examples presented were generated with the visualisation facilities of MAGIC (from the Cerius^2 - MAGIC interface). As will be seen, presentation in this way gives a totally new insight to molecules and their properties.

6.1 Zeise's salt, $K[Pt(C_2H_4)Cl_3]$

The geometry optimisation of $K[Pt(C_2H_4)Cl_3]$, also known as "Zeise's salt" was described in section 5.4. Here, some visual representations of the density and orbitals of the single point energy SCF calculation on the converged geometry are presented. These pictures were created by Cerius^2 [12] through an interface of this software to MAGIC. This interface was developed by Dr Andrew G. Ioannou.

Figure 6.1 shows isosurfaces of the density of the complex for various values of the density. The shape of the isosurfaces varies from spheres surrounding the atoms for large values of the density (0.500 - 10.00 a.u.) to a shape that indicates clearly the bonding between the atoms for medium values (0.050 - 0.100 a.u.), reducing

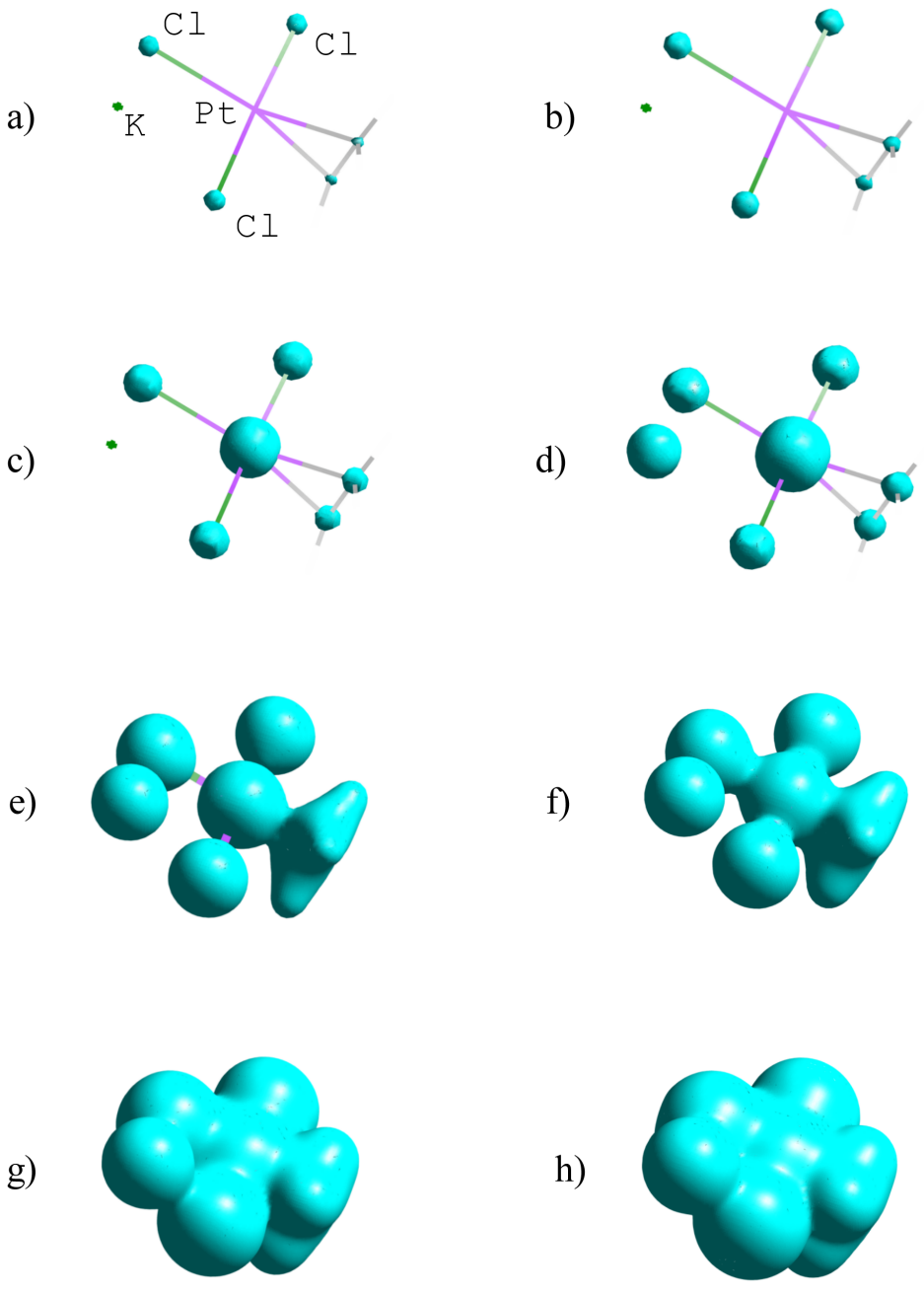

Figure 6.1: Isosurfaces of the density of $K[Pt(C_2H_4)Cl_3]$ for the values: (a) 10.000 a.u., (b) 5.000 a.u., (c) 1.000 a.u., (d) 0.500 a.u., (e) 0.100 a.u., (f) 0.050 a.u., (g) 0.010 a.u. and (h) 0.005 a.u.

gradually to a spherical shape that encloses the whole molecule for values of 0.010 a.u. or less. This picture is consistent with the common notion of chemists that most of the electronic density is contained in the core of the atoms and is unaffected by bonding, while the small fraction of the valence density is responsible for the bonding. Furthermore, at sufficiently long distances the molecule resembles a point charge.

It should be born in mind that the isosurface drawings of Figure 6.1 are not quantitatively correct as far as their shape around the K and Pt atoms is concerned, due to the use of ECPs. In reality the density isosurfaces must include more volume around the K and Pt atoms. However the ECPs reduce the number of electrons of K from 19 to 9 and of Pt from 78 to 18 with a consequent decrease in density around these atoms.

Figure 6.2(a) shows a contour plot of the density of the molecule on the plane defined by the platinum and the two carbon atoms. The values of the density are represented on this surface by different colours ranging from red for the highest values to green for the lowest.

Figure 6.2(b) contains a representation of the density on an isosurface of the Highest Occupied Molecular Orbital (HOMO). The values of the density are represented by the same colour code as in Figure 6.2(a).

Figure 6.2(c) shows an isosurface of the Lowest Unoccupied Molecular Orbital (LUMO). Two colours (blue and yellow) are used to represent the areas of the orbital with different sign (positive and negative). It is just as easy to examine the remainder of the orbitals with the Cerius^2 - MAGIC interface. Their shapes become more complicated as one goes higher in energy and the number of nodes increases. The shapes of these orbitals contain many subtleties that simple LCAO approaches such as Hückel or semiempirical molecular orbital theories are not able to represent. Furthermore, their use to qualitatively describe bonding as consisting mainly of contributions from orbitals of certain atoms becomes extremely difficult for large molecules. They could possibly assist in predicting reaction mechanisms in the context of frontier orbital theory, such as in the case of the Woodward - Hoffmann rules [134]. No such use however seems obvious from the present calculations and

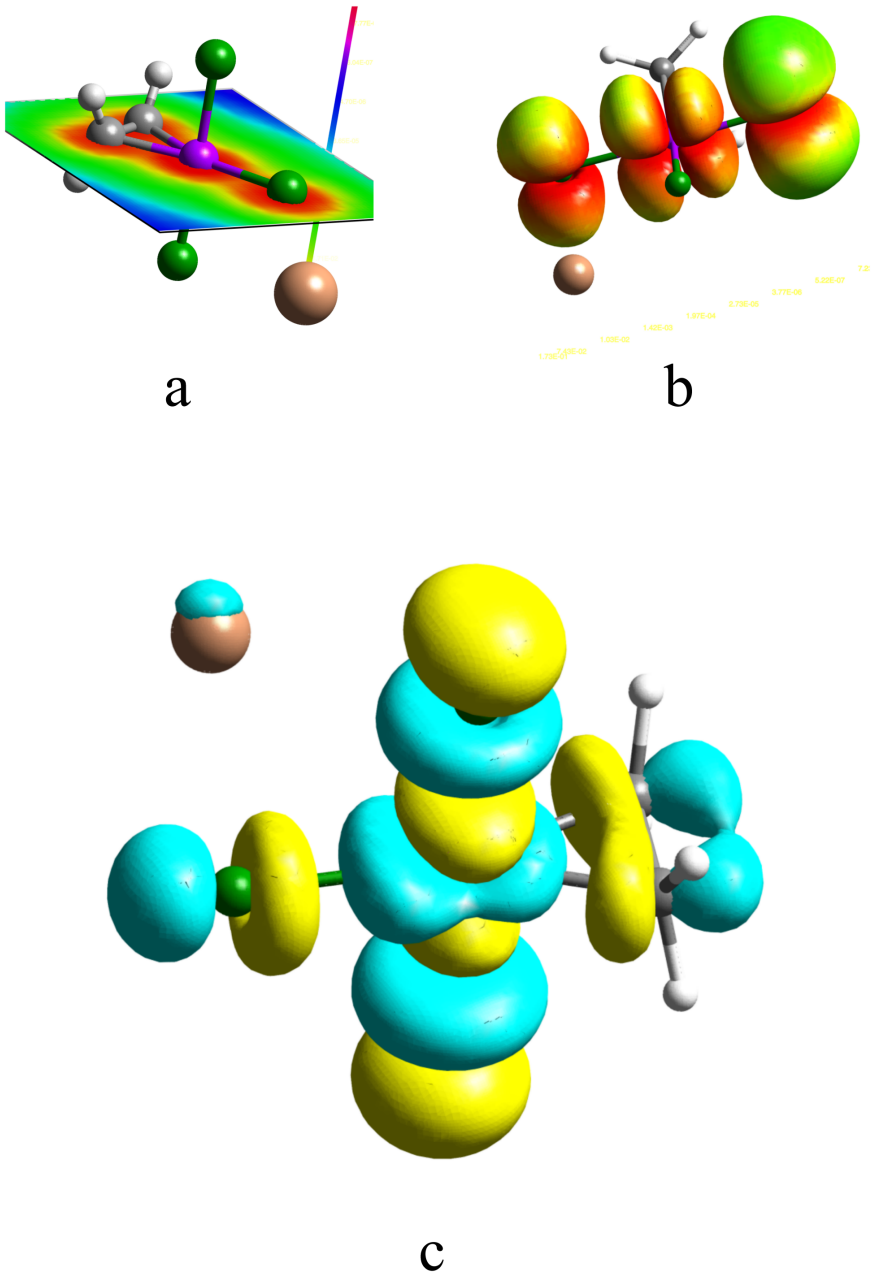

Figure 6.2: $K[Pt(C_2H_4)Cl_3]$. (a) A contour plot of the density on the plane containing the Pt and C atoms. (b) The density plotted on one isosurface of the highest occupied molecular orbital. (c) An isosurface of the lowest unoccupied molecular orbital.

since these are Kohn - Sham DFT orbitals at any rate, their isosurfaces are regarded by the author as an interesting curiosity. Their only definite utility lies in the fact that they contribute to the density. The density appears to be visually substantially more informative than the orbitals and as it will be shown in the following example, there are ways to enhance the information it provides in order to reach qualitative conclusions about the reactivity of a molecule.

6.2 Triphenylsiloxytriphenyllead(IV), $Ph_3SiOPbPh_3$

Alkoxides, such as R−ONa, where R is a hydrocarbon functional group, are common reagents in organic chemistry [157]. The alkoxide oxygen is highy basic with a large negative charge and serves as a strong nucleophile. It is very reactive and is used routinely to displace functional groups on carbon atoms of other organic molecules (nucleophilic substitution reactions) or to eliminate a functional group and a neighbouring hydrogen atom to produce a C−C double bond (elimination reactions). In most cases both reactions take place simultaneously and the relative yields are regulated by the conditions (solvent, temperature, etc.) and by the nature of the R functional group (steric effects and electronic induction and resonance effects). There is extensive experience in using these compounds in various synthetic paths. However less is known about siloxides, a similar class of compounds where the oxygen is connected to a silicon atom or lead siloxides where the sodium atom is replaced by an organolead group.

The crystal structure of the lead siloxide triphenylsiloxytriphenyllead(IV), $Ph_3SiOPbPh_3$ has been investigated by X-ray diffraction [158]. Its isolation was possible because it is relatively inert compared to analogous compounds [159] and does not undergo aerobic hydrolysis, presumably due to the steric hindrance of its phenyl groups.

In order to determine if these experimental observations can be verified by calculations with MAGIC and visualisation of the output with Cerius^2, a single point LDAX calculation on this compound was performed at the geometry of the crystal structure. The STO3G basis [104] was used on all atoms except for the O atom

which contained an SVP basis [76] and the Pb and Si atoms that were described by a quasirelativistic ECP [160, 77] and corresponding valence bases leaving each of them with 4 valence electrons. Overall, the calculation involved 253 basis functions and 2179 auxiliary basis functions. The geometry of the molecule and an isosurface of its density are shown in Figure 6.3. The isosurface of the density shows clearly the bonding but is not much more informative. Furthermore, its shape is not quantitatively correct around the Pb and Si atoms due to the elimination of the core density by the ECPs.

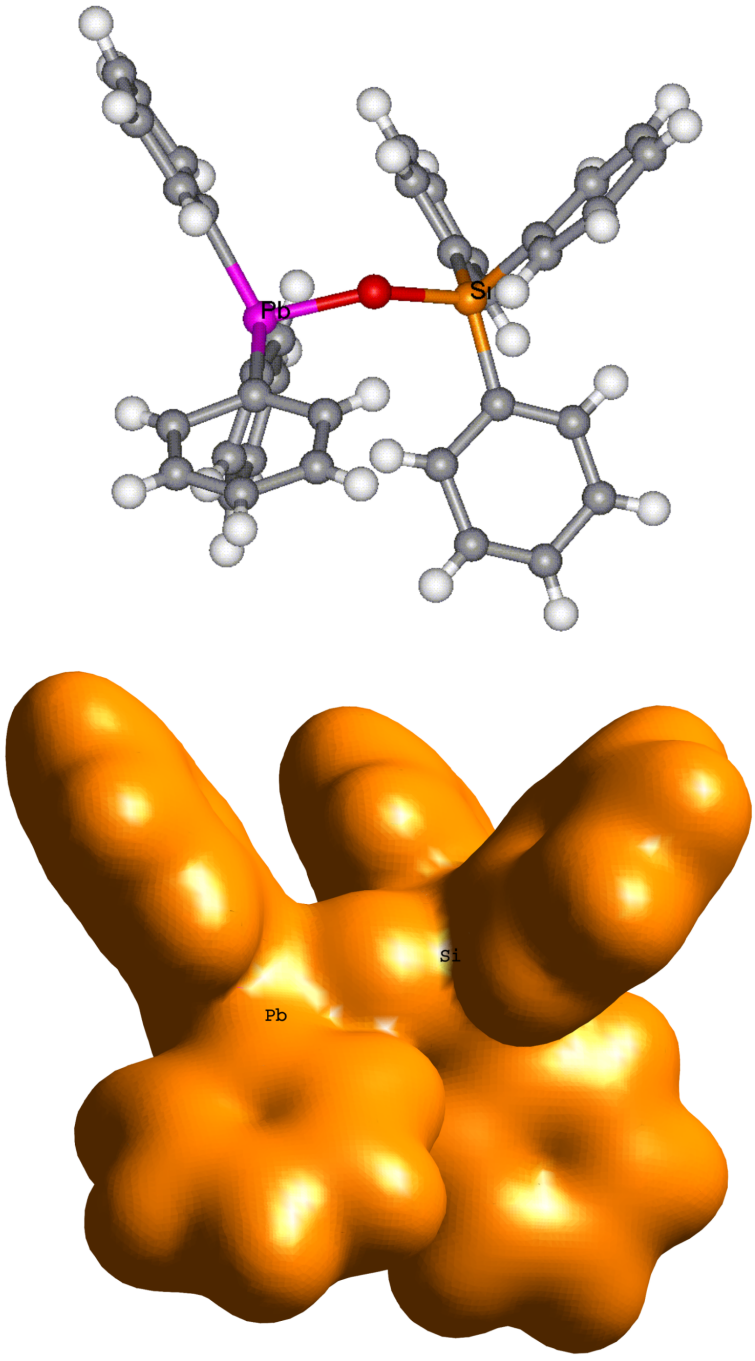

Figure 6.3: The $Ph_3SiOPbPh_3$ molecule (69 atoms) at the crystal structure geometry. Top: A ball and stick drawing. Bottom: A density isosurface at 0.005 a.u.

To extract more information from the density, separate LDAX calculations were performed on the ground state of each of the atoms of the molecule, with the same basis sets, ECPs and auxiliary basis sets as in the molecule. The resulting atomic densities were subtracted from the molecular density. An isosurface of the positive part of the difference is shown in Figure 6.4. This represents the displacement of the electronic density upon molecule formation with respect to the sum of the densities of noninteracting atoms at the molecular geometry and will be referred to here as the *bonding density*. The isosurface of the bonding density in Figure 6.4 extends, as expected for a visual representation of bonding, between the atoms, where the "traditional" chemical bonds are expected to be and its value is zero on the atoms. There is however a single exception to this general trend: the bridging oxygen atom is the only atom that has a buildup of bonding density on it. It is distinct from all other atoms in this sense because the formation of the molecule has increased its density compared to its density as an isolated atom. Based on this observation, the conclusion that this oxygen atom will exhibit strong nucleophilic behaviour in chemical reactions seems plausible.

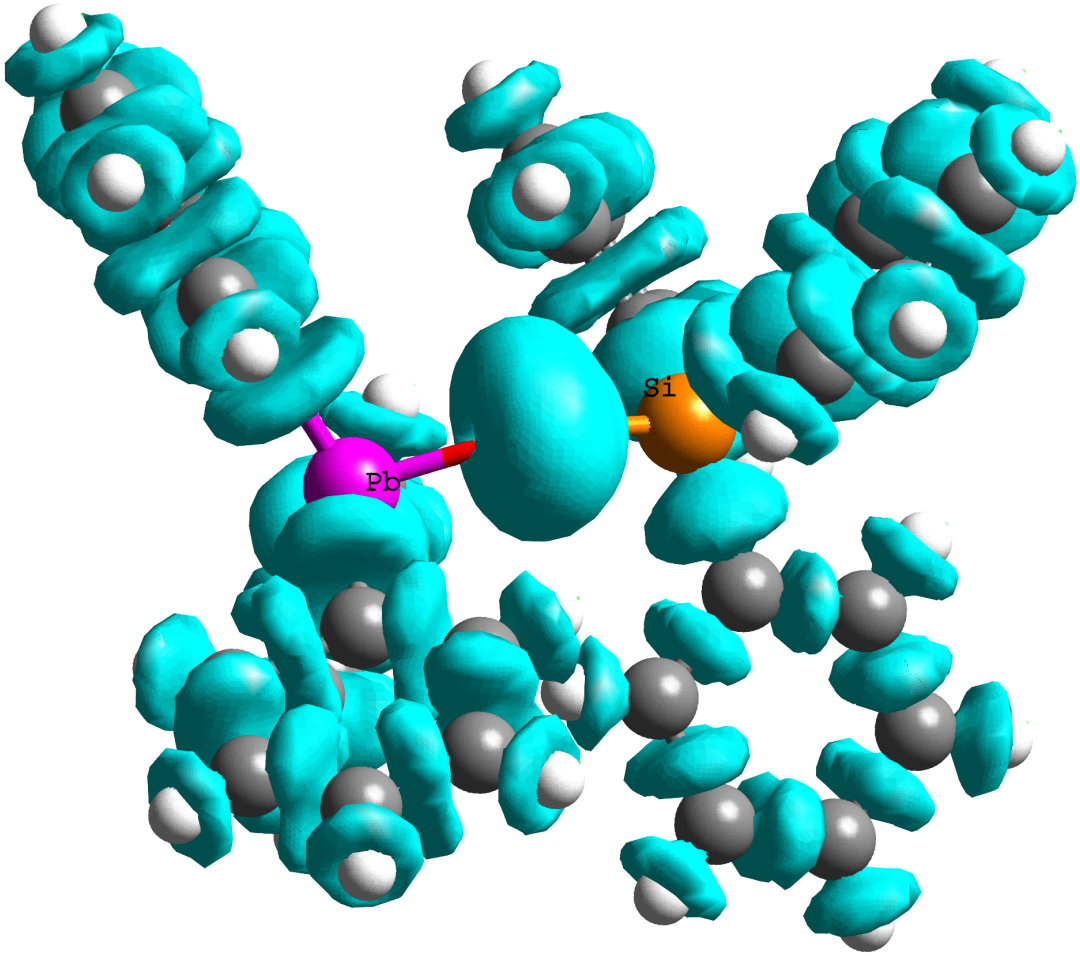

Figure 6.4: An isosurface of the bonding density of $Ph_3SiOPbPh_3$ at 0.005 a.u.

These observations are compounded by Figure 6.5 which shows an isosurface of the negative part of the difference between the molecular density and the sum of atomic densities. This is the *density depletion* upon molecule formation with respect to the sum of the densities of the noninteracting atoms at the molecular geometry. As expected, each atom is surrounded by a density depletion surface with the only exception being the oxygen atom. As a further indication of its electron-rich nature the oxygen has no density depletion and the same is true for the bonding regions of the molecule.

This example demonstrates one of the possible ways in which results from a DFT calculation can be processed to produce visual interpretations for chemical purposes. The nucleophilicity of the oxygen atom of the lead siloxide which was deduced by Figures 6.4 and 6.5 is experimentally observed, and can also be speculated from the rules of organic chemistry. It is expected that analysis along similar lines could be used to derive conclusions regarding the reactivity of molecules where little or no experimental information is available.

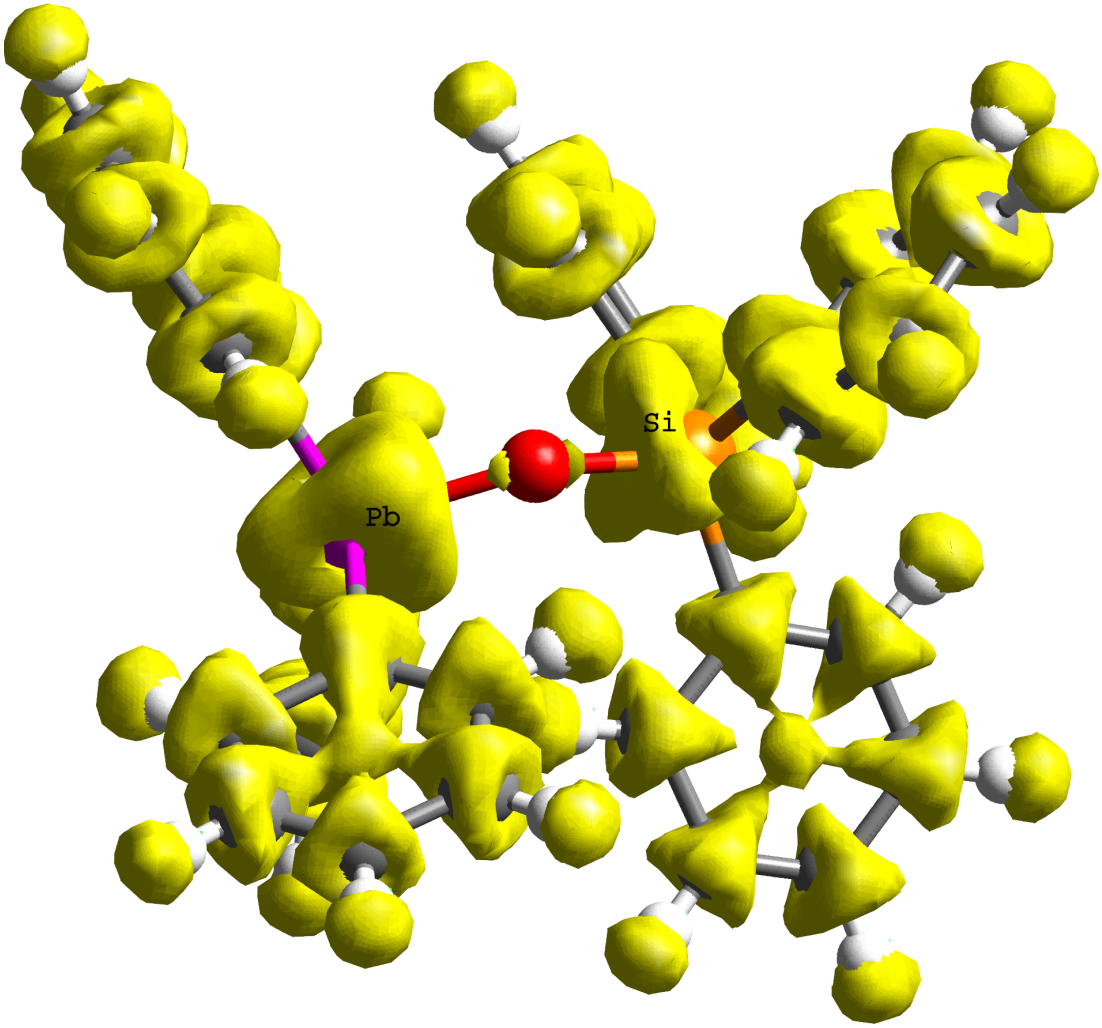

Figure 6.5: An isosurface of the atomic density depletion due to bond formation in $Ph_3SiOPbPh_3$ at 0.005 a.u.

6.3 Acetonitrile ruthenium entecacarbonyl, $Ru_3(CO)_{11}$-(NCMe)

Many low nuclearity transition metal clusters are known and the chemistry derived from triatomic $M_3(CO)_{12}$ clusters of the iron group (M = Fe, Ru, Os) has been studied particularly well [69, 161]. The structure of these clusters is triangular and they are "electronically saturated" because, according to the electron counting rules for clusters, 18 electrons can be attributed to each metal atom. A large amount of interesting chemistry can be developed from these clusters involving reactions with olefins. A common starting point for these reactions is the replacement of one or two CO ligands with CH_3CN (acetonitrile). The resulting species can then lose CH_3CN easily for substitution by olefins. Then reactions on the olefins, promoted by their coordination on the metal cluster, can be studied.

Foulds et al. [162] reported the preparation and some reactions of $Ru_3(CO)_{11}(NCMe)$ and $Ru_3(CO)_{10}(NCMe)_2$. Elemental analysis, IR and ^1H NMR spectroscopy were used to characterise these clusters. Their exact structure is not known but it is expected to be similar to the structure of $Ru_3(CO)_{12}$ for which X-ray crystallographic data is available [163, 164].

A geometry optimisation of the structure of $Ru_3(CO)_{11}(NCMe)$ was performed with MAGIC. The starting geometry was taken from a Molecular Mechanics (MM) optimised structure with the Cerius^2 program [12] using the universal force field of Rappé et al. [78] and corresponds to the equatorial CH_3CN conformer. The LDAX functional [16] in a closed-shell Kohn-Sham formalism was used to describe the electronic structure of the cluster. The quasirelativistic ECP of Hay and Wadt [49] and the corresponding valence basis set were employed to describe the Ru atoms. This ECP has a Kr core (36 electrons) which leaves 8 valence electrons. The 631G* basis set [105] was used on the carbon and nitrogen atoms and the STO3G basis [104] on the oxygen and hydrogen atoms. The auxiliary basis sets of Ahlrichs et al. [94, 95] were used for the RI-J approximation. Overall the calculation involved 200 electrons, 31 atoms, 298 basis functions and 1436 auxiliary basis functions. The optimised structure of the complex at a gradient tolerance of 10^{-3} is shown in

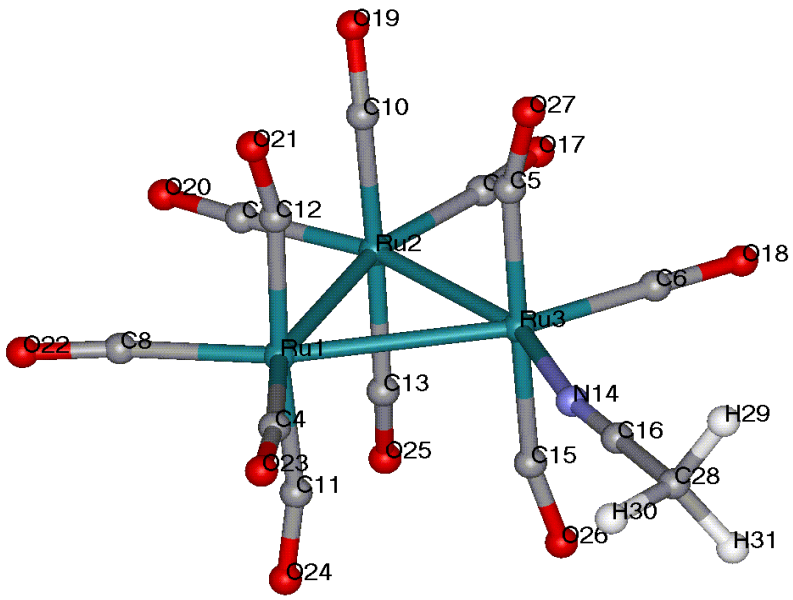

Figure 6.6: The optimised structure of $Ru_3(CO)_{11}(NCMe)$.

Figure 6.6. Selected bond lengths and angles are presented in Table 6.1.

The values of Table 6.1 compare well with the X-ray crystal structure geometry of the similar $Ru_3(CO)_{12}$ cluster [164]. In that crystal structure, the average bond lengths of Ru−Ru, Ru−C, C−O (axial) and C−O (equatorial) are 2.854 Å, 1.920 Å, 1.350 Å and 1.126 Å respectively. Also the average C−Ru−C (equatorial-equatorial), Ru−C−O (axial) and Ru−C−O (equatorial) angles are 104.0°, 173.1° and 178.9° respectively. The lengthening of the N14−C16 bond (1.177 Å) compared to its length of 1.157 Å in the free acetonitrile molecule [157] can be atributed to electronic density back-donation from the ruthenium atom to the antibonding orbitals of acetonitrile. The C−C bond in free acetonitrile is 1.462 Å, very close to the 1.465 Å of C16−C28. It seems reasonable to conclude that at least as far as geometry is concerned, closed shell clusters such as $Ru_3(CO)_{11}(NCMe)$ are described accurately with a combination of quasirelativistic ECPs and the LDAX functional.

Table 6.1: Selected bond lengths and angles from the optimised structure of $Ru_3(CO)_{11}(NCMe)$.

Bond (Å)		Angle (°)	
Ru1−Ru2	2.904	Ru1−Ru2−Ru3	60.9
Ru2−Ru3	2.828	Ru2−Ru3−Ru1	60.8
Ru3−Ru1	2.906	Ru1−Ru3−N14	99.4
Ru3−N14	2.144	N14−Ru3−C6	101.3
N14−C16	1.177	C6−Ru3−Ru2	98.5
C16−C28	1.465	Ru3−N14−C16	171.4
Ru3−C6	1.864	N14−C16−C28	178.8
C6−O18	1.175	Ru3−C6−O18	178.3
Ru3−C15	1.984	Ru3−C15−O26	164.8
C15−O26	1.171	Ru1−C8−O22	169.5
Ru1−C8	1.958	Ru1−C11−O24	164.7
C8−O22	1.170	Ru3−Ru1−C4	100.1
Ru1−C11	1.992	C4−Ru1−C8	100.2
C11−O24	1.171	C8−Ru1−Ru2	101.4

6.4 Uranyl hydroxide, $[UO_2(OH)_4]^{2-}$

The uranyl(VI) cation UO_2^{2+} or dioxouranium(VI), is a very stable species and is common in aqueous solutions of uranium. There is a fair amount of information available regarding its chemical behaviour under acidic conditions [165]. In contrast, little is known about its chemistry in strong alkaline solutions. Such information is important because uranyl forms part of the contents of alkaline solutions in nuclear waste storage tanks. It is known that hydrolysis of uranyl begins at pH = 3 and at near neutral pH the uranyl ion forms a number of polymeric hydroxide species

$$mUO_2^{2+} + nH_2O \rightleftharpoons (UO_2)_m(OH)_n^{2m-n} + nH^+ \tag{6.1}$$

whose relative proportion depends on the concentration of uranyl and hydroxide. Examples of the most important species include $UO_2(OH)^+$, $(UO_2)_2(OH)_2^{2+}$, $(UO_2)_3(OH)_4^{2+}$, $(UO_2)_3(OH)_5^+$, $(UO_2)_3(OH)_7^-$, $(UO_2)_3(OH)_8^{2-}$, $(UO_2)_3(OH)_{10}^{4-}$ and $(UO_2)_4(OH)_7^+$ [166]. At lower pH, uranium precipitates to form a uranate salt, a process used industrially for the precipitation of uranium from ore-leach solutions to form $M_2U_2O_7$ ($M = NH_4^+$, Na^+). This prevents the formation and isolation of $UO_2(OH)_3^-$ and $UO_2(OH)_4^{2-}$ species. However, Clark et al. [167] managed to prepare $UO_2(OH)_4^{2-}$ by using the bulky tetramethylammonium countercation to avoid precipitation of uranate salts. Furthermore, addition of $[Co(NH_3)_6]Cl_3$ led to precipitation of crystals with stoichiometry $[Co(NH_3)_6]_2[UO_2(OH)_4]_3{\cdot}H_2O$, suitable for X-ray crystallography.

In parallel with the experimental isolation and characterisation of $UO_2(OH)_4^{2-}$, Schreckenbach et al. [168] performed DFT calculations on this molecule. They used the B3LYP three-parameter functional of Becke [169] that includes a fraction of Hartree-Fock exchange because they claim that it can reproduce accurate geometries and thermodynamic properties for transition metals even though it was fitted for first row atom molecules. On the basis of some test calculations they determined that the 631+G* basis set of Pople et al. [170] was sufficient and it did not cause errors more significant than the approximate treatment of correlation and relativistic effects. The all-important role of polarisation functions to accurate geometries was stressed once more. For the uranium atom the quasirelativistic ECP of Hay [171]

was used, and its corresponding valence basis was uncontracted. This ECP has a Pt core of 78 electrons and treats explicitly the outer $6s^2 6p^6$ shells and the valence shells (5f, 6d, 7s, 7p) which accommodate fourteen electrons in total. At this level of theory, the geometry of the complex was optimised, using the Gaussian 94 program [172]. The geometry optimisation revealed more than one stable conformation, or local minima of the potential energy surface. In particular, four conformers with a linear UO_2 unit were found, labelled **I** - **IV** and five conformers with a bent UO_2 unit, labelled **V** - **IX**. The bent uranyl is a feature that has not been observed experimentally to date.

In order to investigate the effect of different exchange-correlation functionals and to find out if they can predict the existence of all these conformers, the same geometry optimisations were carried out by the author with MAGIC using the LDAX [16] and BLYP [59, 60] functionals. Exactly the same basis sets and ECPs as in Schreckenbach's paper were used. These calculations also give the opportunity for a further test of the effects of the RI-J approximation. The auxiliary basis of Ahlrichs et. al. [94, 95] was used on the oxygen and hydrogen atoms and the working auxiliary basis described in subsection 3.7.2, was used for the uranium atom. There is an extensive discussion in Schreckenbach et al. [168] about the difficulties of reaching SCF convergence in DFT calculations at the starting geometries of $UO_2(OH)_4^{2-}$ conformers. These were overcome by "building the guess" which involves gradually projecting the density of a converged Hartree-Fock single point energy calculation to an increasing basis set and switching to DFT eventually. In MAGIC this problem was solved by starting with the IADIA density approximation, described in section 4.4, and by improving it with 30 - 40 Density Matrix Search iterations using the Ω_5 function described in subsection 4.5.3. After this, conventional diagonalisation completed SCF convergence. The starting geometries for the optimisation were constructed with the "molecule sketcher" feature of Cerius^2 [12] to visually resemble the ball and stick drawings of the optimised conformers in the paper of Schreckenbach. The geometry optimisations proceeded without any difficulty to produce, at a gradient tolerance of 10^{-3}, all 9 conformer structures that Schreckenbach et. al. reported. Schreckenbach verified that these structures belong to local minima by

Table 6.2: The energies of the optimised $UO_2(OH)_4^{2-}$ conformers, relative to the energy of conformer **I**, in kcal/mol. The B3LYP results are taken from Schreckenbach et al. [168].

Conformer	LDAX	BLYP	B3LYP
I	0.0	0.0	0.0
II	-0.1	-0.3	0.1
III	0.3	0.2	0.5
IV	1.0	1.0	1.4
V	9.8	10.9	18.0
VI	10.5	11.7	19.2
VII	10.3	11.8	19.3
VIII	10.8	11.5	18.5
IX	11.0	12.4	19.3

explicitly evaluating the Hessian of the potential energy surface, and subsequently vibrational frequencies, at these points. The current version of MAGIC is able to locate only minima since the BFGS update formula for the approximation to the inverse Hessian (section 5.3) produces only positive definite matrices.

The energies of the optimised conformers are given in Table 6.2 and the BLYP optimised geometries are shown in Figure 6.7. It can be observed that the energy differences produced with the LDAX and BLYP functionals are smaller than those by the B3LYP functional. Also, **II** appears to be the global energy minimum (most stable conformation) with both the LDAX and BLYP functionals by a very small difference from **I** which is the global minimum with B3LYP. By observing the geometries of the conformers and on the basis of steric considerations, **I** can be predicted as the global minimum. In a recent review of DFT calculations on actinide compounds [173], Schreckenbach et. al. report energies and geometries calculated with the BLYP functional for **I** and **V** only. The energy of **V** relative to **I** they find is 10.8 kcal/mol and compares well with the result of 10.9 kcal/mol obtained with MAGIC. Amongst the reasons responsible for the difference are the

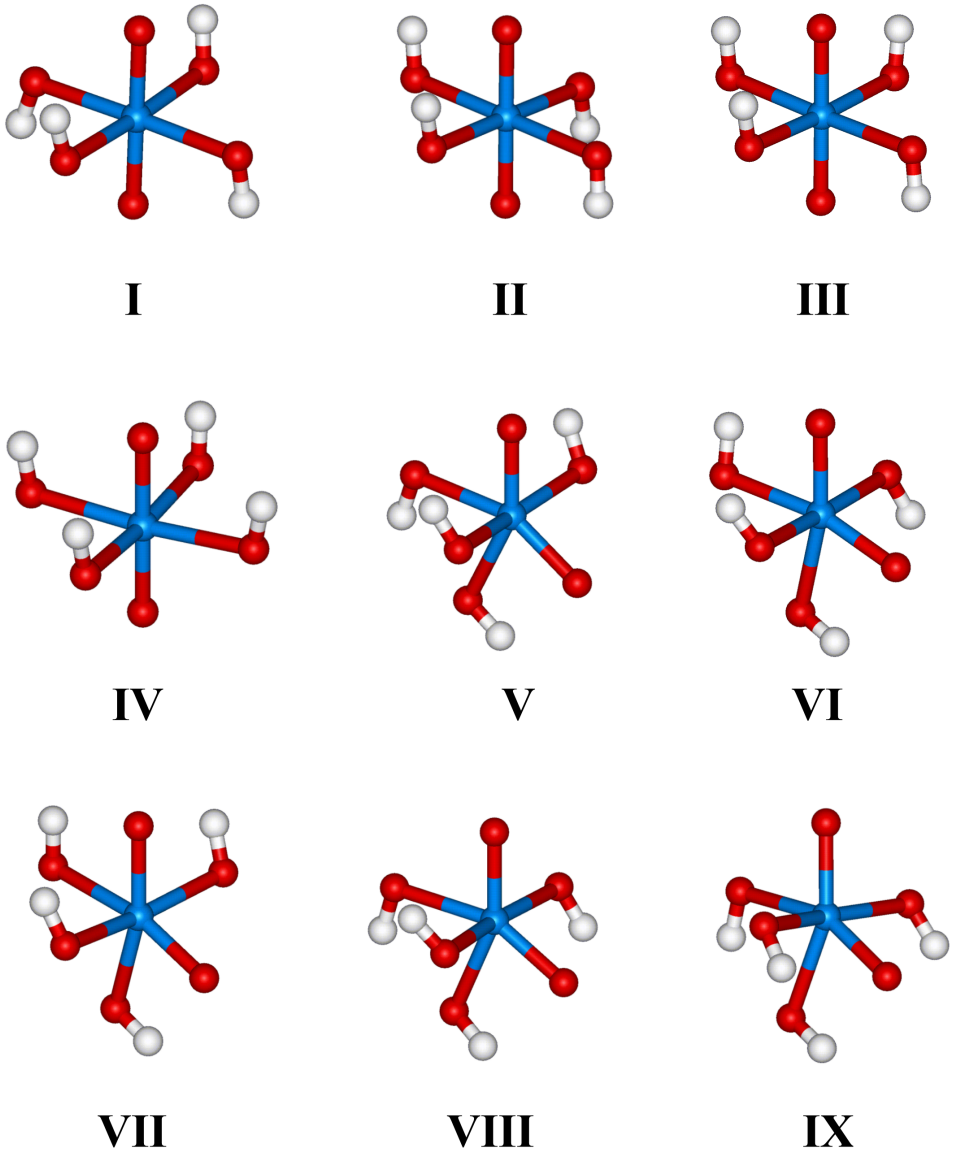

Figure 6.7: The BLYP optimised structures of the conformers of uranyl hydroxide.

different molecular quadrature grid for the exchange-correlation matrix elements and the RI-J approximation. However this difference is small and is probably not the reason for the discrepancy in the relative energy ordering of **I** and **II** which is 0.5 kcal/mol. This is probably due to the different functionals.

Bond lengths and angles of the conformers are given in Table 6.3. The general trend observed is that BLYP gives the longer bond lengths while B3LYP gives the shortest U−O bond lengths and LDAX the shortest U−OH bond lengths. All the methods overestimate bond lengths, BLYP most of all. This is deduced by comparison with the crystal structure and solution (EXAFS) [167] data for the linear uranyl species. The experimental values are U−O = 1.824 Å, U−OH = 2.250 Å for the crystal structure and U−O = 1.80(1) Å, U−OH = 2.21(1) Å for the solution. They do not correspond to any of the conformers **I-IV** in particular but rather they are time-averages of all four conformers. Spectroscopic investigation suggests that the conformers interchange very fast, a fact supported by the small differences in energy that the calculations predict. In fact, energy differences of the order of 0.5 kcal/mol $\simeq 1\text{mE}_h$ define the threshold for "chemical accuracy" (subsection 3.1.2) achieved by DFT and therefore the only safe conclusion that can be drawn about **I-IV** is that they are of comparable energy. There is no obvious trend for the bond angles of the conformers **V-IX**. According to the BLYP geometry optimisations of conformers **I** and **V** only, in the review of DFT calculations on actinides by Schreckenbach et. al. [173], the geometry parameters are U−O = 1.892 Å and U−OH = 2.360 Å for **I** and U−O = 1.923, 1.918 Å, U−OH = 2.301, 2.345, 2.374, 2.374 Å and O−U−O = 125.9° for **V**. These are essentially the same as the BLYP results by MAGIC, U−O = 1.892 Å and U−OH = 2.358 Å for **I** and U−O = 1.921, 1.918 Å, U−OH = 2.297, 2.350, 2.370, 2.370 Å and O−U−O = 126.5° for **V**. The reasons for the not exact coincidence were explained in the previous paragraph.

Another interesting feature of the $UO_2(OH)_4^{2-}$ complex is its oxo ligand exchange that has been confirmed with variable temperature O^{17} NMR spectroscopy. This is a feature unprecedented for uranyl complexes. It is speculated [167] that the oxo ligand exchange happens via migration of hydrogen from the hydroxide ligand to the oxo ligand. The exact mechanism has not been established and it is possible

Table 6.3: Bond lengths (Å) and angles (°) of the optimised $UO_2(OH)_4^{2-}$ conformers. The B3LYP results are taken from Schreckenbach et al. [168].

Conformer	Functional	U−O	U−OH	O−U−O
	LDA	1.894	2.312	178.9
I	BLYP	1.892	2.358	179.8
	B3LYP	1.842	2.334	–
	LDA	1.895	2.316	179.8
II	BLYP	1.895	2.356	179.9
	B3LYP	1.843	2.333	–
	LDA	1.910, 1.889	2.312, 2.313 2.317, 2.302	179.6
III	BLYP	1.904, 1.887	2.355, 2.358 2.359, 2.355	179.6
	B3LYP	1.894, 1.836	2.336, 2.336 2.332, 2.333	–
	LDA	1.919, 1.880	2.313	179.5
IV	BLYP	1.910, 1.879	2.361	179.6
	B3LYP	1.857, 1.829	2.335	–
	LDA	1.940, 1.933	2.259, 2.304 2.305, 2.305	120.6
V	BLYP	1.921, 1.918	2.297, 2.350 2.370, 2.370	126.5
	B3LYP	1.874, 1.870	2.267, 2.320 2.349, 2.349	128.4
	LDA	1.947, 1.947	2.261, 2.261 2.311, 2.311	110.1
VI	BLYP	1.940, 1.940	2.291, 2.291 2.376, 2.376	113.4
	B3LYP	1.899, 1.899	2.252, 2.252 2.346, 2.346	112.7
	LDA	1.969, 1.935	2.263, 2.252 2.313, 2.313	110.2
VII	BLYP	1.952, 1.927	2.301, 2.284 2.380, 2.380	116.0
	B3LYP	1.910, 1.888	2.257, 2.244 2.349, 2.349	114.0
	LDA	1.922, 1.946	2.259, 2.307 2.306, 2.312	119.3
VIII	BLYP	1.914, 1.933	2.298, 2.343 2.373, 2.379	123.9
	B3LYP	1.862, 1.880	2.268, 2.326 2.348, 2.353	129.4
	LDA	1.911, 1.969	2.251, 2.298 2.309, 2.309	116.6
IX	BLYP	1.902, 1.946	2.293, 2.348 2.376, 2.376	124.7
	B3LYP	1.847, 1.891	2.268, 2.336 2.354, 2.354	131.6

Table 6.4: Calculated Mulliken charges of nuclei (a.u.) for the **I** and **V** conformers. The B3LYP results are taken from Schreckenbach et al. [168].

Conformer	Atom	LDA	BLYP	B3LYP
I	U	2.05	2.42	2.42
	O	-0.85	-0.91	-0.90
	O(H)	-1.00	-1.05	-1.06
	H	0.42	0.40	0.42
V	U	1.93	2.32	2.30
	O	-0.85	-0.88	-0.87
	O(H)	-0.87 to -1.03	-1.02 to -1.08	-1.03 to -1.07
	H	0.42 to 0.45	0.39 to 0.44	0.40 to 0.46

that the solvent (water) may participate. Schreckenbach et al. [168] optimised some transition states of the molecule and proposed oxo exchange mechanisms which involve the bent uranyl structures **V**-**IX** as stable intermediates. If this is the case however, the energy gap of approximately 10 kcal/mol between the linear and bent uranyl conformers that LDAX and BLYP predict is more realistic than the corresponding gap of approximately 20 kcal/mol of the B3LYP results, as the activation enthalpy for the ligand exchange was determined from NMR measurements to be $\Delta H^{\ddagger} = 9.8 \pm 0.3$ kcal/mol. The activation enthalpy corresponds to the transition state and should be higher than the enthalpy of the stable intermediate.

A Mulliken population analysis was performed for **I** and **V**. The calculated atomic charges are given in Table 6.4. These charges have only qualitative meaning. They present a rather ionic picture of the molecule and are consistent with the relative electonegativities of the atoms, but considerably smaller than the formal oxidation numbers.

This study of uranyl hydroxide, $UO_2(OH)_4^{2-}$ is a good example of synergy between theory and experiment. The DFT calculations confirm and complement the experimental observations. It is now known that the $UO_2(OH)_4^{2-}$ species exists in solution and in the solid state if the formation of uranate salts is suppressed. The

complex is found in the form of four conformers with linear uranyl units. These conformers are very close in energy (less than 1.5 kcal/mol) and interconvert rapidly. Exchange between the hydroxyl and the oxo ligands takes place and five other conformers with bent uranyl units are believed to play the role of stable intermediates in this process. Further experimental and theoretical investigations need to be carried out in order to elucidate the mechanism of oxo ligand exchange. The bent-uranyl conformers have not been confirmed experimentally. With appropriate multidentate ligands it may be possible to prepare uranyl complexes where the most stable conformer would possess a bent uranyl unit.

Calculations with MAGIC can provide a great deal of insight into the structure and reactivity of heavy atom molecules encountered in industrial processes. To this end, the capabilities of the current version of MAGIC can be increased by further development, such as an extension of the geometry optimisation algorithm for locating transition states.

Chapter 7

Conclusions

The modelling of large heavy atom molecules necessitates the utilisation of many approximations in order to keep the computational cost at an affordable level. The effect of this combination of approximations on the quantities calculated has not been studied extensively, especially in the case of heavy atoms where relativistic effects must be included and constitute one further challenge. The level of approximations needs to be balanced against the errors it causes in the description of molecular properties.

The basic theoretical model of the MAGIC program involves the inclusion of correlation effects through Kohn-Sham density functional theory. Relativistic effects are introduced at no extra computational cost by quasirelativistic effective core potentials.

The implementation of the overlap, kinetic and nuclear attraction integrals was carried out in a fashion not limited by the size of the systems to be studied but only by available computer resources.

A new, efficient, algorithm for evaluating ECP integrals, suited to large systems, was developed and tested.

Also two-electron integral algorithms for calculating the Coulomb energy, in a direct SCF manner, with or without the RI-J approximation were developed and tested. The accuracy of the RI-J approximation was examined extensively with a variety of basis sets and it was determined that existing auxiliary basis sets produce

results of chemical usefulness. Also methods for controlling the error of the RI-J approximation were suggested as well as some simple ways for constructing auxiliary basis sets when properly optimised ones are not available in the literature. The RI-J approximation is very important as it speeds up the evaluation of the Coulomb energy by an order of magnitude, yet the errors it introduces can be controlled. It is therefore used by default in MAGIC.

SCF convergence difficulties are commonly encountered in calculations on molecules involving heavy elements. Standard convergence assistance methods implemented in MAGIC such as DIIS and level shifters solve many of the problems. Their capabilities are greatly enhanced by the independent atomic densities initial approximation and some new density matrix search methods that were also implemented.

The BFGS geometry optimiser for local minima of the potential energy surface (molecular geometries corresponding to stable conformations) and the gradient of the RI-J Coulomb and one-electron energy were implemented and tested.

Example calculations on large inorganic molecules with MAGIC show that the combination of quasirelativistic ECPs with DFT is a level of theory sufficient to provide useful insight into chemical properties. The interpretation of the results is assisted and enhanced through the visualisation facilities provided by the interface of Cerius^2 to MAGIC.

The modern programming conventions and modular structure of MAGIC facilitate the development of new modules that will extend the currently available theoretical model. Some future extensions that could follow naturally from this work are the optimisation of auxiliary basis sets for the actinide and lanthanide elements, the further improvement of density matrix search methods and the implementation of an algorithm for locating transition states.

Appendix A

Single valence electron atomic HF theory

Here a brief derivation of the Hartree-Fock eigenvalue equation for the valence orbital of a single valence electron atom is given. The purpose is to show that the radial part of the resulting valence orbital does not depend on the z-component of its angular momentum. This result comes naturally by intuition but is a bit harder to prove.

Let us consider an atom which consists of filled groups of orbitals of certain angular momenta and a single electron in a shell of angular symmetry β. This is the electronic structure of alkali atoms with the valence electron either in an s orbital (ground state) or in any other orbital of higher angular momentum. We assume that all the spatial orbitals ψ_i are real and of central field type [174].

$$\psi_i(\mathbf{r}_1) = \frac{1}{r_1} R_{n_i l_i}(r_1) Z_{l_i m_i}(\theta_1, \phi_1) \tag{A.1}$$

The real spherical harmonics $Z_{l_i m_i}(\theta_i, \phi_i)$ are defined by equation (2.66). The Hartree-Fock eigenvalue equation for determining the spatial part of the valence orbital, $\psi_v(\mathbf{r}_1) = \frac{1}{r_1} R_{\alpha\beta}(r_1) Z_{\beta\gamma}(\theta_1, \phi_1)$ is

$$(\hat{h} + \hat{J}_c + \hat{K}_c)\psi_v = \epsilon_v \psi_v \tag{A.2}$$

where $\hat{h}$ is the kinetic energy and nuclear attraction operator, $\hat{J}_c$ is the Coulomb

operator due to the core orbitals and $\hat{K}_c$ is the exchange operator due to the core orbitals of alpha spin.

It is instructive to further expand these operators and analyse their effect on the valence orbital ψ_v and then integrate over the angular coordinates to obtain a Hartree-Fock equation with only radial dependence. We will focus on one operator at a time:

$\hat{h}$: This operator, expanded and expressed in spherical polar coordinates, gives the following result

$$\begin{aligned}\hat{h} &= -\frac{Z}{r_1} - \frac{1}{2}\frac{\partial^2}{\partial r_1^2} - \frac{1}{r_1}\frac{\partial}{\partial r_1} + \left(-\frac{1}{2r_1^2}\frac{\partial^2}{\partial\theta_1^2} - \frac{1}{2r_1^2}\cot\theta_1\frac{\partial}{\partial\theta_1} - \frac{1}{2r_1^2\sin^2\theta_1}\frac{\partial^2}{\partial\phi_1^2}\right) \\ &= -\frac{Z}{r_1} - \frac{1}{2}\frac{\partial^2}{\partial r_1^2} - \frac{1}{r_1}\frac{\partial}{\partial r_1} + \frac{1}{2r_1^2}\hat{L}^2 \qquad \text{(A.3)}\end{aligned}$$

where the first term is the nuclear attraction operator and the remaining terms are the kinetic energy operator. The terms with angular dependence are grouped together into the square of the magnitude of the orbital angular momentum operator, $\hat{L}^2$. The real spherical harmonics Z_{lm} are eigenfunctions of the $\hat{L}^2$ operator with eigenvalues $l(l+1)$. Therefore the action of $\hat{h}$ on $\psi_v(\mathbf{r}_1)$ gives

$$\hat{h}\psi_v(\mathbf{r}_1) = \left(-\frac{Z}{r_1} - \frac{1}{2}\frac{\partial^2}{\partial r_1^2} - \frac{1}{r_1}\frac{\partial}{\partial r_1} + \frac{\beta(\beta+1)}{2r_1^2}\right)\frac{1}{r_1}R_{\alpha\beta}(r_1)Z_{\beta\gamma}(\theta_1,\phi_1)$$

and if we multiply this result by $Z_{\beta\gamma}(\theta_1,\phi_1)$ from the left and integrate over solid angles, the following radial equation is obtained

$$\begin{aligned}&\left(-\frac{Z}{r_1} - \frac{1}{2}\frac{\partial^2}{\partial r_1^2} - \frac{1}{r_1}\frac{\partial}{\partial r_1} + \frac{\beta(\beta+1)}{2r_1^2}\right)\frac{1}{r_1}R_{\alpha\beta}(r_1) \\ = &\left(-\frac{Z}{r_1} - \frac{1}{2}\nabla_{r_1}^2 + \frac{\beta(\beta+1)}{2r_1^2}\right)\frac{1}{r_1}R_{\alpha\beta}(r_1) \qquad \text{(A.4)}\end{aligned}$$

where $-\nabla_{r_1}^2/2$ is the radial kinetic energy operator.

$\hat{J}_c$: This operator involves only the core orbitals. First we should note that the density $\rho_c(\mathbf{r}_1)$ due to the N_{core} core spatial orbitals is spherical, or in other words, it has only radial dependence

$$\rho_c(\mathbf{r}_1) = 2\sum_{i=1}^{N_{core}}\psi_i^2(\mathbf{r}_1) = 2\sum_{n=1}^{k}\sum_{l=0}^{n-1}\frac{1}{r_1^2}R_{nl}^2(r_1)\sum_{m=-l}^{l}Z_{lm}^2(\theta_1,\phi_1) \qquad \text{(A.5)}$$

$$= \frac{1}{2\pi}\sum_{n=1}^{k}\sum_{l=0}^{n-1}(2l+1)\frac{1}{r_1^2}R_{nl}^2(r_1) = \rho_c(r_1) \tag{A.6}$$

where the last term is obtained after application of the spherical harmonic addition theorem and k is the highest principal quantum number of the core orbitals. Keeping in mind that the core density is spherical, the Coulomb operator can be expanded as

$$\hat{J}_c = \int \frac{\rho_c(r_2)}{r_{12}}d\mathbf{r}_2 = \sum_{\lambda=0}^{\infty}\sum_{\mu=-\lambda}^{\lambda}\frac{4\pi}{2\lambda+1}Z_{\lambda\mu}(\theta_1,\phi_1) \tag{A.7}$$

$$\times \int Z_{\lambda,\mu}(\theta_2,\phi_2)d\Omega_2\int_0^{\infty}\frac{r_<^{\lambda}}{r_>^{\lambda+1}}\rho_c(r_2)dr_2 \tag{A.8}$$

$$= 4\pi\int_0^{\infty}\frac{\rho_c(r_2)}{r_>}dr_2 \tag{A.9}$$

where we have expanded the $\frac{1}{r_{12}}$ term as a series of spherical harmonics [134] and used the fact that $\int Z_{\lambda,\mu}(\theta_2,\phi_2)d\Omega_2 = \delta_{0\lambda}\delta_{0\mu}$ due to the orthonormality of spherical harmonics. Also, $r_<$ and $r_>$ represent the smaller and larger respectively of r_1 and r_2. Therefore the Coulomb operator for the valence electron has only radial dependence, $\hat{J}_c(\mathbf{r}_1) = \hat{J}_c(r_1)$. Consequently, it is possible to integrate out the angular part of the valence orbital from the result of the action of the Coulomb operator.

$$\hat{J}_c(r_1)\frac{1}{r_1}R_{\alpha\beta}(r_1) = 4\pi\int_0^{\infty}\frac{\rho_c(r_2)}{r_>}dr_2\frac{1}{r_1}R_{\alpha\beta}(r_1) \tag{A.10}$$

$\hat{K}_c$: Due to the non-local nature of the exchange operator we have to consider from the outset its action on the valence orbital. At the same time we will multiply from the left by the angular part $Z_{\beta\gamma}(\theta_1,\phi_1)$ of the valence orbital and integrate over the solid angle $d\Omega_1 = d\theta_1 d\phi_1$.

$$\int Z_{\beta\gamma}(\theta_1,\phi_1)\hat{K}_c\frac{1}{r_1}R_{\alpha\beta}(r_1)Z_{\beta\gamma}(\theta_1,\phi_1)d\Omega_1 \tag{A.11}$$

$$= \sum_{n=1}^{k}\sum_{l=0}^{n-1}\sum_{m=-l}^{l}\frac{1}{r_1}R_{nl}(r_1)\int Z_{\beta\gamma}(\theta_1,\phi_1)Z_{lm}(\theta_1,\phi_1) \tag{A.12}$$

$$\times \left[\int\frac{1}{r_{12}}\frac{1}{r_2^2}R_{nl}(r_2)Z_{lm}(\theta_2,\phi_2)R_{\alpha\beta}(r_2)Z_{\beta\gamma}(\theta_2,\phi_2)d\mathbf{r}_2\right]d\Omega_1 \tag{A.13}$$

The next step is to bring $Z_{lm}(\theta_1,\phi_1)$ into the integral over the coordinates $\mathbf{r}_2$

and apply the addition theorem for the sum over m

$$\sum_{n=1}^{k}\sum_{l=0}^{n-1}\frac{1}{r_1}R_{nl}(r_1)\int Z_{\beta\gamma}(\theta_1,\phi_1)$$
$$\times\quad\left[\int\frac{1}{r_{12}}\frac{1}{r_2^2}R_{nl}(r_2)R_{\alpha\beta}(r_2)Z_{\beta\gamma}(\theta_2,\phi_2)\frac{2l+1}{4\pi}P_l(\cos\zeta)d\mathbf{r}_2\right]d\Omega_1$$

where ζ is the angle between the $\mathbf{r}_1$ and $\mathbf{r}_2$ vectors. Now the $1/r_{12}$ term is expanded as a series of Legendre polynomials

$$\sum_{n=1}^{k}\sum_{l=0}^{n-1}\sum_{s=0}^{\infty}\frac{1}{r_1}R_{nl}(r_1)\int_0^\infty\frac{r_<^s}{r_>^{s+1}}R_{nl}(r_2)R_{\alpha\beta}(r_2)dr_2$$
$$\times\quad\frac{2l+1}{4\pi}\int\int Z_{\beta\gamma}(\theta_1,\phi_1)Z_{\beta\gamma}(\theta_2,\phi_2)P_l(\cos\zeta)P_s(\cos\zeta)d\Omega_1d\Omega_2 \quad \text{(A.14)}$$

In order to proceed further from this point we have to take into account that the Legendre polynomials are a complete set of functions and therefore any function, including the product of two of them, can be expressed as a Legendre series [175]:

$$P_l(\cos\zeta)P_s(\cos\zeta)=\sum_{t=0}^{l+s}\frac{2t+1}{2}C_{tls}P_t(\cos\zeta) \quad \text{(A.15)}$$

The expansion coefficients C_{tls} are integrals of three Legendre polynomials and are zero unless they satisfy the triangle inequality:

$$|t-l|\le s\le t+l \quad \text{(A.16)}$$

Inserting the expansion of equation (A.15) into (A.14) we obtain

$$\sum_{n=1}^{k}\sum_{l=0}^{n-1}\sum_{s=0}^{\infty}\sum_{t=0}^{l+s}\frac{1}{r_1}R_{nl}(r_1)\frac{2t+1}{2}C_{tls}\int_0^\infty\frac{r_<^s}{r_>^{s+1}}R_{nl}(r_2)R_{\alpha\beta}(r_2)dr_2$$
$$\times\frac{2l+1}{4\pi}\int\int Z_{\beta\gamma}(\theta_1,\phi_1)Z_{\beta\gamma}(\theta_2,\phi_2)P_t(\cos\zeta)d\Omega_1d\Omega_2 \quad \text{(A.17)}$$

The addition theorem is used once more, this time to expand $P_t(\cos\zeta)$ into a sum of products of spherical harmonics. This allows to split the double integral over solid angles into a product of integrals of pairs of spherical harmonics.

$$\int\int Z_{\beta\gamma}(\theta_1,\phi_1)Z_{\beta\gamma}(\theta_2,\phi_2)P_t(cos\zeta)d\Omega_1d\Omega_2$$
$$=\frac{4\pi}{2t+1}\sum_{j=-t}^{t}\int Z_{\beta\gamma}(\theta_1,\phi_1)Z_{tj}(\theta_1,\phi_1)d\Omega_1$$
$$\times\int Z_{\beta\gamma}(\theta_2,\phi_2)Z_{tj}(\theta_2,\phi_2)d\Omega_2=\frac{4\pi}{2t+1}\delta_{t\beta} \quad \text{(A.18)}$$

This result shows that in the sum of equation (A.17) only the terms with $t = \beta$ are nonzero. Therefore, (A.17) is simplified.

$$\sum_{n=1}^{k}\sum_{l=0}^{n-1}\sum_{s=0}^{\infty}\frac{1}{r_1}R_{nl}(r_1)\frac{2l+1}{2}C_{\beta ls}\int_0^\infty \frac{r_<^s}{r_>^{s+1}}R_{nl}(r_2)R_{\alpha\beta}(r_2)dr_2 \qquad (A.19)$$

Finally, we can truncate the infinite summation over s by taking into account the triangle inequality that the $C_{\beta ls}$ coefficients have to satisfy according to (A.16):

$$\sum_{n=1}^{k}\sum_{l=0}^{n-1}\sum_{s=|\beta-l|}^{\beta+l}\frac{1}{r_1}R_{nl}(r_1)\frac{2l+1}{2}C_{\beta ls}\int_0^\infty \frac{r_<^s}{r_>^{s+1}}R_{nl}(r_2)R_{\alpha\beta}(r_2)dr_2 \qquad (A.20)$$

This is the expression for the contribution of the exchange operator to the radial part of the Hartre-Fock equation for a one valence electron atom. The most remarkable feature about this result is that it does not depend on γ, the z-component angular momentum quantum number of the valence orbital, $\frac{1}{r}R_{\alpha\beta}(r)Z_{\beta\gamma}(\theta,\phi)$. This was to be expected if we ever had a chance of separating the Hartree-Fock equation into a radial and an angular part but it was not at all obvious at the early stages of the expansion, for example in equation (A.14).

The expressions of equations (A.4), (A.10) and (A.20) combined yield a radial-only equivalent of the Hartree-Fock equation (A.2) for the valence orbital.

$$\left[-\frac{Z}{r_1}-\frac{1}{2}\nabla_{r_1}^2+\frac{\beta(\beta+1)}{2r_1^2}+4\pi\int_0^\infty\frac{\rho_c(r_2)}{r_>}dr_2+\sum_{n=1}^{k}\sum_{l=0}^{n-1}\sum_{s=|\beta-l|}^{\beta+l}\frac{2l+1}{2}C_{\beta ls}\right.$$
$$\left.\times\int_0^\infty dr_2\frac{r_<^s}{r_>^{s+1}}R_{nl}(r_2)r_2\hat{P}_{12}\frac{1}{r_2}R_{nl}(r_2)\right]\frac{1}{r_1}R_{\alpha\beta}(r_1)=\epsilon_{\alpha\beta}\frac{1}{r_1}R_{\alpha\beta}(r_1) \qquad (A.21)$$

where $\epsilon_{\alpha\beta}=\epsilon_v$ and $\hat{P}_{12}$ is an operator which, operating to the right, interchanges r_1 and r_2.

Bibliography

[1] W. J. Hehre, W. A. Lathem, R. Ditchfield, M. D. Newton and J. A. Pople, Quantum Chemistry Program Exchange 11 (1973) 236.

[2] A. Szabo and N. S. Ostlund, *Modern Quantum Chemistry: Introduction to Advanced Electronic Structure Theory*, McGraw-Hill, Inc., (1989).

[3] B. O. Roos, ed., *Lecture Notes in Quantum Chemistry I*, Springer-Verlag, (1992).

[4] B. O. Roos, ed., *Lecture Notes in Quantum Chemistry II*, Springer-Verlag, (1994).

[5] P. D. Wilson, ed., *The Nuclear Fuel Cycle*, OUP, (1996).

[6] M. Douglas and N. M. Kroll, Ann. Phys. 82 (1974) 89.

[7] C. Chang, M. Pellissier and P. Durand, Physica Scripta 34 (1986) 394.

[8] D. Rinaldi, J.-L. Rivail and N. Rguini, J.Comput.Chem 13 (1992) 675.

[9] J. Gao, Rev. Comput. Chem. 7 (1996).

[10] I. Shavitt, *Methods of Electronic Structure*, Plenum, (1977).

[11] R. J. Bartlett and G. D. Purvis, J. Chem. Phys. 76 (1982) 1910.

[12] Molecular Simulations Inc., San Diego, CA, *Cerius*^{2}, Version 3.

[13] R. O. Jones and O. Gunnarsson, Rev. Mod. Physics 61 (1989) 689.

[14] P. Hohenberg and W. Kohn, Phys. Rev. 136 (1964) B864.

[15] W. Kohn and L. J. Sham, Phys. Rev. 140 (1965) A1133.

[16] R. G. Parr and W. Yang, *Density-Functional Theory of Atoms and Molecules*, Oxford University Press, (1989).

[17] R. Car and M. Parrinello, Phys. Rev. Lett. 55 (1985) 2471.

[18] G. Galli and A. Pasquarello, *Computer Simulation in Chemical Physics*, 261–313, Kluwer Academic Publishers, (1993).

[19] S. F. Boys, Proc. R. Soc. London Ser. A 200 (1950) 542.

[20] E. R. Davidson and D. Feller, Chem. Rev. 86 (1986) 681.

[21] M. E. Mura and P. J. Knowles, J. Chem. Phys. 104 (1996) 9848.

[22] V. I. Lebedev, Zh. Vychlisl. Mat. Mat. Fiz. 15 (1975) 48.

[23] V. I. Lebedev, Zh. Vychlisl. Mat. Mat. Fiz. 16 (1976) 293.

[24] V. I. Lebedev, Sibirsk. Mat. Zh. 18 (1977) 132.

[25] V. I. Lebedev and A. L. Skorokhodov, Russ. Acad. Sci. Docl. Math. 45 (1992) 587.

[26] A. D. Becke, J. Chem. Phys. 88 (1988) 2547.

[27] A. M. James and M. P. Lord, *Macmillan's Chemical and Physical Data*, Macmillan Press, (1992).

[28] C. W. Murray, N. C. Handy and G. J. Laming, Mol. Phys. 78 (1993) 997.

[29] N. C. Handy, D. J. Tozer, G. J. Laming, C. W. Murray and R. D. Amos, Isr. J. Chem. 33 (1993) 331.

[30] G. B. Arfken and H. J. Weber, *Mathematical methods for Physicists*, Academic Press, 4th edn., (1995).

[31] H. F. King and M. Dupuis, J. Comput. Phys. 21 (1976) 144.

[32] M. Dupuis, J. Rys and H. F. King, J. Chem. Phys. 65 (1976) 111.

[33] I. Shavitt, *Methods in computational physics*, vol. 2, chap. 1, 1–45, Academic Press, (1963).

[34] P. Pyykkö, Chem. Rev. 88 (1988) 563.

[35] G. L. Malli and N. C. Pyper, Proc. R. Soc. Lond. A 407 (1986) 377.

[36] L. R. Kahn and W. A. Goddard III, J. Chem. Phys 56 (1972) 2685.

[37] L. R. Kahn, P. Baybutt and D. G. Truhlar, J. Chem. Phys. 65 (1976) 3826.

[38] L. E. McMurchie and E. R. Davidson, J. Comput. Phys. 44 (1981) 289.

[39] M. Pelissier, N. Komiha and J. P. Daudey, J. Comput. Chem. 9 (1988) 298.

[40] R. M. Pitzer and N. W. Winter, Int. J. Quantum Chem. 40 (1991) 773.

[41] J. D. Weeks and S. A. Rice, J. Chem. Phys. 49 (1968) 2741.

[42] J. C. Phillips and L. Kleinman, Phys. Rev. 116 (1959) 287.

[43] M. H. Cohen and V. Heine, Phys. Rev. 122 (1961) 1821.

[44] L. Szasz, *The Electronic Structure of Atoms*, John Wiley & Sons, (1992).

[45] L. R. Kahn, Ph.D. thesis, California Institute of Technology, Pasadena, California, (1972).

[46] U. Wedig, M. Dolg and H. Stoll, in A. Veillard, ed., *Quantum Chemistry: The challenge of transition metals and coordination chemistry*, 79–89, D. Reidel Publishing Company, (1986).

[47] P. A. Christiansen, Y. S. Lee and K. S. Pitzer, J. Chem. Phys. 71 (1979) 4445.

[48] P. Durand and J.-C. Barthelat, Theor. Chim. Acta 38 (1975) 283.

[49] P. J. Hay and R. W. Wadt, J. Chem. Phys. 82 (1985) 270.

[50] R. W. Wadt and P. J. Hay, J. Chem. Phys. 82 (1985) 284.

[51] P. J. Hay and R. W. Wadt, J. Chem. Phys. 82 (1985) 299.

[52] M. Dolg, U. Wedig, H. Stoll and H. Preuss, J. Chem. Phys. 86 (1987) 866.

[53] D. Andrae, U. Haussermann, M. Dolg, H. Stoll and H. Preuss, Theor. Chim. Acta 77 (1990) 123.

[54] W. Küchle, M. Dolg, H. Stoll and H. Preuss, J. Chem. Phys. 100 (1994) 7535.

[55] L. R. Kahn, R. H. Cowan and P. J. Hay, J. Chem. Phys. 68 (1978) 2368.

[56] J. H. Wood and A. M. Boring, Phys. Rev. B 18 (1978) 2701.

[57] K. P. Huber and G. Herzberg, *Constants of Diatomic Molecules*, Van Nostrand Reinhold Company, (1979).

[58] A. Schäfer, C. Huber and R. Ahlrichs, J. Chem. Phys. 100 (1994) 5829.

[59] A. D. Becke, Phys. Rev. A 38 (1988) 3098.

[60] C. Lee, W. Yang and R. G. Parr, Phys. Rev. B 32 (1988) 785.

[61] P. J. Hay, *Actinide ECPs*, Private Communication.

[62] A. M. Simper, *Relativistic calculations on molecules*, Ph.D. thesis, Department of Chemistry, University of Cambridge, (1998).

[63] O. Treutler and R. Ahlrichs, J. Chem. Phys. 102 (1995) 346.

[64] W. H. Press, S. A. Teukolsky, W. T. Vetterling and B. P. Flannery, *Numerical Recipes in C*, Cambridge University Press, 2nd edn., (1994).

[65] I. S. Gradshteyn and I. M. Ryzhik, *Table of Integrals, Series and Products*, Academic Press, 5th edn., (1994).

[66] Q. Cui, D. G. Musaev, M. Svensson and K. Morokuma, J. Phys. Chem. 100 (1996) 10936.

[67] Institut für Theoretische Chemie, Universität Stuttgart, *ECPs and corresponding valence basis sets*, http://www.theochem.uni-stuttgart.de/.

[68] O. Kennard and F. Allen, Chemical Design Automation News 8 (1993) 31.

[69] F. A. Cotton and G. Wilkinson, *Advanced Inorganic Chemistry*, John Willey & Sons, 4th edn., (1980).

[70] M. G. Richmond, Coord. Chem. Rev. 168 (1998) 177.

[71] B. F. G. Johnson, Y. V. Roberts, E. Parisini and R. E. Benfield, J. Organometallic Chem. 478 (1994) 21.

[72] M. McPartlin, Polyhedron 3 (1984) 1279.

[73] A. J. Freeman and C. Keller, eds., *Handbook on the Physics and Chemistry of the Actinides*, Elsevier Science Publishers, (1986).

[74] P. Guilbaud and G. Wipff, J. Phys. Chem. 97 (1993) 5685.

[75] S. J. Vosko, L. Wilk and M. Nusair, Can J. Phys. 58 (1980) 1200.

[76] A. Schäfer, H. Horn and R. Ahlrichs, J. Chem. Phys. 97 (1992) 2571.

[77] A. Bergner, M. Dolg, W. Küchle, H. Stoll and H. Preuss, Mol. Phys. 80 (1993) 1431.

[78] A. K. Rappé, C. J. Casewit, K. S. Colwell, W. A. Goddard and W. M. Skiff, J. Am. Chem. Soc. 114 (1992) 10024.

[79] J. Almlöf, K. Korsel and K. Faegri Jr., J. Comput. Chem. 3 (1982) 385.

[80] M. Häser and R. Ahlrichs, J. Comput. Chem. 10 (1988) 104.

[81] H. Horn, H. Weiss, M. Häser, M. Ehrig and R. Ahlrichs, J. Comput. Chem. 12 (1991) 1058.

[82] R. E. Stratmann, G. E. Scuseria and M. J. Frisch, Chem. Phys. Lett. 257 (1996) 213.

[83] C. A. White, B. G. Johnson, P. M. W. Gill and M. Head-Gordon, Chem. Phys. Lett. 230 (1994) 8.

[84] M. C. Strain, G. E. Scuseria and M. J. Frisch, Science 271 (1996) 51.

[85] A. Willetts, L. Gagliardi, A. G. Ioannou, A. M. Simper, C.-K. Skylaris, S. Spencer and N. C. Handy, Int. Rev. Phys. Chem. in press (1999).

[86] L. Gagliardi, A. Willetts, C.-K. Skylaris, N. C. Handy, S. Spencer, A. G. Ioannou and A. M. Simper, J. Am. Chem. Soc. 120 (1998) 11727.

[87] E. J. Baerends, D. E. Ellis and P. Ros, Chem. Phys. 2 (1973) 41.

[88] B. I. Dunlap, J. W. D. Connolly and J. R. Sabin, J. Chem. Phys. 71 (1979) 3396.

[89] L. E. McMurchie and E. R. Davidson, J. Comput. Phys. 26 (1978) 218.

[90] N. H. F. Beebe and J. Linderberg, Int. J. Quantum Chem. 12 (1977) 683.

[91] D. W. O' Neal and J. Simons, Int. J. Quantum Chem. 36 (1989) 673.

[92] G. G. Hall and C. M. Smith, Int. Journal of Quantum Chemistry XXV (1984) 881.

[93] C. M. Smith and G. G. Hall, Theor. Chim. Acta 69 (1986) 63.

[94] K. Eichkorn, O. Treutler, H. Öhm, M. Häser and R. Ahlrichs, Chem. Phys. Lett. 240 (1995) 283.

[95] K. Eichkorn, F. Weingend, O. Treutler and R. Ahlrichs, Theor. Chem. Acc. 97 (1997) 119.

[96] M. W. Schmidt and K. Ruedenberg, J. Chem. Phys. 71 (1979) 3951.

[97] L. Gagliardi, N. C. Handy, A. G. Ioannou, C.-K. Skylaris, S. Spencer, A. Willetts and A. M. Simper, Chem. Phys. Lett. 283 (1998) 187.

[98] S. Spencer, L. Gagliardi, N. C. Handy, A. G. Ioannou, C.-K. Skylaris, A. Willetts and A. M. Simper, J. Phys. Chem. A 103 (1999) 1831.

[99] N. Godbout, D. R. Salahub, J. Andzelm and E. Wimmer, Can. J. Chem. 70 (1992) 560.

[100] O. Vahtras, J. Almlöf and M. W. Feyereisen, Chem. Phys. Lett. 213 (1993) 514.

[101] C. Van Alsenoy, J. Comput. Chem. 9 (1988) 620.

[102] A. Komornicki and G. Fitzgerald, J. Chem. Phys. 98 (1993) 1398.

[103] Basis sets were obtained from the Extensible Computational Chemistry Environment Basis Set Database, Version 1.0, as developed and distributed by the Molecular Science Computing Facility, Environmental and Molecular Sciences Laboratory which is part of the Pacific Northwest Laboratory, P.O. Box 999, Richland, Washington 99352, USA, and funded by the U.S. Department of Energy. The Pacific Northwest Laboratory is a multi-program laboratory operated by Battelle Memorial Institue for the U.S. Department of Energy under contract DE-AC06-76RLO 1830. Contact David Feller, Karen Schuchardt, or Don Jones for further information. The database is accessible via the URL http://www.emsl.pnl.gov:2080/forms/basisform.html.

[104] W. J. Hehre, R. F. Stewart and J. A. Pople, J. Chem. Phys. 51 (1969) 2657.

[105] W. J. Hehre, R. Ditchfield, R. F. Stewart and J. A. Pople, J. Chem. Phys. (1970) 2769.

[106] T. H. Dunning, J. Chem. Phys. 53 (1970) 2823.

[107] T. H. Dunning and P. J. Hay, *Methods of Electronic Structure Theory*, vol. 3, chap. 1, 1–27, Plenum Press, New York and London, (1977).

[108] T. H. Dunning, J. Chem. Phys. 90 (1989) 1007.

[109] D. E. Woon and T. H. Dunning, J. Chem. Phys. 98 (1993) 1358.

[110] R. Gáspár, Acta. Phys. Hung. 35 (1974) 213.

[111] R. Gáspár and A. Nagy, J. Phys. B 20 (1987) 3631.

[112] P. G. Jones and C. Thöne, Chem. Ber. 124 (1991) 2725.

[113] D. F. Feller and K. Ruedenberg, Theor. Chim. Acta 52 (1979) 231.

[114] R. Ahlrichs, Private communication.

[115] J. C. Slater, Phys. Rev. 36 (1930) 57.

[116] C.-K. Skylaris, *Basis functions for large molecule density functional theory studies*, PhD first year dissertation (CPGS), (April 1997).

[117] G. T. Velde and E. J. Baerends, J. Comput. Phys. 99 (1992) 84.

[118] Theoretical Chemistry, Vrije Universiteit, Amsterdam, *Amsterdam Density Functional (ADF)*, (1997), Release 2.3.

[119] J. Rys, M. Dupuis and H. F. King, J. Comput. Chem. 4 (1983) 154.

[120] R. Lindh, U. Ryu and B. Liu, J. Chem. Phys. 95 (1991) 5889.

[121] M. Head-Gordon and J. A. Pople, J. Chem. Phys. 89 (1988) 5777.

[122] U. Ryu, Y. S. Lee and R. Lindh, Chem. Phys. Lett. 185 (1991) 562.

[123] P. M. W. Gill, B. G. Johnson and J. A. Pople, Int. J. Quantum Chem. 40 (1991) 745.

[124] P. M. W. Gill, Private communication.

[125] S. Obara and A. Saika, J. Chem. Phys. 84 (1986) 3963.

[126] P. M. W. Gill and J. A. Pople, Int. J. Quantum Chem. 40 (1991) 753.

[127] P. M. W. Gill, Adv. Quantum Chem. 25 (1994) 143.

[128] H. Taketa, S. Huzinaga and K. O-Ohata, J. Phys. Soc. Japan 21 (1966) 2313.

[129] J. Cízek and J. Paldus, J. Chem. Phys. 47 (1967).

[130] P. Pulay, J. Comput. Chem. 3 (1982) 556.

[131] H. Sellers, Int. J. Quantum Chem. 45 (1993) 31.

[132] V. R. Saunders and I. H. Hillier, Int. J. Quantum Chem. 7 (1973) 699.

[133] I. H. Hillier and V. R. Saunders, Proc. R. Soc. Lond. A 320 (1970) 161.

[134] I. N. Levine, *Quantum Chemistry*, Prentice Hall, 4th edn., (1991).

[135] R. McWeeny, Rev. Mod. Physics 32 (1960) 335.

[136] X. P. Li, W. Nunes and D. Vanderbilt, Phys. Rev. B 47 (1993) 10891.

[137] C. Ochsenfeld and M. Head-Gordon, Chem. Phys. Lett. 270 (1997) 399.

[138] J. M. Millam and G. E. Scuseria, J. Chem. Phys. 106 (1997) 5569.

[139] O. Axelsson, *Iterative solution methods*, Cambridge University Press, (1996).

[140] E. Polak, *Optimization: Algorithms and Consistent Approximations*, Springer-Verlag, (1997).

[141] G. E. Scuseria, *CG-DMS implementation notes*, private communication.

[142] J. A. Pople, R. Krishnan, H. B. Schlegel and J. S. Binkley, Int. J. Quantum Chem.: Quantum Chemistry Symposium 13 (1979) 225.

[143] M. Dupuis and H. F. King, J. Chem. Phys. 68 (1978) 3998.

[144] T. Helgaker and Jørgensen, Adv. Quantum Chem. 19 (1988) 183.

[145] J. F. Gaw and N. C. Handy, Chem. Soc. Spec. Reports 81 (1984) 291.

[146] R. Fournier, J. Andzelm and D. R. Salahub, J. Chem. Phys. 90 (1989) 6371.

[147] R. Fournier, J. Chem. Phys. 92 (1990) 5422.

[148] B. G. Johnson and M. J. Frisch, Chem. Phys. Lett. 216 (1993) 133.

[149] C. G. Broyden, J. Inst. Maths. Appl. 6 (1970) 76.

[150] R. Fletcher, Comp. J. 13 (1970) 317.

[151] D. Goldfarb, Math. Comp. 24 (1970) 23.

[152] D. F. Shanno, Math. Comp. 24 (1970) 647.

[153] J. D. Head and M. C. Zerner, Chem. Phys. Lett. 122 (1985) 264.

[154] J. D. Head and M. C. Zerner, Adv. Quantum Chem. 20 (1988) 1.

[155] J. D. Head, B. Weiner and M. C. Zerner, Int. J. Quantum Chem. 33 (1988) 177.

[156] P. G. Eller, R. R. Ryan and R. O. Schaeffer, Cryst. Struct. Commun. 6 (1977) 163.

[157] K. P. C. Vollhardt and N. E. Schore, *Organic Chemistry*, W. H. Freeman and Company, New York, 3rd edn., (1998).

[158] P. G. Harrison, T. J. King, J. A. Richards and R. C. Phillips, J. Organometallic Chem. 116 (1976) 307.

[159] A. G. Davies and R. J. Puddephatt, J. Chem. Soc. (C) (1967) 2663.

[160] W. Küchle, M. Dolg, H. Stoll and H. Preuss, Mol. Phys. 74 (1991) 1245.

[161] R. D. Adams and I. T. Horvath, Prog. Inorg. Chem. 33 (1985) 127.

[162] G. A. Foulds, B. F. G. Johnson and J. Lewis, J. Organometallic Chem. 296 (1985) 147.

[163] R. Mason and A. I. M. Rae, J. Chem. Soc. (A) (1968) 778.

[164] M. R. Churchill, F. J. Hollander and J. P. Hutchinson, Inorg. Chem. 16 (1977) 2655.

[165] J. J. Katz, G. T. Seaborg and L. R. Morss, *The Chemistry of the Actinide Elements*, Chapman and Hall: London, (1986).

[166] V. Eliet, G. Bidoglio, N. Omenetto, L. Parma and I. J. Grenthe, J. Chem. Soc., Faraday Trans. 91 (1995) 2275.

[167] D. L. Clark, S. D. Conradson, R. J. Donohoe, D. W. Keogh, D. E. Morris, P. D. Palmer, R. D. Rogers and C. D. Tait, Inorg. Chem. 38 (1999) 1456.

[168] G. Schreckenbach, P. J. Hay and R. L. Martin, Inorg. Chem. 37 (1998) 4442.

[169] A. D. Becke, J. Chem. Phys. 98 (1993) 1372.

[170] W. J. Hehre, L. Radom, P. v. R. Schleyer and J. A. Pople, *Ab Initio Molecular Orbital Theory*, John Wiley & Sons: New York, (1986).

[171] P. J. Hay, J. Chem. Phys. 79 (1983) 5469.

[172] M. J. Frisch, G. W. Trucks, H. B. Schlegel, P. M. W. Gill, B. G. Johnson, M. A. Robb, J. R. Cheeseman, T. A. Keith, G. A. Petersson, J. A. Montgomery, K. Raghavachari, M. A. Al-Laham, V. G. Zakrzewski, J. V. Ortiz, J. B. Foresman, C. Y. Peng, P. Y. Ayala, M. W. Wong, J. L. Andres, E. S. Replogle, R. Gomperts, R. L. Martin, D. J. Fox, J. S. Binkley, D. J. Defrees, J. Baker, J. P. Stewart, M. Head-Gordon, C. Gonzalez and J. A. Pople, *Gaussian 94 (Revision E1)*, Gaussian, Inc., Pittsburgh PA, (1995).

[173] G. Schreckenbach, P. J. Hay and R. L. Martin, J. Comput. Chem. 20 (1999) 70.

[174] D. R. Hartree, *The calculation of atomic structures*, John Wiley & Sons, (1957).

[175] E. U. Condon and G. H. Shortley, *Theory of Atomic Spectra*, Cambridge, (1935), §9^6, formula (11).

Index

Typeset with LaTeX 2_ε in Computer Modern 11pt. using the MiKTeX, version 1.11 beta 3, distribution for Microsoft Windows (95, 98 and NT 4). Thanks to Christian Schenk (http://www.snafu.de/~cschenk/miktex/), Willem Minten (http://www.esat.kuleuven.ac.be/~minten/NTTeXing/NTTeXing.html) and the GNU emacs and GSview developers. Also thanks to Donald Knuth, Leslie Lamport and the LaTeX3 project team.